การวิเคราะห์ระบบเซลล์เชื้อเพลิงชนิดออกไซด์แข็งที่ใช้เอทานอลเป็นเชื้อเพลิง เพื่อการผลิตพลังงานไฟฟ้า ความร้อน และความเย็นร่วม

นางสาวพนิชา ทิพวรรณ

วิทยานิพนธ์นี้เป็นส่วนหนึ่งของการศึกษาตามหลักสูตรปริญญาวิศวกรรมศาสตรดุษฎีบัณฑิต
สาขาวิชาวิศวกรรมเคมี ภาควิชาวิศวกรรมเคมี
คณะวิศวกรรมศาสตร์ จุฬาลงกรณ์มหาวิทยาลัย
ปีการศึกษา 2557

ANALYSIS OF ETHANOL-FUELLED SOLID OXIDE FUEL CELL SYSTEMS FOR COMBINED COOLING, HEAT AND POWER GENERATION

Miss Phanicha Tippawan

A Dissertation Submitted in Partial Fulfillment of the Requirements
for the Degree of Doctor of Engineering Program in Chemical Engineering
Department of Chemical Engineering
Faculty of Engineering
Chulalongkorn University
Academic Year 2014

Thesis Title	ANALYSIS OF ETHANOL-FUELLED SOLID OXIDE FUEL CELL SYSTEMS FOR COMBINED COOLING, HEAT AND POWER GENERATION
By	Miss Phanicha Tippawan
Field of Study	Chemical Engineering
Thesis Advisor	Assistant Professor Amornchai Arpornwichanop, D.Eng.

Accepted by the Faculty of Engineering, Chulalongkorn University in Partial Fulfillment of the Requirements for the Doctoral Degree

.....Dean of the Faculty of Engineering
(Professor Bundhit Eua-arporn, Ph.D.)

THESIS COMMITTEE

.....Chairman
(Associate Professor Sarawut Rimdusit, Ph.D.)
.....Thesis Advisor
(Assistant Professor Amornchai Arpornwichanop, D.Eng.)
.....Examiner
(Assistant Professor Kasidit Nootong, Ph.D.)
.....Examiner
(Pimporn Ponpesh, Ph.D.)
.....External Examiner
(Assistant Professor Woranee Paengjuntuek, D.Eng.)

พนิชา ทิพวรรณ : การวิเคราะห์ระบบเซลล์เชื้อเพลิงชนิดออกไซด์แข็งที่ใช้เอทานอลเป็นเชื้อเพลิงเพื่อการผลิตพลังงานไฟฟ้า ความร้อน และความเย็นร่วม (ANALYSIS OF ETHANOL-FUELLED SOLID OXIDE FUEL CELL SYSTEMS FOR COMBINED COOLING, HEAT AND POWER GENERATION) อ.ที่ปรึกษาวิทยานิพนธ์หลัก: ผศ. ดร.อมรชัย อาภรณ์วิชานพ, 186 หน้า.

การใช้เอทานอลเป็นเชื้อเพลิงสำหรับเซลล์เชื้อเพลิงชนิดออกไซด์แข็ง ได้จัดว่าเป็นวิธีการที่ช่วยให้ได้กระบวนการผลิตไฟฟ้าที่สะอาดและมีประสิทธิภาพสูงยิ่งขึ้น งานวิจัยนี้จึงนำเสนอการวิเคราะห์ระบบเซลล์เชื้อเพลิงชนิดออกไซด์แข็งที่ใช้เอทานอลเป็นเชื้อเพลิง ในส่วนแรกคือ การศึกษาเกี่ยวกับกระบวนการรีฟอร์มมิงเอทานอลโดยประยุกต์ใช้หลักการทางเทอร์โมไดนามิกส์ กระบวนการรีฟอร์มมิงที่พิจารณามี 3 กระบวนการ ได้แก่ การรีฟอร์มมิงด้วยไอน้ำ (steam reforming) การออกซิเดชันบางส่วนด้วยอากาศ (partial oxidation) และการรีฟอร์มมิงแบบออโตเทอร์มัล (autothermal reforming) โดยพิจารณาถึงองค์ประกอบของก๊าซผลิตภัณฑ์ที่ได้และเปรียบเทียบกระบวนการดังกล่าวด้วยการวิเคราะห์พลังงานและเอ็กเซอร์ยี เพื่อหากระบวนการที่เหมาะสมสำหรับการผลิตก๊าซไฮโดรเจนจากเอทานอลสำหรับเซลล์เชื้อเพลิงชนิดออกไซด์แข็ง ผลที่ได้พบว่ากระบวนการรีฟอร์มมิงด้วยไอน้ำสามารถผลิตไฮโดรเจนได้มากที่สุด ถึงแม้ว่ากระบวนการนี้จะต้องการพลังงานความร้อนจากภายนอกมาก แต่จากการวิเคราะห์ด้วยเอ็กเซอร์ยีกลับพบว่าเป็นกระบวนการที่ใช้พลังงานได้อย่างคุ้มค่ามากกว่ากระบวนการอื่น สภาวะที่เหมาะสมของกระบวนการนี้คือดำเนินการที่อุณหภูมิ 980 K อัตราส่วนเชิงโมลของไอน้ำต่อเอทานอลคือ 1.8 ในลำดับต่อมาได้ศึกษากลไกการเกิดปฏิกิริยารีฟอร์มมิงด้วยไอน้ำของเอทานอล และค้นพบว่ากระบวนการนี้สามารถหลีกเลี่ยงการเกิดคาร์บอนได้ โดยให้เกิดปฏิกิริยาแบบสองขั้นตอนผ่านตัวกลาง ซึ่งมีความว่องไวต่อการเกิดคาร์บอนต่ำ โดยเริ่มแรกให้เอทานอลเกิดปฏิกิริยาดีไฮโดรจีเนชันเกิดเป็นอะซีทัลดีไฮด์เสียก่อน แล้วจึงให้ทำปฏิกิริยากับน้ำในขั้นตอนที่สองได้เป็นก๊าซที่มีไฮโดรเจนเป็นองค์ประกอบหลัก แต่อย่างไรก็ตามวิธีการดังกล่าวต้องเผชิญกับข้อจำกัดของปฏิกิริยาสมดุลเคมี ซึ่งเต็มไปด้วยผลิตภัณฑ์ที่ไปเจือจางก๊าซไฮโดรเจน อาทิ ก๊าซคาร์บอนไดออกไซด์และไอน้ำ ด้วยเหตุนี้ในลำดับต่อมาจึงศึกษาผลกระทบของการกำจัดก๊าซคาร์บอนไดออกไซด์และไอน้ำที่มีต่อสมรรถนะของเซลล์เชื้อเพลิงชนิดออกไซด์แข็งขึ้น ผลการศึกษาพบว่าเซลล์เชื้อเพลิงชนิดออกไซด์แข็งมีสมรรถนะดีขึ้นจริง ต่อมาได้นำการวิเคราะห์ทางเศรษฐศาสตร์ได้ถูกนำเสนอเพื่อเปรียบเทียบกระบวนรีฟอร์มมิงด้วยไอน้ำของเอทานอลแบบสองขั้นตอนที่ทำงานร่วมกับการใช้ตัวดูดซับคาร์บอนไดออกไซด์ กับกระบวนการรีฟอร์มมิงด้วยไอน้ำของเอทานอลแบบดั้งเดิม การศึกษานี้ช่วยให้เห็นถึงความเป็นไปได้ทางเศรษฐศาสตร์ของการรีฟอร์มมิงด้วยไอน้ำแบบสองขั้นตอนที่ทำงานร่วมกับการใช้ตัวดูดซับคาร์บอนไดออกไซด์มากขึ้น ในลำดับสุดท้าย เพื่อนำความร้อนจากเซลล์เชื้อเพลิงกลับมาใช้ใหม่และปรับปรุงประสิทธิภาพการใช้พลังงานในระบบให้ดียิ่งขึ้น การทำงานร่วมกันของเซลล์เชื้อเพลิงชนิดออกไซด์แข็งและเครื่องทำความเย็นแบบดูดซับ เพื่อผลิตพลังงานไฟฟ้า ความร้อน และความเย็นร่วม จึงถูกศึกษาขึ้นในงานนี้ การวิเคราะห์พลังงานและเอ็กเซอร์ยียังเป็นเครื่องมือวิเคราะห์ที่สำคัญในการหาปริมาณพลังงานที่ต้องการและยังสามารถอธิบายความคุ้มค่าของพลังงานที่ถูกป้อนเข้าไปได้ นอกจากนี้การวิเคราะห์เอ็กเซอร์ยีร่วมกับสิ่งแวดล้อม ยังชี้ให้เห็นศักยภาพในการลดการปลดปล่อยมลพิษของระบบดังกล่าวอีกด้วย

ภาควิชา วิศวกรรมเคมี ลายมือชื่อนิสิต .....

สาขาวิชา วิศวกรรมเคมี ลายมือชื่อ อ.ที่ปรึกษาหลัก .....

ปีการศึกษา 2557

5371811021 : MAJOR CHEMICAL ENGINEERING
KEYWORDS: SOLID OXIDE FUEL CELL / ETHANOL / ABSORPTION CHILLER / ENERGY ANALYSIS / EXERGY ANALYSIS

PHANICHA TIPPAWAN: ANALYSIS OF ETHANOL-FUELLED SOLID OXIDE FUEL CELL SYSTEMS FOR COMBINED COOLING, HEAT AND POWER GENERATION. ADVISOR: ASST. PROF. AMORNCHAI ARPORNWICHANOP, D.Eng., 186 pp.

A solid oxide fuel cell (SOFC) fuelled by ethanol, an attractive green fuel that can be renewably produced from agricultural products, is regarded as a promising clean process to generate electricity with high efficiency. Therefore, this research concentrates on the analysis of ethanol-fuelled solid oxide fuel cell systems. Firstly, the thermodynamic analysis of three different ethanol reforming processes (i.e., steam reforming, partial oxidation and autothermal reforming) is investigated in term of product compositions and compared on the basis of energy and exergy analyses to find the most suitable process for solid oxide fuel cell applications. The simulation results show that although the steam reforming process provides the highest hydrogen yield, it is the highest energy requiring process. The exergy analysis shows that the lowest exergy destruction is found in the steam reforming. The integration of ethanol steam reformer operated at temperature of 980 K and steam-to-ethanol ratio of 1.8 and solid oxide fuel cell provides the best energetic and exergetic performances. Secondly, the improvement of the ethanol steam reforming is further investigated by considering the reforming reaction mechanism. To avoid a carbon formation, the steam reforming of ethanol should be carried out into two steps via a reaction intermediate which has a lower coking activity. Ethanol is firstly dehydrogenated to be acetaldehyde and then steam reform into hydrogen rich gas. However, this method faces a limitation of chemical equilibrium reactions which typically produce more dilute products such as CO_2 and water. For this reason, the removal of CO_2 and excess steam in the reforming environment and its effect on SOFC performance are studied. Thirdly, an economic analysis of improved reforming processes (two-step steam reforming and two-step steam reforming with CO_2 capture) is presented and compared with a conventional steam reforming. The study illustrates the feasibility of the two-step steam reforming and CO_2 capture integrated processes in the economic aspect. Finally, a heat recovery of the SOFC system is considered to improve the efficiency of the system energy usage. The ethanol-fuelled solid oxide fuel cell system integrated with an absorption chiller is proposed in this study for combined cooling, heat and power generation. The energy and exergy analyses of such system is performed to determine an energy demand and to describe how efficiently the energy usage. The exergoenvironmental analysis is also performed providing useful insights in terms of heat recovery and environmental aspects and the results indicate the benefit of this system.

Department:	Chemical Engineering	Student's Signature	----------
Field of Study:	Chemical Engineering	Advisor's Signature	----------
Academic Year:	2014		

ACKNOWLEDGEMENTS

I would like to express my gratitude to Assistant Professor Amormchai Arpornwlchanop for giving me the opportunity to pursue the doctoral study at Chulalongkorn University. His support and encouragement have inspired and motivated me to push through the fight of researching environment. It has been a great experience for me to work with him.

I would like to thank the members of my thesis committee, Associate Professor Sarawut Rimdusit, Assistant Professor Kasidit Nootong, Dr. Pimporn Ponpesh and Assistant Professor Woranee Paengjuntuek, for their time and useful comments on this research.

Financial support by the Dutsadiphiphat Scholarship, the Ratchadaphiseksomphot Endowment Fund of Chulalongkorn University and the Thailand Research Fund is gratefully acknowledged.

My appreciation is also expressed to Professor Ibrahim Dincer who provides me the opportunity to spend a period of eight months in his research group at University of Ontario Institute of Technology (UOIT), Canada. His ideas and suggestion are of great benefits to my research area. Special thanks go to Dr. Rami El-Emam for his technical assistances on EES programming. I also thank to all my friends at UOIT for their valuable friendship and the Polinkiewicz family for their help during my visit to Canada.

I am very thankful to all of the members of Control and Systems Engineering Research Laboratory, Department of Chemical Engineering, Chulalongkorn University for their moral support, advice and very nice friendship. Most importantly, I am very grateful for the unconditional love and support from my mother and my aunts. They are never given up to believe in me, which I appreciate sincerely. Also, special thanks go to Mr. Songphon Lornaowarat for making me believe in myself as well as unwinding me when needed by means of a talent of humor and wit. I learn to create self-disciplines from his approach.

My deepest gratitude goes to Venerable Luangta Maha Bua Yanasampanno, Luang Pu Oom Sukakamo and Luang Pu Awaan Kemmako for teaching me to know the real happiness and helping me to find the life purpose.

CONTENTS

Page

Page

Page

Page

Page

LIST OF TABLES

Page

LIST OF FIGURES

Page

LIST OF FIGURES

Page

LIST OF FIGURES

Page

LIST OF FIGURES

Page

NOMENCLATURES

a	Extent of steam reforming reaction for methane, kmol/h
a_{ik}	The number of atoms of element k in a component i
b	Extent of water gas shift reaction, kmol/h
c	Extent of electrochemical reaction, kmol/h
C	The number of components in the reaction system
C_P	Specific heat capacity, J/kg K
D_{eff}	Diffusion coefficient, m^2s^{-1}
D_P	Depletion number
E	Theoretical open-circuit voltage, V
E^0	Reversible open-circuit voltage, V
$E_{electrode}$	Activation energy of electrode, kJ mol^{-1}
$Emi(CO_2, tri)$	Normalized CO_2 emissions of the trigeneration, kg/MW h
ex_i	Specific molar exergy for each stream flow, kJ/kmol
ex_{ch}	Specific molar chemical exergy, kJ/kmol
$\dot{E}x_d$	Exergy destruction, kW
$\dot{E}x_f$	Exergy of the fuel, kW
F	Faraday constant, C/mol
F_{coke}	Molar flow rate of carbon, kmol/h
$F_{C_2H_5OH}$	Molar flow rate of ethanol, kmol/h
F_{H_2}	Molar flow rate of hydrogen, kmol/h
G	Total Gibbs free energy of the system, kJ/kmol
h_i	Specific molar enthalpy, kJ/kmol
i	Current density, A/cm^2
i_0	Exchange current density, A/m^2
$k_{electrode}$	Pre-exponential factor of electrode, $\Omega^{-1}m^{-2}$

NOMENCLATURES

LHV	Lower Heating Value, kJ/kg
$\dot{m}$	Mass flow rate, kg/h
n	Number of electrons
$\dot{n}$	Molar flow rate, kmol/h
n_i	The number of moles of each gases component.
p	Partial pressure, kPa
P	Pressure, kPa
$\dot{Q}$	Heat flow rate, kW
r	SOFC anode circulation ratio
R	Universal gas constant, kJ/kmol K
R_{ohm}	Total cell internal resistance, Ω cm^2
$r_{el,c}$	Electrical to cooling energy ratio
$r_{el,h}$	Electrical to heating energy ratio
s_i	Specific molar entropy, kJ/kmol K
SI	Sustainability index
T	Temperature, K
U_f	Fuel utilization ratio
U_{O_2}	Oxygen utilization ratio
V	Cell voltage, V
$\dot{W}$	Work rate, kW
$X_{C_2H_5OH}$	Ethanol conversion, %
y	Mole fraction
Y_{H_2}	Hydrogen yield, mol H_2/mol ethanol

NOMENCLATURES

Greek symbols

α	Transfer coefficient
τ	Layer thickness, μm
σ	Electronic or ionic conductivity, $\Omega^{-1}m^{-1}$
η	Efficiency or energy efficiency, %
ψ	Exergy efficiency, %

Subscripts

0	Dead state conditions
act	Activation
c	Cooling
cop	Compressor
cog,c	Cooling cogeneration
cog,h	Heating cogeneration
conc	Concentration
cv	Control volume
DC	DC current
el	Electrical power
ER	Ethanol Reforming
EV	Evaporator
f	Fuel
h	Heating
HP	Heating Process
i	Inlet, component
in	State, or device inverter (DC to AC inverter)
k	Element
ohm	Ohmic
out	Outlet
tri	Trigeneration

NOMENCLATURES

w	The number of elements appearing in all of the components

Superscripts

·	Rate of a component
0	At standard pressure

Acronyms

AB	Absorber
AC	Absorption chiller
C	carbon
C_2H_4	Ethylene
C_2H_5OH	Ethanol
$CaCO_3$	Calcium carbonate
CaO	Calcium oxide
CH_3CHO	Acetaldehyde
CH_4	Methane
CO	Condenser, carbon monoxide
CO_2	Carbon dioxide
EES	Engineering equation solver
EV	Evaporator
GE	Generator
H_2	Hydrogen
H_2O	Water
HP	High Pressure
N_2	Nitrogen
O_2	Oxygen
SG	Steam Generator
LHV	Lower Heating Value
LP	Low Pressure

NOMENCLATURES

SOFC	Solid Oxide Fuel Cell
TPB	Three Phase Boundary

CHAPTER I

INTRODUCTION

1.1 Background and motivation

Today, energy demand continues to increase considerably because of rapid population growth and economic development. Among the developing technologies for power generation, a fuel cell has been accepted to be a potential alternative. It is an electrochemical device that can directly convert chemical energy from fuel (i.e., hydrogen) to electrical energy via an electrochemical process. Leading to an environmentally friendly process (Abdullah S. et al., 2014), this is quite different from conventional power plants, which is based on a combustion process to convert fuel into high-temperature gas for driving an electrical generator via a turbine engines.

A solid oxide fuel cell (SOFC) is among the various types of a fuel cell. It is operated at high temperature (600-1000°C), allowing internal conversion of a wide range of fuels in SOFC itself (Coutelieris et al., 2003; Douvartzides et al., 2004b; Piroonlerkgul et al., 2008) and generation of high quality by-product heat for cogeneration (Verda and Calí Quaglia, 2008; Hong et al., 2014) or trigeneration (Blarke and Lund, 2008) applications. In addition, a solid electrolyte is employed and thus, corrosion and electrolyte management problems can be avoided. SOFC is considered to be used as a large scale power plant since highly efficient combined cycle plants can be established. It has proven lifetimes sufficient for stationary applications. In general, both non-renewable fuels (e.g., natural gas, liquefied petroleum gas) and renewable fuels (e.g., ethanol, biogas, glycerol) can be used to produce hydrogen for SOFC (Lin et al., 2013); however, regarding a cost effectiveness, only the utilization of renewable fuel from agricultural residues will allow SOFC be competitive potential in the near-term future.

Hydrogen has been identified as an ideal energy carrier to support a sustainable energy development and can be used in a fuel cell to generate electricity. Nowadays a

steam reforming of hydrocarbons, such as natural gas, is the most commonly used process for hydrogen production (Angeli et al., 2014; De Falco et al., 2014). However, use of natural gas, which is a limited energy resource, has caused environmental problems, i.e., air pollutant and greenhouse gas emissions. Consequently, there is a new interest in the search for effective alternatives to produce renewable hydrogen cleanly and safely. Although SOFC offers the feasibility of using various fuel types, ethanol is one of the promising candidates (Saebea et al., 2013). Ethanol is considered an attractive green fuel for use in SOFC because it can be produced renewably from various agriculture products. Thus, it is suitable for agricultural country like Thailand. Ethanol production supports farmers and creates domestic jobs. In addition, ethanol is produced domestically, from domestically grown crops, reducing dependence on foreign oil and increasing the nation's energy independence. Compared with other fuels, ethanol presents several advantages, including a high heat of vaporization, a low photochemical reactivity, ease of storage and handling safety (Cardona and Sánchez, 2007; Hong et al., 2011; Casas-Ledon et al., 2014; Ebner et al., 2014).

As mentioned earlier, fuel cells utilize hydrogen as fuel of the system. Although hydrogen is the lightest, the simplest, and one of the most abundant elements in nature, it is not a free element. There are different methods to extract pure hydrogen from ethanol, such as steam reforming (SR), partial oxidation (POX) and autothermal reforming (ATR) (Rabenstein and Hacker, 2008; Sun et al., 2012). Each reforming process differs in operating method, composition of obtained reforming gas and energy demand. A number of researchers take great effort to find the most suitable reforming process in order to achieve a commercial application. A steam reforming is among the widely used processes due to its high hydrogen yield; however, this process involves a highly endothermic reaction and requires high energy supply. To minimize the external heat requirement, partial oxidation and autothermal reforming processes are alternative routes for hydrogen production (Rabenstein and Hacker, 2008).

Regarding the first law of thermodynamics, an energy balance can determine energy requirements in the forms of streams of matter, heat and work, but fails to provide accurate information on how efficiently the supplied energy is used in a system.

This is due to the fact that such an energy analysis cannot identify the real thermodynamic inefficiencies associated with the energy conversion system. On the other hand, an entropy balance determines the entropy generation within the system, which is an indicator of its inefficient energy usage. However, since entropy values still fail to account for the quality of energy, the true thermodynamic value (quality) of an energy carrier is characterized by its exergy. Exergy destruction which is one of the exergy-based variables represents the exergy destroyed due to irreversibility (entropy generation) within the system (El-Emam and Dincer, 2011). The irreversibility may be caused by chemical reaction, heat transfer through a finite temperature difference, mixing of matter, unrestrained expansion and friction.

The first law of thermodynamics gives information about the conservation of energy involved through energy analysis while the second law of thermodynamics can be used to assess and improve energy systems, leading to a better understand of the energy utilization through exergy analysis. Clearly, these insights to the process operation cannot be attained by an energy analysis alone (Rosen et al., 2008). To identify a suitable ethanol reforming process for hydrogen production in SOFC applications, energy and exergy analyses of each ethanol reforming process should be investigated.

Although the steam reforming process is widely used in chemical industries, steam reforming of ethanol for hydrogen production involves a complex multiple reaction system and thus, the purity of hydrogen product is affected by many undesirable by-products. This causes the yield of hydrogen depend on a complex manner on process variables such as pressure, temperature and reactant ratio. In order to maximize the yield of hydrogen, it is necessary to know the effect of these variables on the product composition (Fishtik et al., 2000). However, there are several reaction pathways that could occur in ethanol and water system, depending on the catalysts used. Various kinds of intermediate by-products, such as acetaldehyde and ethylene, are usually formed. Other important problems during the reforming of ethanol involve catalyst coking and formation of undesirable products (Freni S. et al., 2000). It is well known that trend of carbon formation increases dramatically in the presence of

ethylene, which is derived from the dehydration of ethanol, via a polymerization process (Lima da Silva et al., 2009). From this problem, it seems reasonable to convert ethanol first into other species with a lower coking activity and then convert these species into hydrogen-rich gas. Acetaldehyde is one of the desired species that can be easily produced from ethanol dehydrogenation, which is favored at a relative low temperature operation (Freni S. et al., 2000; Nishiguchi et al., 2005). Conceptually, ethanol steam reforming may be divided into two steps. First, ethanol is dehydrogenated to acetaldehyde using a dehydrogenation unit. Secondly, gas product from the first unit is fed into the steam reforming environment in order to produce more hydrogen and reduce the amount of reactants which could cause a carbon formation (e.g., methane and carbon monoxide). Thus, a carbon-free hydrogen production should be studied in details for a two-step steam reforming system.

The concept of a two-step ethanol steam reforming is proposed in order to avoid carbon formation by producing only desired species in the first step of a dehydrogenation unit, and then converting these species into hydrogen-rich gas in a reformer. However, the steam reforming of acetaldehyde in the second step is limited by chemical equilibrium reactions which typically produce more dilute products such as CO_2 and water. For this reason the removal of CO_2 and excess steam in the reforming environment is an interesting alternative to enhance the purity of hydrogen-rich gas. Using CaO sorbent for CO_2 capture (Elzinga et al., 2011; Cormos and Simon, 2013) and installing a dehumidifier (Harriman, 1990) are conceptually designed to remove portion of undesirable products. Therefore, the analysis of removal effects should be required for an appropriate operation. To illustrate the potential of two-step steam reforming process integrated with SOFC system in the market place, analysis of the two-step reforming and CO_2 capture integrated processes should also be studied in term of economic consideration (Biegler et al., 1997; Piroonlerkgul et al., 2010; Lopes et al., 2012).

To further improve the energy and exergy efficiencies of the SOFC system, exhaust gas released from SOFC and contained useful fuels and heat can be utilized and recovered; an integration of SOFC and other heat recovery units can improve the

overall system efficiency. Afterburner, heat exchanger networks and absorption chiller are among the process that can be integrated with the SOFC system (Tse et al., 2011; Chen and Ni, 2014; Fong and Lee, 2014). Presently, an increase in demand for cooling and heating power calls for resurveying traditional energy production. One method for sustainable development is to adopt the technology of combined cooling, heating, and power (CCHP) or trigeneration system. The possibility of such an integrated system should be also performed under energy, exergy and environmental aspects (Rosen et al., 2008; Dincer and Naterer, 2010; Dincer and Rosen, 2013) to improve understanding in the whole ways of energy sustainability world.

1.2 Objectives of research

The objectives of this research are to design and analyze a SOFC system consisting mainly of a fuel processor and SOFC stack and to recover useful heat obtained from SOFC exhaust gas to improve an overall efficiency of the ethanol-fuelled SOFC systems for combined cooling, heat and power generation.

1.3 Scopes of research

1.3.1 To identify the most suitable ethanol reforming process from three different processes, i.e., steam reforming, partial oxidation, and auto-thermal reforming with respect to the first and second laws of thermodynamics.

1.3.2 To investigate the ethanol steam reforming mechanisms and design a two-step steam reforming process for carbon-free hydrogen production.

1.3.3 To perform the enhancement of hydrogen production by using CaO sorbent for CO_2 capture and installing a dehumidifier for steam removal.

1.3.4 To assess the performance of SOFC system integrated with the improved ethanol steam reformer. A thermally auto-sustainable condition and economic issues are also considered.

1.3.5 To design the heat recovery obtained from SOFC exhaust gas by integrating with absorption chiller for combined cooling, heat and power generation.

1.3.6 To analyze the integrated ethanol-fuelled SOFC systems and absorption chiller by using energy, exergy and exergoenvironmental analyses.

1.4 Dissertation overview

This dissertation is divided into nine chapters as follows:

Chapter I describes the background and motivation of this research. The research objectives, scopes of research, research procedures and dissertation overview are also presented.

Chapter II presents literature reviews on the technological developments in ethanol reforming for hydrogen production, with an emphasis on steam reforming, partial oxidation and autothermal reforming processes. The improvements of hydrogen production are present to enhance the hydrogen purification. Research studies on the design and modeling of SOFC are also revealed and the significance of studies in energy and exergy analyses to improve the system efficiency is addressed.

Chapter III presents the main principles of this thesis. The general basic concepts of fuel cells and solid oxide fuel cell (SOFCs) which is the fuel cell type of this interest in this thesis are described. The details of fuel processing for SOFC, the ways to enhance the hydrogen production and absorption chiller are also given.

Chapter IV explains a mathematical model of reforming process, SOFC under isothermal condition and double effect absorption chiller based on the use of H_2O/LiBr as the refrigerant-absorber pair. The simulation models of all main units are validated with the data reported in published literatures.

Chapter V presents the application of a thermodynamic concept to identify a suitable reforming process for an ethanol-fueled solid oxide fuel cell (SOFC). Three

different reforming technologies, i.e., steam reforming, partial oxidation and autothermal reforming, are considered by using energy and exergy analyses to determine an energy demand and to describe how efficiently the energy supplied to the reforming process.

Chapter VI presents the use of a two-step ethanol steam reforming, which consists of ethanol dehydrogenation and steam reforming, as a fuel processor to replace a conventional ethanol steam reforming (single step steam reforming) for carbon-free hydrogen production. The effect of operating conditions on equilibrium compositions, carbon formation boundary, reforming efficiency and process energy consumptions is studied.

Chapter VII presents the effect of removing CO_2 and steam from the reforming gas on the performance of SOFC. The addition of CaO to capture CO_2 and the installation of a dehumidifier to remove steam in the reformer are proposed to improve hydrogen production efficiency. Performance of the steam reformer and SOFC integrated system with and without an enhancement unit is compared and analysed with respect to key operating parameters.

Chapter VIII presents the performance of the SOFC integrated with the two-step steam reforming of ethanol is analyzed under thermally self-sufficient condition. The addition of CaO to capture CO_2 in the reformer is proposed to improve hydrogen production efficiency. The economic analysis is used to point out the benefit of the proposed system.

Chapter IX presents an integrated SOFC system with an absorption chiller that uses heat recovery of the SOFC exhaust gas for combined cooling, heating, and power generation (trigeneration) through energy and exergy analyses. A combined analysis of exergy and environmental impact (through greenhouse gas emissions) of the chilled water production process using the SOFC exhaust heat are also performed under exergoenvironmental analysis.

CHAPTER II

LITERATURE REVIEWS

This chapter aims to review the technological developments in ethanol reforming for hydrogen production, with an emphasis on steam reforming, partial oxidation and autothermal reforming processes. Then, the improvements of hydrogen production are present to enhance the hydrogen purification. Because the purified hydrogen is utilized for solid oxide fuel cell (SOFC) application, research studies on the design and modeling of SOFC are also revealed in this chapter. In the end, energy and exergy analyses to improve the system efficiency is addressed to show the significance of studies.

2.1 Ethanol reforming technologies

Hydrogen is likely to be an important part of a new set of technological requirement that concerns about sustainability and environmental friendliness. Since 1990s, the hypothesis stated that “Hydrogen has been identified as an ideal energy carrier.” leads to a strong interest of international scientific and industrial community towards the possible development of hydrogen production. Although hydrogen is the most common element in the universe, and its molecule has the highest energy content per unit weight of any known fuel, it never occurs by itself on earth, as it always combined with other elements such as oxygen or carbon. Thus, it needs to be produced and for this reason it is not a primary source, but only an energy carrier, which could be used in combination with the efficient device for converting hydrogen into convenient form of electrical energy.

On the advantages of using hydrogen as energy carrier is that all primary resources such as fossil fuels, renewable energy resources (solar, wind, hydro, geothermic, biomass) and nuclear power could be used for its production (Holladay et al., 2009). In particular, it can be extracted from any substance containing hydrogen atoms such as hydrocarbons, water and even some organic matter, etc., with different

production processes, as shown in Figure 2.1. Nowadays almost half of the hydrogen used worldwide comes from steam reforming of natural gas (48%), as it is the most economically competitive method from hydrocarbon feedstock. In Table 2.1, the contributions of different sources to the world hydrogen production capacity reveal that almost 96% of the total production of hydrogen involves fossil fuels (natural gas, refinery oil and coal). However, the use of fossil fuels causes the huge amount of carbon dioxide emission and for secondary energy production this pathway is non-sustainable. As a result, there is a growing interest in the search for effective alternatives to produce renewable hydrogen cleanly and safely.

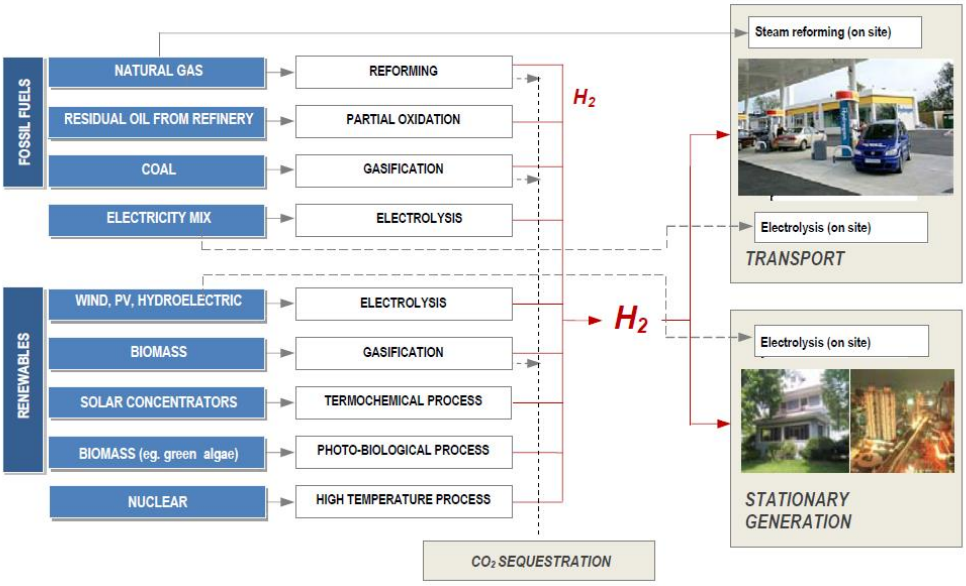

Figure 2.1 Hydrogen production processes (Conte M. et al., 2009).

Table 2.1 Current worldwide hydrogen production from different sources (Chorkendorff and Niemantsverdriet, 2003).

Raw material	Technology	%
Natural gas	Catalytic steam reforming	48
Refinery oil	Partial oxidation	30
Coal	Gasification	18
Water	Electrolysis	4

Among the various feedstocks, ethanol is considered an attractive green fuel because of its relatively high hydrogen content, availability, non-toxicity, ease of storage and handling safety. More importantly, ethanol can be produced renewably by fermentation of various biomass resources, such as agricultural products, energy plants, agro-industrial wastes, forestry residue materials as well as organic fraction of municipal solid waste. Moreover, as biomass removes carbon dioxide from the atmosphere during its growth, when biomass-derived ethanol is reformed, the carbon released back to the atmosphere will be recycled into the next generation of growing plants and not contribute to global warming (Ni et al., 2007a).

Ethanol reforming technologies for hydrogen production can be generally classified into three processes: (1) steam reforming, (2) partial oxidation and (3) autothermal reforming. These thermal processes require the use of thermal energy associated with chemical reactions to obtain directly hydrogen. In steam reforming, ethanol reacts with steam at relatively high energy supply, producing mainly hydrogen and carbon dioxide. In partial oxidation, ethanol reacts with a controlled oxidant mixture (air or/and oxygen) producing the similar product mixtures but providing some exothermic heat. A further method that should be considered as "thermally self-sufficient" is the autothermal technology based on the combination of steam reforming and partial oxidation by involving both steam and oxygen as chemical reagents.

Ethanol steam reforming

Steam reforming was introduced in Germany at the beginning of twentieth century to produce hydrogen for ammonia synthesis, and it was further developed in the 1930s when natural gas and other hydrocarbon feedstocks became available on large scale. After 1908 model T designed by Henry Ford had been driven on alcohol, ethanol began to use in cars. In fact, this story is the origin of greater use of ethanol ever since. In 1991 Garcia and Laborde mentions that if ethanol is used as vehicle fuel, the heterogeneous catalytic process could be an important alternative in order to transform ethanol to hydrogen and fuel cell is an important application for hydrogen generated from ethanol. Their thermodynamic study of ethanol steam reforming was published to

solve the chemical equilibrium of ethanol-water system and analyze the effects of process variables such as temperature, pressure and the water to ethanol feed ratio. The thermodynamic analysis gives fundamental information because the equilibrium conversion will be always the best one, whatever catalyst is used (García and Laborde, 1991). The thermodynamic feasibility of ethanol steam reforming has been re-examined by Vasudeva et al., (1996) under conditions conducive to carbon formation. The findings are compared with the previously published results of Garcia and Laborde (1991). In addition, the computations are extended to high range of operating conditions. Equilibrium hydrogen yields as high as 5.5 moles per mole of ethanol in the feed are obtainable as against the Garcia and Laborde's value of 4.41. The kinetics study of ethanol steam reforming was preliminary investigated by Freni et al., (1996). Their simulation shows the feasibility of steam reforming process at temperature between 800 and 1000 K, and pressures up to 100 bar. In the experimental results, they conclude that the use of a $CuO/ZnO/Al_2O_3$ catalyst exhibits good activity, and no more expensive catalysts are necessary.

These three studies ignite a number of researchers for taking a great effort on the study of ethanol steam reforming. Latterly, it became widely studied both experiments and simulations. Llorca et al., (2002) showed a positive effect of cobalt addition to several oxides in the catalytic studies of ethanol steam reforming. They identified that under 100% ethanol conversion, ZnO-supported samples provided selectivity up to 73.8% to H_2 and 24.2% to CO_2. A new strategy for maximizing the hydrogen production and minimizing the CO formation was proposed by Auprêtre et al., (2002). Their catalytic study suggested that CO_2 and H_2 should be primary products in any highly selective catalytic formulation to avoid using high and low temperature water gas shift units. The catalytic wall reactor which eliminated heat transfer boundary layers by coupling catalytic methane combustion on Pt with catalytic ethanol steam reforming on Rh and Rh-Ce was examined by Wanat et al., (2004). At steam/carbon ratio of 3/1 the reactor gave >99% conversion of ethanol. Morgenstern and Fornango, (2005) presented a now technically attractive pathway to exhibit ethanol steam reforming for low temperature (250-300 C) over their novel copper-nickel catalyst, which retains a Raney-type structure. A lot of studies have also relied on experiments

(Diagne et al., 2002; Srinivas et al., 2003; Fatsikostas and Verykios, 2004; Kaddouri and Mazzocchia, 2004; Aupretre et al., 2005; Biswas and Kunzru, 2007; Casanovas et al., 2010; Nedyalkova et al., 2010; Akiyama et al., 2012; Chen et al., 2012) to investigate the effects of catalysts on the various supports and to identify their optimal conditions. Recently, thermodynamic analysis of ethanol steam reforming has been investigated by many researchers (Hernández and Kafarov, 2009; Lima da Silva et al., 2009; Rossi et al., 2009; Díaz Alvarado and Gracia, 2010). Most researches point to increase hydrogen yield by studying various parameters and finding the suitable operating condition and even catalysts used.

However, one of most interesting topics that most studies reported on is the carbon formation trend. Carbon formation is mainly caused by Boudouard reaction, polymerization of ethylene, or decomposition of methane formed during ethanol steam reforming. Carbon formation is faster when dehydration of ethanol occurs (Ni et al., 2007a). Carbon can destroy catalyst structure and occupy catalyst surface and thus reduce catalyst activity. A complex multiple reaction system of ethanol steam reforming illustrated by Fishtik et al., (2000). They predicted the behavior of the system by selecting a particular set of reactions. The key finding they discovered is that if no additional intermediate species are observed under nonequilibrium condition, the same set of unique overall reactions obtained from chemical thermodynamics. It should be noted that if intermediates are found, they may be the significant species for shifting the reactions to the most desirable way and avoid the carbon formation. For this reason, there are controversial issues concerning the participation of acetaldehyde species as an intermediate that takes part in the reaction mechanism (Frusteri et al., 2004; Benito et al., 2005; Haryanto A. et al., 2005; Ni et al., 2007a). Benito et al., (2005) proposed the simplified reaction scheme of ethanol steam reforming as represented in Figure 2.2. They indicated that the behavior of cobalt catalyst favors dehydrogenation reactions. Ethanol dehydrogenation yields hydrogen and acetaldehyde. Acetaldehyde decomposition leads to methane and carbon monoxide. Methane is reformed with steam in the next reaction step to obtain hydrogen and carbon monoxide. The last reaction step in this proposed mechanism is the water gas shift reaction which produces hydrogen and carbon dioxide. On the other hand, at the beginning if ethanol is

dehydrated to ethylene. Ethylene is easily decomposed to carbon and deposited on the catalyst. Similar to Frusteri et al., (2004)'s work, they investigated the performance of MgO-supported metal catalyst. They found that Rh/MgO was most resistant to coke formation and proposed a reaction mechanism for ethanol steam reforming as show in Figure 2.3.

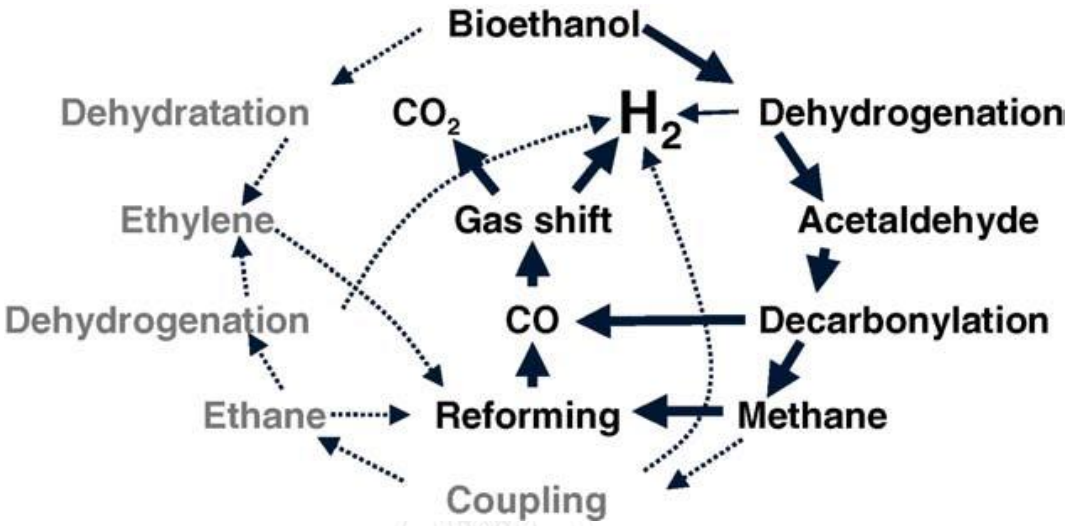

Figure 2.2 Reaction scheme proposed by Benito et al., (2005).

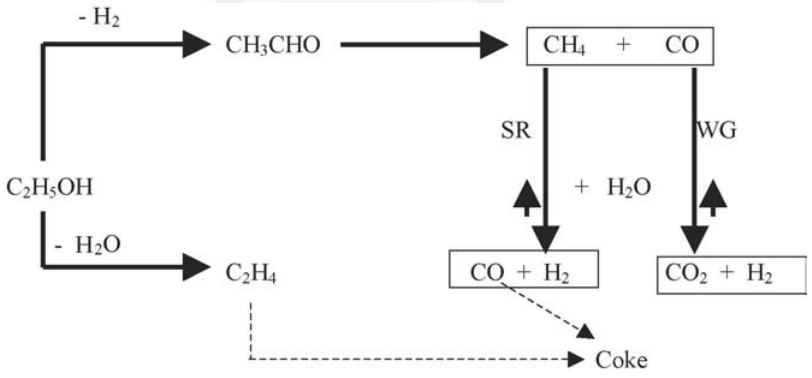

Figure 2.3 Reaction mechanisms for ethanol steam reforming (Frusteri et al., 2004).

Haryanto A. et al., (2005) showed that there are several reaction pathways that could occur in ethanol steam reforming process, depending on the catalysts used (Figure

2.4). They concluded that due to the very complex reactions, it is important to reduce the production of undesirable intermediate compounds. Reactions to avoid are those that lead to ethylene. The present of ethylene especially hinders the overall hydrogen production reaction by inducing the pathways toward carbon formation and thus causing coking of catalysts.

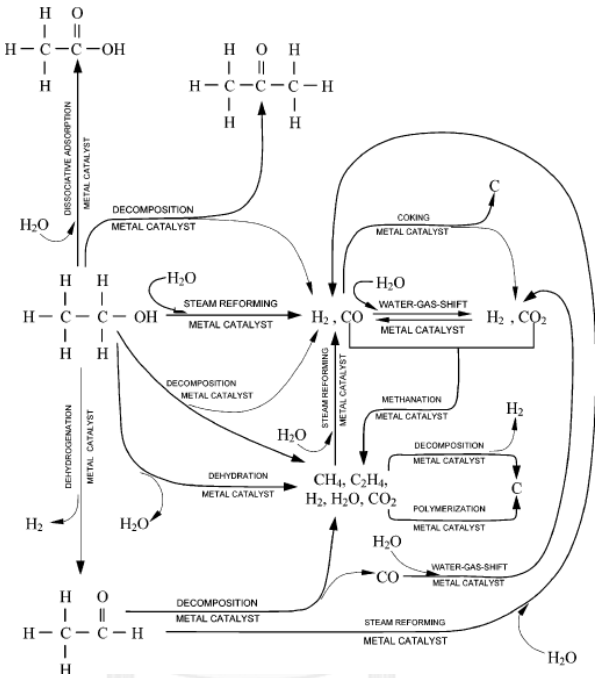

Figure 2.4 Reaction pathways of ethanol steam reforming over metal catalysts (Haryanto A. et al., 2005).

To assure that acetaldehyde is a significant intermediate of ethanol reforming, there are several works focusing on the dehydrogenation reaction of ethanol. Iwasa and Takezawa, (1991) concluded that the dehydrogenation of ethanol to acetaldehyde occurs much more rapidly than its decomposition to ethyl acetate and acetic acid, and it is the intermediate product in the steam reforming environment. Freni S. et al., (2000) studied a two-layer fixed-bed reactor for hydrogen-rich gas production with the first layer composed of a Cu-based catalyst for ethanol dehydrogenation at 370 ˚C and the second one composed of a Ni-based catalyst under steady-state conditions at 650 ˚C. In addition, Nishiguchi et al., (2005) studied steam reforming of ethanol over CuO/CeO_2. They revealed that acetaldehyde and hydrogen are mainly produced at low temperatures

(260 ˚C). In the conclusions of Freni S. et al., (2000) and Ni et al., (2007a), a two-step process of ethanol steam reforming is proposed. To overcome the coking problem by preventing ethylene formation, ethanol passes through the first step at 573-673 K to perform dehydrogenation to acetaldehyde and hydrogen, followed by acetaldehyde steam reforming or decomposition at higher temperature. Experiments of ethanol dehydrogenation were also studied by Deng et al., (1995), Iwasa and Takezawa, (1991) and Lin and Chang, (2004).

Ethanol partial oxidation

Although several studies have been made on steam reforming of ethanol, this process presents some disadvantages, such as energy-consuming and severe catalyst deactivation. On the contrary, partial oxidation process has the merit of fast start up and response time because of the exothermic nature of the oxidation reaction. Furthermore, since this reaction does not need the external addition of heat via a heat exchanger the partial oxidation reactor is more compact than a steam reformer (Mattos and Noronha, 2005a; Mattos and Noronha, 2005b; Silva et al., 2008; Wang and Wang, 2008). A few works have been done concentrated on ethanol reforming by partial oxidation. Christensen et al., (2004) studied the ethanol partial oxidation in a quartz integral reactor at temperatures ranging from 973 K to 1173 K, for different oxygen to ethanol ratios and residence time. Liguras et al., (2004) found that Ru-containing catalysts supported on alumina pellets showed very good catalytic behavior in catalytic partial oxidation process of ethanol. Mattos and Noronha, (2005a) studied the effect of reaction conditions and catalyst reducibility on the performance of the Pt/CeO_2 catalyst in the partial oxidation of ethanol. The Pt/CeO_2 catalyst can perform good stability and activity at 573 K. At higher temperature and higher residence times, the only by-product detected on this catalyst is methane. In another study of Mattos and Noronha, (2005b), they show more information about supported Pt catalysts. The results showed that the support plays an important role in the products distribution of the partial oxidation of ethanol. Methane and acetaldehyde were the products detected on Pt/ZrO_2, Pt/CeO_2 and $Pt/Ce_{0.50}Zr_{0.50}O_2$ catalysts whereas ccetic acid was only the main product on Pt/Al_2O_3 catalyst. Thermodynamic equilibrium is studied by Wang and Wang, (2008) in the wide ranges of operating conditions. and also noted that ethanol dehydration and

decomposition should be minimized. Thermodynamics and kinetics investigations for the thermal partial oxidation of ethanol were performed by Al-Hamamre and Hararah, (2010). In their results, the maximum reforming efficiency can be reached 90% at air ratio of 0.2 and temperature > 1000 K.

Ethanol autothermal reforming

Autothermal reforming is a combination of steam reforming (endothermic) and partial oxidation (exothermic) providing the great advantage of a reasonable compromise between energy supplied to or released from the reaction (Cai et al., 2008). Using ethanol and the mixture of water and oxygen with the molar ratio of 1:1.78:0.61, the overall reaction can be thermally neutral in which the exothermic ethanol partial oxidation provides the heat necessary for the concurrent endothermic ethanol steam reforming (Graschinsky et al., 2012). Therefore autothermal reforming does not require an external heat source resulting in simpler design and higher energy management efficiency (Markova et al., 2009). Moreover, autothermal reforming is suitable for the on-board hydrogen production for portable applications requiring high hydrogen selectivity and rapid response (Chen et al., 2009). With respect to the ethanol autothermal reforming, Casanovas et al., (2010) used the benefit of autothermal reforming process to design a two-side platelet microreactor (Figure 2.5) and tested the hydrogen production from ethanol. They concluded that microreactor technology can be used to generate hydrogen at low temperature (733K) with the overall efficiency of 71% under autothermal regime. Cai et al., (2008) found that the Rh/CeO_2 catalyst was highly active and stable for autothermal reforming of ethanol with a stoichiometric feed composition. Experimental researchs have been conducted by Chen et al., (2009), Chen et al., (2010) and Gutierrez et al., (2011) to study ethanol autothermal reforming on various catalysts. Ethanol autothermal reforming and carbon monoxide removal process is optimized by Markova et al., (2009). The optimization results showed that the maximum hydrogen concentration of 42% and maximum hydrogen yield of 3.8 can be obtained at air-to-fuel combustion ratio of 0.2-0.3, steam-to-carbon feed ratio of 2.5, inlet and average temperatures of reactant are 230 ˚C and 640 ˚C respectively.

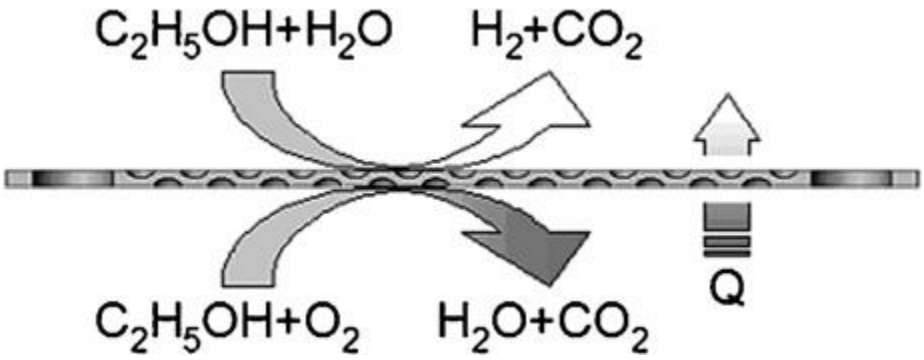

Figure 2.5 Scheme of the interchangeable platelet of the microreactor that allows good heat transfer between the two parts of reactions (Casanovas et al., 2010).

A thermodynamic approach of the autothermal reforming of ethanol was published by Graschinsky et al., (2012). They detailed the study by using the total Gibbs method to estimate product distribution. The results showed that for steam to ethanol ratios higher than 3, hydrogen production reaches a maximum with the temperature but the addition of oxygen reduces hydrogen production. They also concerned about the important phenomenon of carbon formation. Thermodynamic study proves that the addition of water and oxygen reduces carbon formation in all conditions under their study.

As mentioned earlier, each ethanol reforming process has certain advantages and disadvantages. In the past, there are few studies concerning about a comparison of hydrogen production from ethanol using different reforming processes. Rabenstein and Hacker, (2008) investigated the ethanol processing, i.e., steam reforming, partial oxidation and autothermal reforming, and the ranges of optimal operating conditions for each process were given. Based on their results, it is difficult to determine exactly the suitable operational policy of the reforming processes. Furthermore, the process performance in terms of the energy demand was only focused. The thermodynamic analysis of different ethanol reforming processes was also studied by Sun et al., (2012). The optimal conditions for operating the ethanol reformer were proposed. It was found that the partial oxidation of ethanol tends to be the lowest theoretical H_2 yield and highest coke formation so it is not a suitable process for hydrogen production but it is necessary to consider this process when integrated with energy requiring system

because the ethanol partial oxidation produces a maximum heat that may provide the most suitable thermal management.

Until now, for the in situ ethanol reforming to supply hydrogen for fuel cell, three aspects must be questioned: first, how can produce hydrogen in carbon free condition? Second, what is the most suitable ethanol reforming process for fuel cell application? And third, is there possible to find the new analysis tool to identify the most suitable ethanol reforming process?

2.2 Improvement of hydrogen production

There is no doubt that hydrogen powered vehicles are the way forward if the world is serious about reducing damage to the environment, but at present there are still huge barriers to overcome in order to make any significant improvement of hydrogen production. Current methods of ethanol reforming first yield hydrogen combined with carbon dioxide, or hydrogen combined with carbon dioxide and methane. Therefore, hydrogen needs to be purified before it can be used as fuel for fuel cells. To this aim, different forms of in situ separation obtained by removing either hydrogen or CO_2 have been widely reported in the literatures.

Common technologies employed for hydrogen separation and purification include partial condensation, absorption, adsorption, permeation through membranes, and chemical reaction as shown in Table 2.2, various processes to separate and purify hydrogen are based on physical or chemical principles. In practical operations, some of these processes are employed according to its intended application. However, there are two aspects of importance to be considered in selecting a purification method. The first is its ability to cope with a range of gas feedstocks in term of hydrogen content and the second concerns that the limitation of impurities in the gas feed.

All techniques can operate well with hydrogen-rich gas feedstocks. Partial condensation can tolerate a wider range of hydrogen content, typically 30 to 90 %, but is limited in gas composition that may selectively condense at very low temperatures. Although the partial condensation of hydrogen is not so popular these days, it has been mainly used for recovery of hydrogen from petrochemical off-gases. These gases are

compressed and cryogenically cooled in order to condense the hydrocarbon compositions.

Various absorption processes using solvents or solutions have been under industrial operation for many years. The absorption processes are roughly classified into physical ones that utilized the differences in solubility between hydrogen and other components, and chemical ones based on chemical reactions between impurity components and the absorbent. The equipment consists of an absorption column where soluble components are trapped in an absorbent at a higher pressure or a lower temperature, followed by a regeneration column where the absorbed components are released at a lower pressure or a higher temperature. The absorbent is circulated between the two columns.

The most well-known adsorption technology is pressure swing adsorption (PSA). Its operation is based on a physical binding of gas molecules to adsorbent material. Specific adsorptive materials (e.g., activated carbon, zeolites, molecular sieves, etc.) are used as a trap, preferentially adsorbing the target gas species at high pressure. The process then swings to low pressure to desorb the adsorbed material.

Metal hydride separation and the two diffusion techniques, polymer membrane and palladium membrane, have the ability to deal with feed gases lean in hydrogen. The hydride separation and palladium diffusion techniques are based on the very selective adsorption and diffusion of hydrogen, respectively, and the purity of output hydrogen is not affected by the leanness of the gas feed. However, polymer membrane diffusion is based on a differential diffusion rate principle and purity of the output hydrogen will be affected by the hydrogen concentration and by the nature of the other impurities in the input gas stream.

By considering hydrogen production from ethanol, two techniques are actually utilized over this whole range of capability, namely membrane separation technology and chemical absorption of alkaline carbonates which is known as “Sorption-enhanced steam reforming technology”. Compared with another method, membrane techniques have economic potential in reducing operating costs, minimizing unit operations and

lowering energy consumption (Paglieri and Way, 2002). There have been many applications of palladium (Pd) in membrane reactors involving ethanol reforming for hydrogen production such as composite Pd supported on porous stainless steel (Basile et al., 2011; Seelam et al., 2012), coupled with proton exchange membrane fuel cell (PEMFC) for automobile applications (Song et al., 2005; De Falco, 2011), the comparison of the membrane reactor with a traditional reactor (Gallucci et al., 2008b; Manzolini and Tosti, 2008; Yu et al., 2009), the study of co-current and counter-current configurations (Gallucci et al., 2008a), low temperature steam reforming of ethanol (Tosti et al., 2008a; Tosti et al., 2008b), the effects of pressure (Tosti et al., 2011) and correlations in palladium membranes have been reviewed by Yun and Ted Oyama, (2011).

Table 2. 2 Performance characteristics of typical processes for purifying hydrogen (Grashoff et al., 1983)

Methods	Means Media	Operating conditions		Hydrogen concentration		Hydrogen recovery (%)	Typical process (Impurities)
		Pressure (KPa)	Temperature (K)	Feed (%)	Product (%)		
Partial Condensation	Cooling agents	2-5	90	30-90	90-98	95	H_2 recovery
Physical Absorption	Organic solvents	1-15	RT*	60-90	80-95	90-95	H_2 recovery
Chemical Absorption	Alkaline carbonates	0.5-3	330-380	< 85	98	> 95	CO_2 removal
	Amine solutions	0.3-2	> RT	< 85	98	> 95	CO_2 removal
Adsorption	Adsorbents	> 0.1	< RT	< 99.9	> 99.99	> 95	H_2O removal
	Adsorbents Liquid Nitrogen	> 0.5	80	< 99.999	> 99.9999	> 95	Final purification
Pressure swing adsorption	Adsorbents	2-15	RT	60-90	> 99.9	70-90	H_2 recovery
	Adsorbents	1-4	RT	50-80	< 99.999	70-85	H_2 production
Polymer Membrane	Polyamide Polysulfone	2-20	273-373	70-95	85-99	85-95	H_2 recovery
Palladium Membrane	Pd-Ag alloys	< 2	573-723	> 98	99.9999	< 90	H_2 purification
Metal hydride	$LaNi_5$-based alloy	< 4	> RT	< 60	99	> 90	H_2 recovery
	$LaNi_5$-based alloy	< 1	> RT	> 95.5	> 99.5	> 90	H_2 purification

* RT is room temperature.

Sorption-enhanced steam reforming technology

Sorption-enhanced steam reforming is a new field of research for to develop steam reforming process with in situ CO_2 separation. Solid sorbent is added to the reactor and then converts CO_2 into a solid carbonate as soon as it is formed. Calcium oxide has been investigated thoroughly as a suitable sorbent for SERP processes (Abanades, 2002; Feng B. et al., 2007; Sakadjian B.B. et al., 2007) and is believed to be thermodynamically the best candidate among metal oxides for CO_2 capture in zero emission power generation systems (Abanades, 2002). Rostrup-Nielsen, (1984) reported that the first description of the addition of a CO_2 sorbent to a hydrocarbon steam reforming reactor was published in 1868. The several studies of the Sorption-enhanced are widely demonstrated in steam methane reforming process including stabilization of cyclic capacity (Cobden et al., 2009), technical and economic study of system integrated with solid oxide fuel cell (Piroonlerkgul et al., 2010) ,the performance study of lithium carbonate doped CaO properties (Derevschikov et al., 2011), reaction kinetics and sorbent capacity of CO_2 adsorbent (Halabi et al., 2012), the comparative exergy analysis of sorption enhanced and a conventional methane steam reforming (Tzanetis et al., 2012) and the studies in a fluidized bed reactor (Johnsen et al., 2006; Chen et al., 2013b). A novel hybrid material for reforming catalyst and CO_2 sorbent is developed by Martavaltzi and Lemonidou, (2010) and operational window as well as efficiency penalty in sorption-enhanced steam methane reforming is performed by (Solieman et al., 2009). Moreover, there is some research studied sorption-enhanced steam reforming of other substances such as bio-oil/biogas mixture (Iordanidis et al., 2006), hydroxyacetone (Fu et al., 2013), glycerol (Fermoso et al., 2012; Dou et al., 2013), and oxygenated hydrocarbons (Lima da Silva and Müller, 2011).

In ethanol reforming process, ethanol is almost totally reformed but the primary products involving CH_4 and CO are limited by equilibrium reactions of methane steam reforming and water gas shift. From the concept of sorption-enhanced reforming, if the CO_2 can be removed from the gas as it is formed, the normal equilibrium limits are displaced and complete conversion can be closely approached.

Comas et al., (2004) compared ethanol steam reforming process with and without the presence of CaO as a CO_2 sorbent. Potential advantages of the presence of

CaO as CO_2 sorbent include higher energy efficiency, higher hydrogen production and lower CO content in the reformer gas exit. The presence of CaO eliminates the need of a WGS reactor for PEMFC application. Favorable operation conditions in the presence of CaO are (1) atmospheric pressure, (2) reactor temperatures around 700 ◦C, and (3) water/ethanol molar ratio of 4.

The analysis using ASPEN PLUS software was done by Mahishi et al., (2008) and the Gibbs energy minimization approach was followed. The effects of temperature, pressure, steam/ethanol ratio, and CaO/ethanol ratio on product yield were investigated. The case studies were conducted to understand the effect of sorbent addition on the hydrogen yield. Thermodynamic studies showed that the use of sorbents has the potential to enhance the equilibrium hydrogen yield and reduce the equilibrium CO_2 content of product gas by 50.2%. Sorbent-enhanced gasification is a promising technology with a potential to improve the yield and lower the cost of hydrogen production so it tends to be usable for the ethanol reforming process.

Thermodynamic analysis of steam reforming of different oxygenated hydrocarbons (ethanol, glycerol, n-butanol and methanol) with and without CaO as CO_2 sorbent was carried out by Lima da Silva and Müller, (2011). The results indicated that the sorption enhanced steam reforming is a fuel flexible and effective process to produce high-purity H_2 with low contents of other compositions in the temperature range of 723-873 K. For all the oxygenated hydrocarbons investigated in this work, thermodynamic study predicted that high-purity hydrogen with CO content within 20 ppm required for proton exchange membrane fuel cell applications can be directly produced by a single-step sorption-enhances ethanol steam reforming process in the temperature range of 723-773 K at pressures of 3-5 atm. Thus, further processes involving water-gas shift and preferential CO oxidation reactors are not necessary.

Saebea et al., (2011) applied an adsorption-membrane hybrid system in which a carbon dioxide adsorbent is used to remove undesired carbon dioxide and a membrane to improve the performance of an ethanol steam reforming. It was found the boundary of carbon formation is likely to decrease when carbon dioxide adsorption is considered. The use of the adsorption-membrane hybrid system in ethanol steam reforming process does not only provide the highest hydrogen yield but also obtain pure hydrogen product.

CuMgAl based materials was employed by Cunha et al., (2013) to be the ensemble of catalyst and adsorbent for reaction enhancement of catalytic steam reforming of ethanol. It was experimentally proved that hydrogen was generated in the temperature range between 473 K and 873 K and these materials have s similar CO_2 adsorption capacity as pure hydrotalcites at 673 K.

Wu et al., (2013) used the NiMgAl multifunctional materials to perform sorption-enhances steam reforming of ethanol on their experimental and numerical work. The kinetic results obtained that the support material with nickel impregnation has a similar CO_2 adsorption capacity as pure hydrotalcites. To achieve the highest possible enhancing performance, the reaction conditions were found as steam-to-ethanol molar ratio of 10, weight of active metal per ethanol molar flow rate in the feed of 0.25 kg h/mol at temperature of 773 K. It was also found that the use of a CO_2 adsorbent can improve the yield of H_2 and the thermal efficiency.

2.3 Solid Oxide Fuel Cell (SOFC)

There have been several publications focusing on the performance of solid oxide fuel cell. Among various papers, three approaches are presented, i.e., 1) design of solid oxide fuel cell stack to avoid the possible problems of practical operations and improve the efficiency of system to reach the maximum, 2) solid oxide fuel cell modeling by using mathematical solver or process simulator investigated the internal processes inside the cell including the electrochemical reactions in the catalyst layers, the ion transfer in the electrolyte layer and mass and heat transport within all regions and 3) the abilities of solid oxide fuel cell integrated systems for various applications.

2.3.1 SOFC Design

Recently, there have been several publications focusing on designing of SOFCs. Such designs can be for different geometries (planar, tubular, or monolithic), flow configurations (co-, cross-, or counter-flow), support structures (anode-, cathode-, or electrolyte-support), ion-conducting electrolytes (proton-, or oxygen-conductor), temperatures (low-, intermediate-, or high-temperature SOFC), materials and their

applications. These common designs have been studied both experimentally and computationally in literatures.

The cell geometries of SOFC can be developed into planar, tubular and monolithic configurations. One of these configurations, the planar type design has received much attention recently (Tseronis et al., 2012; Chen et al., 2013a; Dey et al., 2013; He et al., 2013; Yan et al., 2013), because it is simpler to fabricate and easier to be made into various shapes than the other type designs. Besides, the planar type SOFC offers higher power density relative to the tubular type SOFC, which is ascribed to the low electrical resistance due to shorter current paths and lower ohmic loss (Tanim et al., 2014). A typical planar SOFC is analyzed by Tseronis et al., (2012) in parametric and transient studies for non-isothermal conditions. However, the interest in tubular cells is unique to SOFC: sealing around cell edges and controlling temperature gradients are among the major issues to be resolved in planar SOFCs. In SOFC, the benefit of a simple sealing arrangement potentially outweighs the disadvantages of low volumetric power density and long current path that are inherent in tubular cell geometries. A numerical model to simulate the effect of combustion zone geometry on the steady state and transient performance of a tubular solid oxide fuel cell (SOFC) has been developed by Jia et al., (2007). The simulations predicted that increasing the length of the combustion zone would lead to an increase of the overall cell tube temperature and a shorter response time for transient performance. Enlarging the combustion zone, however, makes only a negligible contribution to electricity output properties, such as output voltage and power. These numerical results show that the developed model can reasonably simulate the performance properties of a tubular SOFC and is applicable to cell stack design. The flat-tube SOFC (FT-SOFC) exhibits the advantages of ease in sealing, low stack volume and low current-collecting resistance. However, due to its weak strength, the FT-SOFC may get deformed or break during the manufacturing process. To improve the cell strength, the cell support must be thickened. However, as the support thickness is increased, the electrons must travel a longer distance, which leads to an increase in the electrical resistance. In another method, the hydrogen channel diameter can be reduced for the strong strength. But, it may lead to a corresponding decrease in the hydrogen mass transfer rate. Although in

manuscript of Park et al., (2012) study the performance of several FT-SOFC designs and suggest the better design of tubular, planar design has an advanced benefit.

The effects of flow configurations are investigated by Aguiar et al., (2004) and Sohn et al., (2010). Aguiar et al., (2004) studied the planar-SOFC system behavior under co and counter-flow operations. The results showed that the co-flow configuration is better than the counter-flow because the counter-flow leads to steep temperature gradients with a consequent uneven current density distribution. However, a two-dimensional micro/macro scale model as an efficient numerical framework for simulating intermediate temperature solid oxide fuel cells (IT-SOFCs) proposed by Sohn et al., (2010) showed that the counter-flow configuration was higher performance than the co-flow configuration. But the co-flow configuration had a more uniform current density distribution than the counter-flow configuration. In addition, the co-flow configuration exhibited more uniform temperature distribution, which is advantageous to long-term of IT-SOFC performance and durability. The concept of a single-chamber solid-oxide fuel cell (SC-SOFC) has been proposed by Wang et al., (2008) due to large internal stress during the heating and cooling processes resulting from the thermal expansion mismatch between cell components and sealant. The fuel cell envisaged not only an increase of the peak power density to ~200 $mWcm^{-2}$ but also a significant improvement of the anodic coking resistance. Wang et al., (2011) also proposed the single-chamber solid oxide fuel cell (SC-SOFC) with a right-angular configuration. It is shown that the cell exhibits the smallest ohmic resistance when the two electrodes are symmetrically located on the two planes. Compared with the conventional coplanar SC-SOFC, this configuration can make full use of the edge area of the electrolyte substrate and shorten the conductive channel of oxygen ion, leading to a remarkable reduction in ohmic resistance, an elevation of the open-circuit voltage, and, ultimately, an improved performance.

Different support structures (anode-, cathode-, or electrolyte-support) in planar SOFC affect on the performance. So Patcharavorachot et al., (2008) presented a performance analysis of a planar solid oxide fuel cell (SOFC) with different support structures. An electrochemical model, taking into account structural and operational

parameters and gas diffusion at the electrodes, is used to analyze the characteristics of the planar SOFC. Analysis of individual cell voltage loss indicates that ohmic loss dominates the performance of an electrolyte-supported SOFC whereas activation and ohmic overpotentials constitute the major loss in an electrode-supported counterpart. Sensitivity analyses of the anode-supported SOFC show that decreasing the electrolyte and anode thickness can improve cell performance. A decrease in operating temperature causes the cell to operate at a lower range of current density due to an increase in ohmic and activation overpotentials. Further, increasing the operating pressure and degree of pre-reforming reduces the concentration overpotential and thereby enhances cell performance. Chan et al., (2001) also shows the performance of an anode-supported cell is superior to that of an electrolyte-supported cell or a cathode-supported cell for the same materials used, same electrode kinetics and same operational constraints. When all three components are of the same thickness, the sensitivity of cell voltage due to the change of electrolyte thickness is the highest, then sensitivity of cell voltage due to the change of cathode thickness and finally the sensitivity of cell voltage due to the change of anode thickness. Reducing all three component thicknesses causes, in general, reduced sensitivity strength with an improved operating current density range.

Solid electrolytes of SOFCs can be divided into two types, namely oxygen ion-conducting (SOFC-O^{2-}) and proton-conducting electrolytes (SOFC-H^{+}). Obviously, most SOFC studies have employed oxygen ion-conducting electrolytes although proton-conducting electrolytes are also applied in SOFC. The performance of ethanol-fuelled solid oxide fuel cells (SOFCs) with two types of electrolytes was investigated by Jamsak et al., (2007). When all resistances are taken into account, the actual performance of the SOFC-O^{2-} becomes significantly better than that of SOFC-H^{+}. The maximum power density of the SOFC-O^{2-} is about 34 times higher than that of SOFC-H^{+}. However, there are a few studies on the development of proton- and mixed ions conducting electrolytes (Fan et al., 2011; Bertei et al., 2012; Zhao et al., 2012). Fan et al., (2011) measured electrochemical impedance spectroscopy of the samaria doped ceria-carbonate (SCC) and found that mixed H^{+}/O^{2-} conduction improves the effective ionic conductivity of composite electrolyte.

Conventional SOFCs operated at high temperature around 1000 ˚C to achieve maximum ionic conductivity of electrolytes. However, such a severe condition poses some disadvantages on commercialization, e.g. expensive material, thermal stress, long start-up and shut down time and high running cost (Zhao et al., 2013). Therefore, lower temperature-SOFCs also known as intermediate temperature SOFCs have attracted an increasing interest in recent years. Zhu, (2001) presented the several advantages of intermediate temperature SOFCs for stationary and vehicle applications. The materials for intermediate-to-low temperature operation have been developed by Mat et al., (2007), Gao et al., (2010), Suzuki et al., (2011), Fan et al., (2011), Huang et al., (2011), Huang et al., (2012), Qin et al., (2012).

More recently, SOFCs have a wide variety of applications from use as auxiliary power units in vehicles (Zhu, 2001; Brett et al., 2006a; Brett et al., 2006b; Baniasadi and Dincer, 2011; Tanim et al., 2014), for marine applications (Tse et al., 2011), residential applications (Braun et al., 2006; Fujita et al., 2012) and for combine cooling, heating and power generation (Al-Sulaiman et al., 2010a; Yu et al., 2010; Ma et al., 2011; Al-Qattan et al., 2014).

2.3.2 SOFC modeling

Mathematical models are essential tool for design and selecting the optimum operating conditions of SOFC and for studying and development the performance of SOFC. In general, the modeling of SOFC consists of an electrochemical model and mass and energy balances. A great number of researchers had investigated in the development of mathematical models SOFC in various aspects.

An electrochemical model has been developed to describe multiple phenomena contributed to irreversible losses in an actual fuel cell. The losses, which are called polarization, overpotential, or overvoltage in the SOFC caused by three main sources: 1) activation polarization; 2) ohmic polarization; and 3) concentration polarization. Electrochemical models of solid oxide fuel cells are studied by Virkar et al., (2000), Chan et al., (2001), Suwanwarangkul et al., (2003), Zhu and Kee, (2003), Costamagna

et al., (2004), Aguiar et al., (2004), Noren and Hoffman, (2005), Sánchez et al., (2006), (Patcharavorachot et al., 2008), Hofmann and Panopoulos, (2010), Lo Faro et al., (2011), Park and Bae, (2012), Pirkandi et al., (2012), Kromp et al., (2013). Chan et al., (2001) presented a complete polarization model of a solid oxide fuel cell (SOFC) that eliminates the ambiguity of the suitability of such model when used under different design and operating conditions. The Butler-Volmer equation is used in the model to describe the activation overpotential instead of using simplified expressions such as the Tafel equation and the linear current potential equation. The detailed Butler-Volmer equation was also discussed by Noren and Hoffman, (2005). They focused on the importance of including the activation losses in a model designed to accurately predict the voltage–current relationship of a modern solid oxide fuel cell. To predict the concentration overpotential, both ordinary and Knudsen diffusions are considered by Chan et al., (2001) to cater for different porous electrode designs. And Suwanwarangkul et al., (2003) developed models for mass transport inside a porous SOFC anode based on Fick's model (FM), the dusty-gas model (DGM) and the Stefan–Maxwell model (SMM) to show the effect of pore size on all model predictions. They concluded that the dusty-gas model is the most appropriate model to simulate gas transport phenomena inside a SOFC anode. However, this model requires numerical solution, whereas Fick's and Stefan–Maxwell's do not. It was found that the SMM, rather than the FM, is a good approximation of the dusty-gas model for H_2–H_2O system, except in the case of high current density, low H_2 concentration and low porosity, where only the DGM is recommended. For the CO–CO_2 system, there is no simple rule for selecting an alternate model to DGM. Depending on the CO concentration, porosity and current density, the FM or the SMM could be used. The only restriction is for small porosities where only the DGM should be used. Their work also demonstrated that only the DGM is recommended for a multicomponent system (H_2–H_2O–CO–CO_2). Moreover, activation and concentration polarization effects in anode-supported solid oxide fuel cells (SOFC) were examined by Virkar et al., (2000) in term of the role of electrode microstructure. In Zhu and Kee, (2003)'s work, concentration overpotentials are based on a dusty-gas representation of transport through porous electrodes.

Mass transport phenomena taking place in solid oxide fuel cells are modeled and discussed by Tseronis et al., (2008), Bertei et al., (2012), Novaresio et al., (2012) and Wang et al., (2012). Tseronis et al., (2008) used the dusty-gas model to predict species composition profiles with more realistic operating conditions. Mathematical models of mass and charge transport have been described by Bertei et al., (2012). Their design analysis allowed the identification of how geometrical and morphological parameters affect the cell performance. Novaresio et al., (2012) revealed the open-source library for the numerical modeling of mass transfer in solid oxide fuel cells which is essential for the design and optimization of this technology. The performance of three different types of models, the dusty-gas model, the binary-friction model and the cylindrical pore interpolation model, were compared by Wang et al., (2012). However, they concluded that all three models gave a similar performance in term of predicting the concentration overpotential and fuel composition profiles for different cases. A lot of investigations have been also presented in order to simulate the heat transfer within SOFCs. The full and steady-state heat transfer equations were analytically solved by Coutelieris et al., (2005) for both solid and gas phase with appropriate boundary conditions. They obtained analytical expressions for the local and the overall heat transfer coefficients. Transient heat transfer models were presented by Colpan et al., (2011). Their successful model of a planar solid oxide fuel cell operated with humidified hydrogen was used to simulate at the heat-up and start-up states. Amiri et al., (2013) detailed a mathematical model the account for mass, momentum, heat, and electrical charge transfer for a tubular micro-solid oxide fuel cell.

The models that include mass and energy balances and an electrochemical model have been used to study the complicated interactions between the various phenomena occurring inside the cell and to optimize the system performance. For complete work, Aguiar et al., (2004) developed a model predicted the SOFC characteristics both in the steady and the transient states. It consisted of mass and energy balances, and an electrochemical model. For the mass balance the molar flux in the gas channels was considered convective in the flow direction. It was assumed that only hydrogen was electrochemically oxidized and that all of CO was converted through the shift reaction, considered to be at equilibrium. In the fuel channel, three reactions are

taken into account: 1) methane steam reforming; 2) water gas-shift; and 3) hydrogen electrochemical oxidation. In the air channel, only the reduction reaction of O_2 was considered. Faraday's law related the flux of reactants and products to the electric current arising from an electrochemical reaction. In the energy balance were included the released heat from electrochemical reactions and ohmic losses; the convective heat transfer between cell components and gas streams; and the in-plane heat conduction through cell components. The thermal fluxes were supposed to be conductive and radiate between the PEN and the interconnect components. However, in the gas channels, they were assumed to be convective in the gas flow direction and from the gas channels to the solid parts. In the electrochemical model the OCV was calculated by the Nernst equation and the SOFC stack was considered isopotential.

2.3.3 SOFC system

Solid oxide fuel cells are considered as one of the most promising technology characterized by a high efficiency, low CO_2 emissions, and high flexibility in term of fuels and installation requirements; however, this technology is too expensive to stand alone. The challenges for the commercialization are to reduce cost and increase the reliability of the system. And then the challenges extend to the integration of SOFC system for more applications.

The high temperature exhaust gas from SOFC can be utilized in energy requiring units like preheaters and reformers and in even other cycles i.e. Rangkine, Brayton for additional power generation. The simulation and heat integration of a solid oxide fuel cell (SOFC) integrated with an ethanol steam reforming system was carried out by Arteaga-Perez et al., (2009). Two heat exchanger networks were designed being demonstrated that when the fuel utilization coefficient in the SOFC is 80%, the reforming reactor temperature 823 K and the ethanol to water molar ratio 1:5.5 the auto-sustainability condition is reached. It was also demonstrated that an efficient ethanol processor not only depends on the reaction but also depends on well designed heat exchanger network and process integration. On the Brayton cycle operation, gas turbine power plant suffers from low efficiencies. To improve system efficiencies and economics, the SOFC is proposed for integration into gas turbine power plant (Cheddie,

2011). The integration of SOFC technology with turbine cycles has been also analyzed by many researchers. For examples, Zhang et al., (2011) discussed the effects of some key irreversibilities existing in the fuel cell and gas turbine such as electrochemical reactions, electronic/ionic resistances in the fuel cell, heat leakage from the fuel cell, finite-rate heat transfer, and irreversibilities adiabatic processes in the gas turbine on the performance of the hybrid system. System layouts for integrated gasification solid oxide fuel cell/gas turbine systems were performed by Park et al., (2011) with carbon dioxide capture. The results shows that the oxy-combustion technology provided much higher efficiency that the pre-combustion. The solid oxide fuel cell and micro gas turbine system were analyzed by Sanaye and Katebi, (2014) in energy, exergy, economic and environmental aspects. Moreover, the exergy analysis of the integration of SOFC technology with gas turbine has been also studies by Calise et al., (2006), Haseli et al., (2008), Stamatis A. et al., (2012) and (Ishak et al., 2012).

Cogeneration or Combined Heat and Power (CHP) are defined as the use of a heat engine or power station to generate electricity and useful heat at the same time. While trigeneration or Combined Cooling Heat and Power (CCHP) refers to the simultaneous generation of electricity and useful heating and cooling. An absorption chiller is a closed loop cycle that uses waste heat to provide cooling or refrigeration (Somers et al., 2011), which has attracted increased interest throughout the world because of its advantages over other vapor-compression refrigeration systems, including its quiet operation, high reliability, and long service life (Dincer and Rosen, 2013). To date, the use of absorption chillers has been limited by their relatively poor efficiency at delivering cooling compared to vapor compression cycles. However, absorption chillers are still widely used because they can utilize low temperature (<100 $^{\circ}$C) heat to provide cooling (Somers et al., 2011). Thus, in processes where low temperature waste heat is available and cooling is desired, it is often beneficial to implement an absorption chiller to increase the overall energy efficiency of the process (Maidment et al., 1999; Moné et al., 2001). There are few existing studies which examine the feasibility of using absorption chillers based on SOFCs for trigeneration plants. Tse et al., (2011) investigated the feasibility of combining a SOFC-gas turbine system and a double effect absorption chiller in a trigeneration system to drive the

heating ventilation and air conditioning (HVAC) and electrical base-load system. They found that the net electric power increases by 47% relative to the electrical power available for a conventional SOFC-gas turbine –HVAC system. A total energy system integrating the SOFC with the absorption chiller has been developed by Yu et al., (2010) and simulated by using a program based on MATLAB soft package. The program is divided into three modules based on the modular programming principle: SOFC module, exhaust combusting and reactant preheating module, and the absorption chiller module. The results show that the cooling efficiency increased when the current density is increased, while the electrical efficiency and total efficiency decreased at the same conditions. The electrical efficiency and total efficiency have a maximum value, whereas the cooling efficiency gets a minimum value at fuel utilization of 0.85 with variation of the fuel utilization factor. A more detailed integrated trigeneration system incorporating a solid oxide fuel cell (SOFC) and a double-effect water/Lithium Bromide absorption chiller with a typical gas produced from a gasification process has been presented by Yu et al., (2011). This study mainly focused on the effect of several parameters: the fuel utilization ratio, fuel flow ratio and air inlet temperature. The results also showed that the proposed tri-generation can achieve a combined cooling and power efficiency of 89% or a combined heating and power efficiency of approximately 84%.

According to the use of ethanol as fuel in SOFCs, the integration of traditional technology of sugar production, ethanol and bagasse cogeneration with a SOFC has been studied by (Casas et al., 2011). The results demonstrated that the system is likely to be environmental friendliness with respect to greenhouse gas emission, renewability and exergy efficiency. From these results, it may bring forward in economic and social impacts.

2.4 Energy and exergy analyses

The existent studies that rely on the energy and exergy analyses of fuel processors, solid oxide fuel cells, and their integrated system are reviewed in this section. Douvartzides et al., (2004a) analyzed the effect of the reforming factor on the optimum exergetic efficiency for a solid oxide fuel cell (SOFC) power plant involving

external ethanol steam reforming. They found that the exergy destruction rate is maximized in unit operation which conducts combustion process as the afterburner. The study on ethanol fueled proton exchange membrane fuel cell for automobile applications was integrated by Song et al., (2005). They concluded that the utilization of excess steam results in an increase of the overall exergy destruction and lowering to the plant efficiency. Recently, a more detailed mathematical model was reported by Casas et al., (2010). They developed an energy-exergy analysis in order to optimize the operating parameters of a SOFC power plant and suggested that the efficient use of wasted heat by the cell in a combined cycle can reduce the irreversibilities in the system as well as the energy and exergy efficiencies. Because the use of too high temperature of SOFC exhaust gas for a refrigeration cooling system may led to the main causes of irreversibility, in this regard, an exergy analysis reveals minimizing thermodynamic inefficiency through energy systems. It is well known that different energy has different energy quality and it is important to efficiently and scientifically dispatch the energy among multiple products of cooling, heating, and power. However, exergy analysis cannot completely solve the energy matching problem between supply and demand (Gao et al., 2015). Thermodynamically, developing energy and exergy strategies to provide guidelines are needed for more effective use of exhaust heat for this combined cycle. At present, considerable efforts are devoted to develop SOFC-trigeneration system by applying energy and/or exergy analysis. Al-Sulaiman F.A. et al., (2011) demonstrated an energetic performance comparison of three trigeneration systems: SOFC-trigeneration, biomass-trigeneration, and solar-trigeneration systems. The comparative study showed that the SOFC-trigeneration system exhibited the highest electrical efficiency among the three systems. Al-Sulaiman et al., (2010a) also conducted an energy analysis of a trigeneration plant based on an SOFC and an Organic Rangkine Cycle (ORC) in another. The study revealed that there was at least a 22% gain in efficiency when a trigeneration system was used compared to only the power system. The study also determined that the efficiency of the SOFC decreased as the current density increased. However, the change in the current density of the SOFC had a negligible effect on the trigeneration efficiency, whereas increasing the SOFC inlet flow temperature afforded significantly improved trigeneration efficiency. A comprehensive exergy analysis of a trigeneration plant based on an SOFC and an ORC

was also performed by Al-Sulaiman et al., (2010b) The study revealed that the operating condition increased the gain in the exergy efficiency when trigeneration was used compared to a power cycle alone from 3 to 25%. In addition, it was shown that the most significant sources of exergy destruction rates are the ORC evaporator, air heat exchanger at the SOFC inlet and the heating process heat exchanger. Therefore, further improvements in designing these three components are needed.

CHAPTER III

THEORY

This chapter presents the main principles of this thesis. There are as follows: firstly, presenting the description general basic concepts of fuel cells, such as principle, type of fuel cell in section 3.1; secondly, presenting the details of solid oxide fuel cell (SOFCs) which is the fuel cell type of this interest in this thesis in section 3.2; thirdly, Ethanol reforming for SOFC by describing each reforming process and the development of the hydrogen product through sorption-enhanced steam reforming and reformate gas dehumidification technology in section 3.3; finally, principle of SOFC integrated system for combined cooling, heat and power generation in section 3.4.

3.1 Fuel Cells

3.1.1 Principle of fuel cells

Fuel cells are electrochemical devices that convert chemical energy in fuels into electrical energy directly without the intermediate steps of producing mechanical work. The interest in fuel cells has increased during the past decade due to the fact that the use of fossil fuels for power has resulted in many negative consequences such as severe pollution, extensive mining of the world's resources, and political control and domination of countries that have extensive resources. Because combustion is avoided, fuel cells produce power with minimal pollutant and they have the ability to fulfill all of the global power needs while meeting the efficacy since fuel cells are not limited by thermodynamic limitations of heat engines such as the Carnot efficiency (EG&G Technical Services, 2004). In 1839, William Grove discovered the basic operating principle of fuel cells by reversing water electrolysis to generate electricity from hydrogen and oxygen. The principle that he discovered remains unchanged today while fuel cells are now closer to commercialization than ever.

3.1.2 Types of fuel cell and applications

A variety of fuel cells are classified by the type of electrolyte used in the cells and the choice of electrolyte dictates the operating temperature range of the fuel cell representing the physicochemical and thermo-mechanical properties of materials used in the cell components (i.e., electrodes, electrolyte, interconnect, current collector, etc.). The operating temperature also plays an important role in dictating the degree of fuel processing required. Table 3.1 provides an overview of the key characteristics of the main fuel cell types.

3.2 Solid oxide fuel cell (SOFC)

3.2.1 SOFC features

Solid oxide fuel cell (SOFC) has all-solid-state construction which has a three-layer sandwich structure: two porous electrode; anode and cathode, serving as the chemical reaction, and the electrolyte, serving a three-diffusion layer of oxygen ions but electrically nonconductive. Along with high operating temperatures, SOFC offers several advantages over the other types of fuel cell as follows:

- Because the electrolyte is solid, the cell can be cast into various shapes, such as tubular, planar, or monolithic. The solid ceramic construction of the unit cell alleviates any corrosion problems in the cell and avoids electrolyte movement or flooding in the electrodes.
- The kinetics of the cell is relatively fast; therefore, expensive noble metal catalysts are not needed.
- SOFC can tolerate relatively high impurity content in the fuel. It can be operated by hydrogen or renewable fuels including ethanol, biomass and glycerol.
- SOFC do not suffer from CO poisoning. Indeed, CO is a directly useable fuel in SOFC.
- The high operating temperature allows use of most of the waste heat for cogeneration or in bottoming cycles. The overall efficiency of the system can be significantly increased when this waste gas is fully utilized.

Table 3.1 Different types of fuel cell and applications.

Fuel cell type	Electrolyte	Operating temperature	Mobile ion	Fuel	Applications
Alkaline FC (AFC)	KOH	50-200 °C	OH^-	Pure H_2	Used in space vehicles, e.g. Apollo,Shuttle.
Proton exchange membrane FC (PEMFC)	Solid polymer (such as Nafion)	30-100 °C	H^+	Pure H_2 (tolorates CO_2)	Vehicles and mobile applications, and for lower power CHP systems
Phosphoric acid FC (PAFC)	Phosphoric acid	~220 °C	H^+	Pure H_2 (tolorates CO_2, approx. 1% CO)	Large numbers of 200-kW CHP systems in use
Molten carbonate FC (MCFC)	Lithium and potassium carbonate	~650 °C	CO_3^{2-}	H_2, CO, CH_4, other hydrocarbons (tolerates CO_2)	Suitable for medium- to large-scale CHP systems, up to MW capacity
Solid oxide FC (SOFC)	Solid oxide electrolyte	600-1000 °C	O^{2-}	H_2, CO, CH_4, other hydrocarbons (tolerates CO_2)	Suitable for all sizes of CHP systems, 2kW to multi-MW

However, the high temperature of the SOFC has its drawbacks. There are thermal expansion mismatches among materials, and sealing between cells is difficult in the flat plate configurations. The high operating temperature places severe constraints on materials selection and results in difficult fabrication processes. Corrosion of metal stack components is a challenge.

3.2.2 SOFC operation

A schematic representation of an SOFC operation is depicted in Figure 3.1. In SOFC operation, oxygen or air is reduced to oxygen ions at the cathode:

$$0.5O_2 + 2e^- \rightarrow O^{2-} \qquad (3.1)$$

The oxygen ions diffuse into the electrolyte material and migrate to the other side of the cell where they contact the anode. The high ionic conductivity and the high electrical resistance of electrolyte allow only O^{2-} ions to migrate from the cathode to the anode. At the anode, O^{2-} reacts with hydrogen producing water:

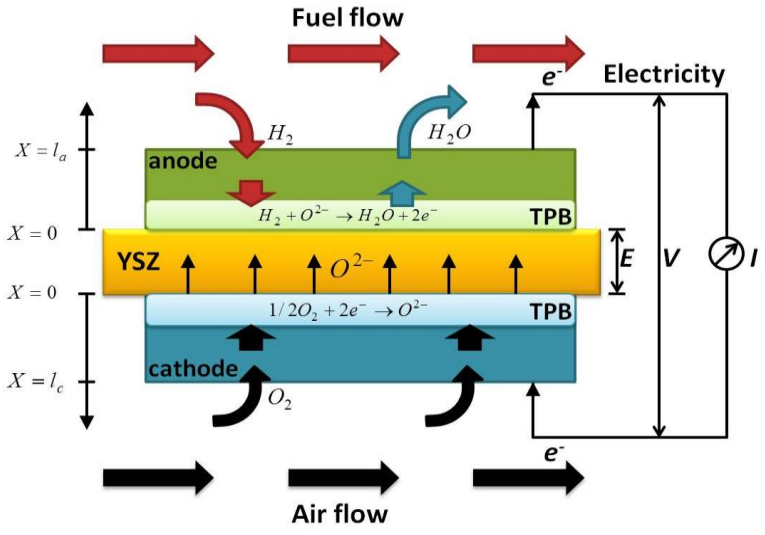

Figure 3.1 Schematic representation of a Solid Oxide Fuel Cell

$$H_2 + O^{2-} \rightarrow H_2O + 2e^- \quad (3.2)$$

As reaction 3.2 occurs, electrons are released at the anode and migrate from the cathode through an external electric circuit, thus generating an electric current. The overall reaction occurring in the cell is:

$$H_2 + 0.5O_2 \rightarrow H_2O \quad (3.3)$$

As a result, the fuel gas is diluted by water vapor, and the cell performance deteriorates unless the fuel gas is circulated to remove vapor.

3.2.3 SOFC characteristic

The key performance measure of a fuel cell can be determined by the actual voltage. When a fuel cell is operating, it is found that the actual voltage is less than the theoretical voltage which is the maximum voltage that can achieved by a fuel cell at no load conditions. The theoretical voltage can be calculated by the Nernst equation. However, as current passes though the cell, the voltage is expected to drop from the theoretical voltage due to the irreversibilities in fuel cell. Three main voltage losses are (1) activation loss, (2) concentration loss and (3) ohmic loss. The different loss mechanisms dominate at different levels of current density as seen in Figure 3.2. The current density is defined as the current produced per unit fuel cell area. These loss mechanisms are discussed in more detail in section 4.3.2.

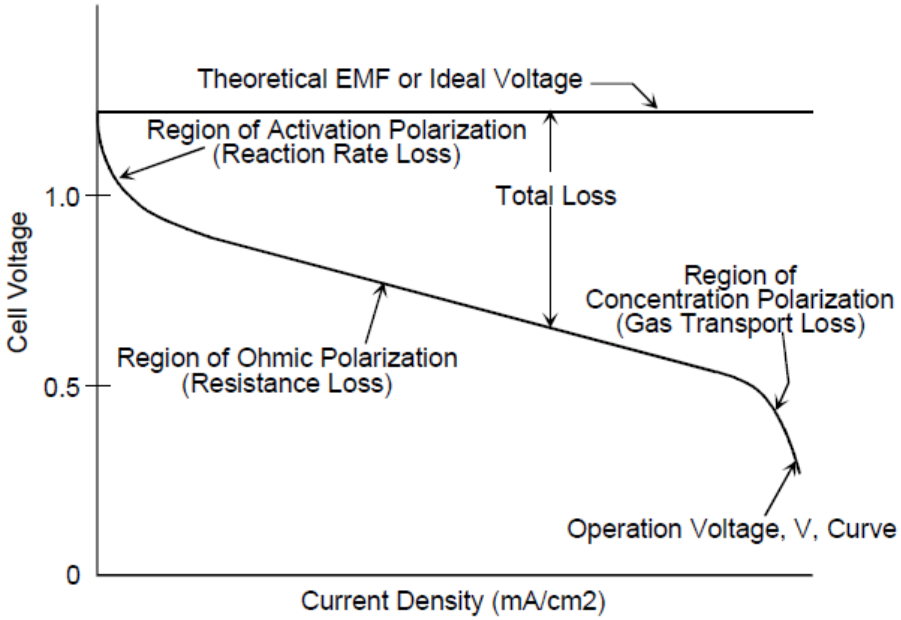

Figure 3.2 Current-Voltage characteristics of fuel cell

3.2.4 SOFC materials

To avoid separation and cracking during fabrication and operation at high temperature, the components for ceramic SOFC must have similar coefficient of thermal expansion. Both the anode and cathode must be porous to allow gas transport to the reaction site, whereas the electrolyte must be dense in order to separate the oxidant and fuel gases. The selection of materials is usually the result of a compromise between the below characteristics:

- High chemical stability under the relative operational conditions
- High electrical conductivity for the electrodes and electrical interconnects
- High ionic conductivity and almost zero electrical conductivity for the electrolyte
- Low cost

In this study, materials used for SOFC components are summarized in Table 3.2.

Table 3.2 Materials used for SOFC components

Component	**composition**
Anode	Ni-YSZ cermet
Cathode	strontium-doped lanthanum manganite (LSM)
Electrolyte	yttria-stabilized zirconia (YSZ)

3.3 Ethanol reforming for SOFC

Fuel cells utilize hydrogen as fuel of the system. Although hydrogen is the lightest, the simplest, and one of the most abundant elements in nature, it is not a free element. There are different configurations and reforming processor which are presented in this section. Moreover, this section also provides the principle of ethanol reforming mechanism, sorption-enhanced reforming and dehumidification in the reforming reaction, which leads to the technologies of improvement for ethanol reforming.

3.3.1 Ethanol

Ethanol, is an alcohol, is a clear, colorless liquid with a characteristic, flammable and high octane number (99.8% ethanol has an octane number of 113). Ethanol has widespread use as a solvent of substances intended for human contact or consumption, including scents, flavorings, colorings, and medicines. In chemistry, it is both an essential solvent and a feedstock for the synthesis of other products. It has a long history as a fuel for heat and light, and more recently as a fuel for internal combustion engines. It can be mixed with petrol; this increases the octane number of petrol such as gasohol.

In this research, ethanol (Ethanol) is considered to be a promising candidate as a source for renewable hydrogen because it can be produced renewably through the

fermentation of biomass, waste material from agro-industries, or even organic fraction of municipal solid waste. It present several advantages over other fuels related to natural availability, easy to store, handle, and transport in a save way due to its lower toxicity and volatility. The properties of ethanol used as fuel shown in Table 3.3.

Table 3.3 The properties of ethanol used as fuel

Properties	**Value**
Name	Ethanol or Ethyl Alcohol
Chemical formula	C_2H_5OH
Molecular weight	46.07 g/mol
Density	0.789 g/cm^3
Melting point	-114.3 ◦C
Boiling point	78.4 ◦C
Viscosity	1.20 mPa·s (cP) at 20.0 ◦C
Flash point	13 ◦C
Lower heating value	1,230 kJ/mole of ethanol
Higher heating value	1,300 kJ/mole of ethanol

3.3.2 Ethanol reforming processes

The generic term most often applied to the process of converting ethanol to hydrogen and carbon monoxide is “reforming”. There are a number of methods to reform fuel. The three most commercially developed and popular methods are 1) steam reforming, 2) partial-oxidation reforming, and, 3) autothermal reforming. Steam reforming (SR) provides the highest concentration of hydrogen and can obtain a conversion efficiency. Partial oxidation (POX) is a fast process, good for starting, fast response, and a small reactor size. Non-catalytic POX operates at temperatures of approximately 1,400 °C, but adding a catalyst (catalytic POX or CPOX) can reduce this temperature to as low as 870 °C. Combining steam reforming closely with CPOX is termed autothermal reforming (ATR).

a) Steam reforming

At present, ethanol steam reforming is the most widely used process because it provides a higher hydrogen yield and a lower rate of side reactions. This process, however, has some limitations, e.g., slow start-up time, high energy consumption and severe catalyst deactivation. Ethanol steam reforming is an endothermic process that combines ethanol with steam over catalysts at high temperatures as:

$$C_2H_5OH + H_2O \leftrightarrow 2CO + 4H_2 \quad (3.4)$$

However, there are several reaction pathways that could occur in ethanol/water system, depending on the catalysts used. Various kinds of intermediate by-products such as acetaldehyde and ethylene are usually formed the feasible reactions of ethanol/water system are ethanol dehydrogenation, acetaldehyde decomposition, ethanol dehydration, methane steam reforming and water gas shift reaction as shown in Table 3.4. According to the complete steam reforming reaction, which gives the maximum hydrogen yield, is given by the following reaction:

$$C_2H_5OH + 3H_2O \leftrightarrow 2CO_2 + 6H_2 \quad (3.5)$$

b) Partial oxidation

The partial oxidation of ethanol is an exothermic process in which ethanol and oxygen are combined in proportions to partially combust ethanol into a gaseous mixture of H_2 and CO. The advantages of the ethanol partial oxidation are fast start-up and less system complexity because it does not need an external heat source and a water balance. However, this process provides low hydrogen yield. The incomplete ethanol oxidation reaction is shown as:

$$C_2H_5OH + \frac{1}{2}O_2 \leftrightarrow 2CO + 3H_2 \quad (3.6)$$

c) Autothermal reforming

The autothermal reforming of ethanol, also known as an oxidative steam reforming, is an exothermic process. This type of the reforming method combines the steam reforming and the partial oxidation reactions in a single process, in order to achieve the minimum energy input necessary to maintain the reformer at a desired temperature. The autothermal reforming reaction is shown in Eq. (3.7), which 0.61 mol of oxygen is needed to react with one mole of ethanol (Graschinsky et al., 2012).

$$C_2H_5OH + 1.78H_2O + 0.61O_2 \leftrightarrow 2CO_2 + 4.78H_2 \quad (3.7)$$

One of the most important things that should be concerned is the carbon formation problem. The possible reaction pathways of each ethanol reforming process including carbon formation reactions are summarized in Table 3.4 (Ni et al., 2007a; Wang and Wang, 2008; Gutierrez et al., 2011).

Table 3.4 Possible reactions of ethanol reforming process

Possible reactions	Steam reforming	Partial oxidation	Autothermal reforming
$C_2H_5OH + H_2O \leftrightarrow 2CO + 4H_2$	✓		✓
$C_2H_5OH + 3H_2O \leftrightarrow 2CO_2 + 6H_2$	✓		✓
$C_2H_5OH + CO_2 \rightarrow 3CO + 3H_2$	✓		✓
$C_2H_5OH + 3O_2 \leftrightarrow 2CO_2 + 3H_2O$		✓	✓
$C_2H_5OH + 2O_2 \leftrightarrow 2CO + 3H_2O$		✓	✓
$2C_2H_5OH + O_2 \leftrightarrow 4CO + 6H_2$		✓	✓
$C_2H_5OH + O_2 \leftrightarrow CO_2 + CO + 3H_2$		✓	✓
$C_2H_5OH + 1.5O_2 \leftrightarrow 2CO_2 + 3H_2$		✓	✓
$CO + H_2O \leftrightarrow CO_2 + H_2$	✓	✓	✓
$C_2H_5OH \rightarrow CH_3CHO + H_2$	✓	✓	✓
$C_2H_5OH \rightarrow C_2H_4 + H_2O$	✓	✓	✓
$C_2H_5OH \rightarrow CH_4 + CO + H_2$	✓	✓	✓
$2C_2H_5OH \rightarrow 3CH_4 + CO_2$	✓	✓	✓
$CH_3CHO + H_2O \rightarrow 2CO + 3H_2$	✓		✓
$CH_3CHO \rightarrow CH_4 + CO$	✓	✓	✓
$C_2H_5OH + 2H_2 \rightarrow 2CH_4 + H_2O$	✓	✓	✓
$CH_3CHO + H_2O + O_2 \rightarrow 2CO_2 + 3H_2$		✓	✓
$CH_4 + H_2O \leftrightarrow CO + 3H_2$	✓		✓
$CO + 3H_2 \rightarrow CH_4 + H_2O$	✓	✓	✓
$CO_2 + 4H_2 \rightarrow CH_4 + 2H_2O$	✓	✓	✓
$2CO \leftrightarrow CO_2 + C$	✓	✓	✓
$C_2H_4 \rightarrow \text{polymer} \rightarrow 2H_2 + 2C$	✓	✓	✓
$CH_4 \leftrightarrow 2H_2 + C$	✓	✓	✓
$H_2O + C \leftrightarrow H_2 + CO$	✓	✓	✓
$2H_2O + C \leftrightarrow 2H_2 + CO$	✓	✓	✓

3.3.3 Sorption-Enhanced Reforming Process (SERP)

In any ethanol reforming process, ethanol is almost totally reformed but the primary products involving CH_4 and CO are limited by equilibrium reactions of methane steam reforming and water gas shift. However, if the CO_2 can be removed from the gas as it is formed, the normal equilibrium limits are displaced and complete conversion can be closely approached.

One way of enhancing the reaction is by removing the CO_2 produced. This can be done by adding a CO_2 sorbent (acceptor) to the reactor. Sorption enhancement enables lower reaction temperatures while maintaining the conversion, which may also reduce catalyst coking and sintering, while enabling use of less expensive reactor wall materials (Johnsen et al., 2006). Furthermore a CO_2/H_2 separation step integrated with the reforming step has potentially a positive impact on efficiency and could lower the efficiency penalty and thus the costs. Upon reaction of carbon dioxide (CO_2) and the solid sorbent (adsorption/ carbonation step), CO_2 is converted to a solid carbonate. Regenerating the sorbent (desorption/calcination step) results in releasing CO_2 suitable for storage. The carbonation/calcination (or adsorption/desorption) equilibrium reaction is written as in Eq. (3.8):

$$CO_2 + CaO \leftrightarrow CaCO_3 \tag{3.8}$$

The SERP process can be carried out as batch process using two or more parallel externally heated fixed reactors, one being in adsorption mode and the other in desorption mode. Alternatively, an interconnected fluidised bed system could be used in which sorbent is circulated. While this places more demands on the mechanical stability of the sorbent, it also simplifies the system operation to some extent such that both processes no longer need to take place in the same reactor. A fluidised system also enjoys a greater degree of flexibility with regard to heat integration than fixed-bed options. Temperature swing for regeneration is more easily achieved in a dedicated reactor with good heat transfer characteristics. Additionally, a fluidised bed can much more easily handle a sorbent that loses capacity during cycling. In the fixed-bed

situation, this would require constant tweaking of the timing of the different steps, or possibly running under conditions where only use of the lowest stable capacity is available. In the fluidised bed situation, there are many options available for optimisation, such as a constant replenishment of sorbent. It is also possible to regenerate the sorbent online with such a configuration (Harrison, 2008).

3.4 Absorption chiller

Combined Cooling, Heat and Power (CCHP) or trigeneration refers to the simultaneous generation of electricity and useful heating and cooling, typically in an absorption chiller. Absorption chillers differ from the vapor compression systems, which use electrically-driven compressors, in that the absorption cooling effect, is driven by any type of waste heat, steam, hot liquid or hot gas.

The basic principle of absorption chiller cycle is similar to vapor compression cycles; the main difference being that the compressor is replaced by a chemical cycle taking place between the absorber, pump, and generator as shown in Figure 3.3. Basically, the evaporator allows the refrigerant to evaporate and to be absorbed by the absorbent, a process that extracts heat from the building. The combined fluids then go to the generator, which is heated by the gas or steam, driving the refrigerant back out of the absorbent. The refrigerant then goes to the condenser to be cooled back down to a liquid, while the absorbent is pumped back to the absorber. The cooled refrigerant is released through an expansion valve into the evaporator, and the cycle repeats.

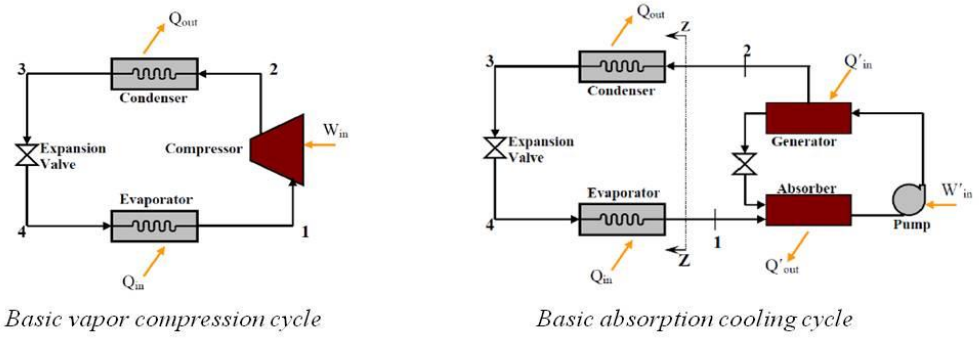

Figure 3.3 The operation of absorption cooling cycle compared with vapor compression cycle.

The coolant and the absorbent constitute what is called a working pair. Essentially, absorption chillers are either lithium bromide-water ($LiBr/H_2O$) or ammonia-water equipment. The $LiBr/H_2O$ system uses lithium bromide as the absorber and water as the refrigerant. The ammonia-water system uses water as the absorber and ammonia as the refrigerant. Table 3.5 highlights a summary of the most important properties of absorption cooling systems.

Table 3.5 Absorption cooler's characteristics

Indices	**NH_3 Absorption**	**LiBr Absorption**	
Effect	Single	Single	Double
Cooling capacity (kW)	20 - 2500	300 - 5000	300 - 500
Thermal COP	0.6 – 0.7	0.5 – 0.6	0.9 – 1.1
Temperature range (°C)	120 - 132	120 - 132	150 - 172
Machine costs (€/ton)	1250 to 1750	870 to 920	930 to 980

As shown in Table 3.5, LiBr absorptions come as single-effect or double-effect cycles. The single-effect cycle refers to the transfer of fluids through the four major components of the refrigeration machine - evaporator, absorber, generator and condenser. Differ from the single-effect, the double-effect chiller has two condensers and two generators to allow for more refrigerant boil-off from the absorbent solution (Figure 3.4). The double-effect machines are thermally more efficient but are more complex and require higher grade heat input. However, triple effect machines have not been developed in practice.

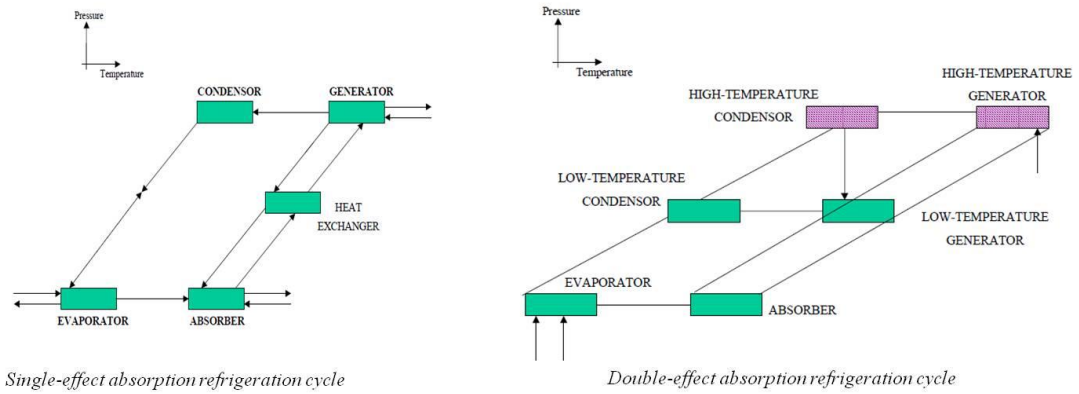

Figure 3.4 Single- and double-effect absorption refrigeration cycles

Utilizing waste heat that would otherwise be unused greatly increases the cost-effectiveness of the systems, compared to consuming gas directly. Gas absorption systems have several non-energy benefits over conventional electric systems including:

- Elimination of the use of CFC and HCFC refrigerants
- Quiet, vibration-free operation
- Lower pressure systems with no large rotating components
- High reliability
- Low maintenance

The contribution that gas cooling technologies can make to the goal of improved emissions is substantial. Natural gas-powered air-conditioning equipment offers substantial advantages to the environment in regard to CFCs and HCFCs, because they are not used in the absorption cycle. Legislative activities are focused on pushing the nation toward energy-efficient technologies that reduce harmful emissions. While gas-fired chillers produce emissions at the site, combustion efficiencies can be high and harmful emissions comparatively low for a well-operated absorption unit.

However, Cost is the primary constraint on the widespread adoption of absorption chiller systems. The low thermal efficiency of single-effect absorption systems has made them non-competitive except in situations with readily available free waste heat. Even double effect systems are not cost-effective in many applications.

Although absorption chillers can be quite economical in the right situation, their exact economics must be worked out on a project-by-project basis.

Absorption systems also require greater pump energy than electric chillers. The size of condenser water pumps is generally a function of the flow rate per unit cooling capacity. Cooling technologies with lower COPs typically require a significantly higher condenser water flow rate than those technologies with higher COPs, therefore requiring larger pumps. Similarly, absorption chillers require larger cooling tower capacity than electric chillers, due to the larger volume of water

3.5 Energy and exergy analyses

The First Law of Thermodynamics (FLT) is the law of the conservation of energy, which states that, although energy can change form, it can be neither created nor destroyed. If energy is conserved and then the amount of energy must be constant but why do we hear on the news that the world is experiencing an energy shortage? How could we be running out of energy? How should we find a new renewable energy candidate?

The answer to these questions lies in the difference between the term energy that is commonly used in everyday conversations and the term energy that means only thought of "the capacity to do work". In fact, energy has both quantity and quality. The capacity to do work of energy is its quality and is not conserved. The Second Law of Thermodynamics (SLT) can be interpreted as system for assigning quality to energy. It explains the directional nature of all real processes that continuously degrade the quality of energy. Latterly, it can be expresses in the term as exergy.

Energy analysis is only dealing with the energy balance that no information on the degradation of energy or resources during a process and does not quantify the usefulness or quality of the various energy and material streams flowing through a system and exiting as products and wastes. But exergy analysis can do. The thermodynamic imperfections can be quantified as exergy destructions, which represent losses in energy quality or usefulness. Exergy analysis clearly indicates the locations of

energy degradation in a process and can therefore lead to improved operation or technology.

It is important to distinguish between energy and exergy in order to avoid confusion with traditional energy-based methods of thermal system analysis and design. Table 3.6 presents a general comparison of energy and exergy.

Table 3.6 Comparison of energy and exergy

Energy	Exergy
Dependent on properties of only a matter or energy flow, and independent of environment properties	Dependent on properties of both a matter or energy flow and the environment
Has values different from zero when in equilibrium with the environment (including being equal to mc^2 in accordance with Einstein's equation)	Equal to zero when in the dead state by virtue of being in complete equilibrium with the environment
Conserved for all processes, based on the FLT	Conserved for reversible processes and not conserved for real processes (where it is partly or completely destroyed due to irreversibilities), based on the SLT
Can be neither destroyed nor produced	Can be neither destroyed nor produced in a reversible process, but is always destroyed (consumed) in an irreversible process
Appears in many forms (e.g., kinetic energy, potential energy, work, heat) and is measured in that form	Appears in many forms (e.g., kinetic exergy, potential exergy, work, thermal exergy), and is measured on the basis of work or ability to produce work
A measure of quantity only	A measure of quantity and quality

CHAPTER IV

PROCESS MODELING

Process modeling is an essential tool for the analysis of physical, chemical, and electrochemical processes in fuel cell systems. In this research, the thermodynamic model by using minimization of Gibb free energy is applied for the ethanol reforming process in section 4.1. The electrochemical model of SOFC is also described in Section 4.2. Section 4.3 and 4.4 shows models of auxiliary units and absorption chiller respectively. Additionally, the validation of all main units is presented in each section.

4.1 Fuel processor

4.1.1 Ethanol reforming processes

Thermodynamic analysis of ethanol reforming processes is performed based on steady-state. The equilibrium composition of the reforming products was determined by the minimization of a total Gibbs free energy (a non-stoichiometric approach). The total Gibbs free energy of the system, regarded as an ideal gas, may be expressed as:

$$G = \sum_{i=1}^{C} n_i G_i^0 + \sum_{i=1}^{C} n_i RT \ln y_i + \sum_{i=1}^{C} n_i RT \ln P \qquad (4.1)$$

where C is the total number of components in the reaction system, n_i is the number of moles of each gases component. It is assumed that the reformer is run at atmospheric pressure and a pressure drop is neglected, thus the last term of Eq. (4.1) vanishes. The equilibrium state is found by minimizing G, calculated using Eq. (4.1). Resulting from the conservation of atomic species, n_i have to satisfy the element balance as given by

$$\sum_{i=1}^{C} n_i a_{ik} - A_k = 0 \qquad \text{for } k = 1,2,...,w \qquad (4.2)$$

where a_{ik} is the number of atoms of element k in a component i, A_k is the total number of atoms of element k and w is the total number of elements appearing in all of the components.

The primary components involved in the ethanol reforming process are C_2H_5OH, H_2O, O_2, CH_3CHO, C_2H_4, H_2, CH_4, CO_2, CO and C (Lima da Silva et al., 2009) and the reactions would occur as shown in Table 4.1 (Gutierrez et al., 2011).

The following assumptions are made in the development of the model.

- Steady state and isothermal operation
- All gases behave as an ideal gas.
- The distributions of pressure and temperature are negligible.
- To analyze carbon formation from a thermodynamic point of view, it is assumed that pure carbon is presented in the graphitic form; the chemical potential of carbon at 298 K and its vapor pressure are zero.
- Heat required for the reforming process is supplied by an external source.
- There is no heat loss to the surroundings.

4.1.2 Fuel processor efficiency

To evaluate the performance of the fuel processor, the equilibrium conversion of ethanol ($X_{C_2H_5OH}$), yield of hydrogen (Y_{H_2}) and carbon formation are defined as the following:

$$X_{C_2H_5OH}(\%) = \frac{F_{C_2H_5OH,in} - F_{C_2H_5OH,out}}{F_{C_2H_5OH,in}} \times 100 \quad (4.3)$$

$$Y_{H_2}(\text{mole } H_2/\text{mole Ethanol}) = \frac{F_{H_2}}{F_{C_2H_5OH,in}} \quad (4.4)$$

$$\text{Carbon formation (mole C/mole Ethanol)} = \frac{F_{coke}}{F_{C_2H_5OH,in}} \quad (4.5)$$

The reforming efficiencies are related to the ratio between the LHV of hydrogen leaving the reformer and the LHV of the total ethanol feeding into the reformer.

$$\eta_{ER}(\%) = \frac{\dot{n}_{H_2,out} LHV_{H_2}}{\dot{n}_{C_2H_5OH,in} LHV_{C_2H_5OH}} \times 100 \quad (4.6)$$

Table 4.1 Possible reactions in the ethanol reformer (Gutierrez et al., 2011).

Possible reactions	ΔH (kJ/mol) T = 700 °C	ΔG (kJ/mol) T = 700 °C
$C_2H_5OH + H_2O \leftrightarrow 2CO + 4H_2$	278.1	-203.7
$C_2H_5OH + 3H_2O \leftrightarrow 2CO_2 + 6H_2$	207.8	-211.1
$C_2H_5OH + CO_2 \rightarrow 3CO + 3H_2$	313.2	-199.9
$C_2H_5OH + 3O_2 \leftrightarrow 2CO_2 + 3H_2O$	-1277.5	-1376.3
$C_2H_5OH + 2O_2 \leftrightarrow 2CO + 3H_2O$	-712.1	-980.5
$2C_2H_5OH + O_2 \leftrightarrow 4CO + 6H_2$	61.1	-795.8
$C_2H_5OH + O_2 \leftrightarrow CO_2 + CO + 3H_2$	-252.2	-595.8
$C_2H_5OH + 1.5O_2 \leftrightarrow 2CO_2 + 3H_2$	-534.9	-793.7
$CO + H_2O \leftrightarrow CO_2 + H_2$	-35.1	-3.7
$C_2H_5OH \rightarrow CH_3CHO + H_2$	73.9	-47.5
$C_2H_5OH \rightarrow C_2H_4 + H_2O$	45.2	-79.6
$C_2H_5OH \rightarrow CH_4 + CO + H_2$	53.7	-183.6
$2C_2H_5OH \rightarrow 3CH_4 + CO_2$	-152.0	-351.0
$CH_3CHO + H_2O \rightarrow 2CO + 3H_2$	204.2	-156.2
$CH_3CHO \rightarrow CH_4 + CO$	-20.2	-136.2
$C_2H_5OH + 2H_2 \rightarrow 2CH_4 + H_2O$	-170.6	-163.6
$CH_3CHO + H_2O + O_2 \rightarrow 2CO_2 + 3H_2$	-361.2	-551.9
$CH_4 + H_2O \leftrightarrow CO + 3H_2$	224.4	-20.0
$CO + 3H_2 \rightarrow CH_4 + H_2O$	-224.3	20.0
$CO_2 + 4H_2 \rightarrow CH_4 + 2H_2O$	-189.2	23.7
$2CO \leftrightarrow CO_2 + C$	-170.8	0.01
$C_2H_4 \rightarrow \text{polymer} \rightarrow 2H_2 + 2C$		
$CH_4 \leftrightarrow 2H_2 + C$	-88.6	16.3
$H_2O + C \leftrightarrow H_2 + CO$	135.7	-3.7
$2H_2O + C \leftrightarrow 2H_2 + CO$	100.6	-7.4

4.1.3 Model validation

Here, the simulation model used to predict the equilibrium composition of ethanol reforming processes is validated with experimental and simulation data reported in literatures. Figure 4.1 (a) shows the model prediction of H_2 yield from the steam reforming compared with experimental data (Biswas and Kunzru, 2007). In their experiment, the reforming of ethanol was carried out using Ni/ZrO_2. It is observed from Figure 4.1 (a) that the model can reliably predict the H_2 product under different operating temperatures. Further, it is found that the use of model in the operating temperature range of 773-923 K can make more precise predictions with only 3-10 % error. Figure 4.1 (b) compared the H_2 yield of the ethanol partial oxidation process obtained from the simulation and the studies by Sun et al., (2012) and Wang and Wang, (2008). The model prediction agrees very well with the reported data. Comparison of the modeling result and experimental data of the ethanol autothermal reforming based on $RhPt/ZrO_2$ catalyst (Gutierrez et al., 2011) are shown Figure 4.1 (c) and a good agreement of the model prediction and experimental data of the H_2 yield is observed Most simulation results are not exceed 5 % error.

(a)

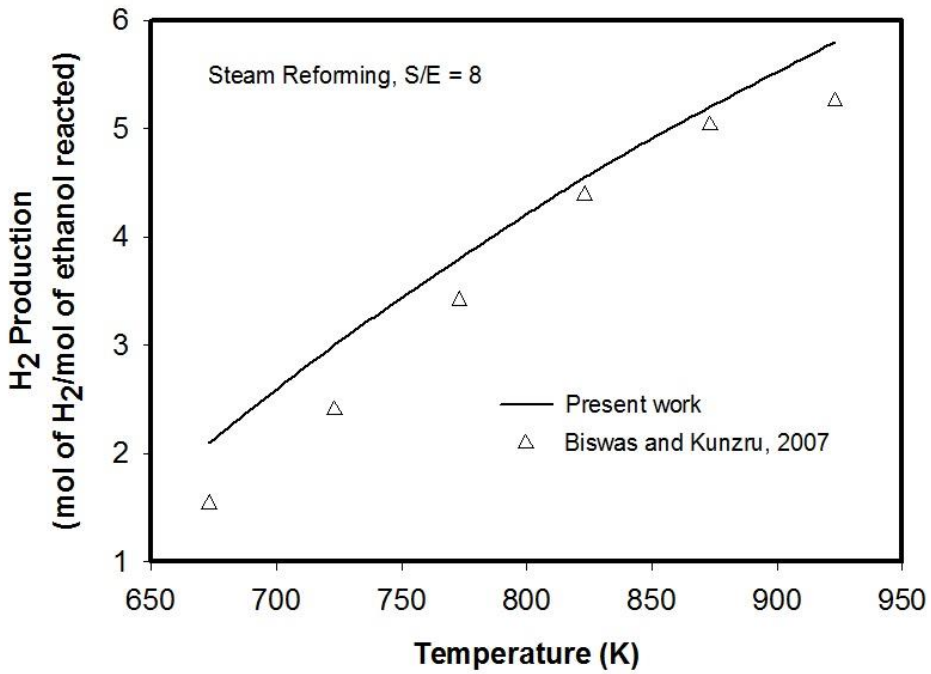

(b)

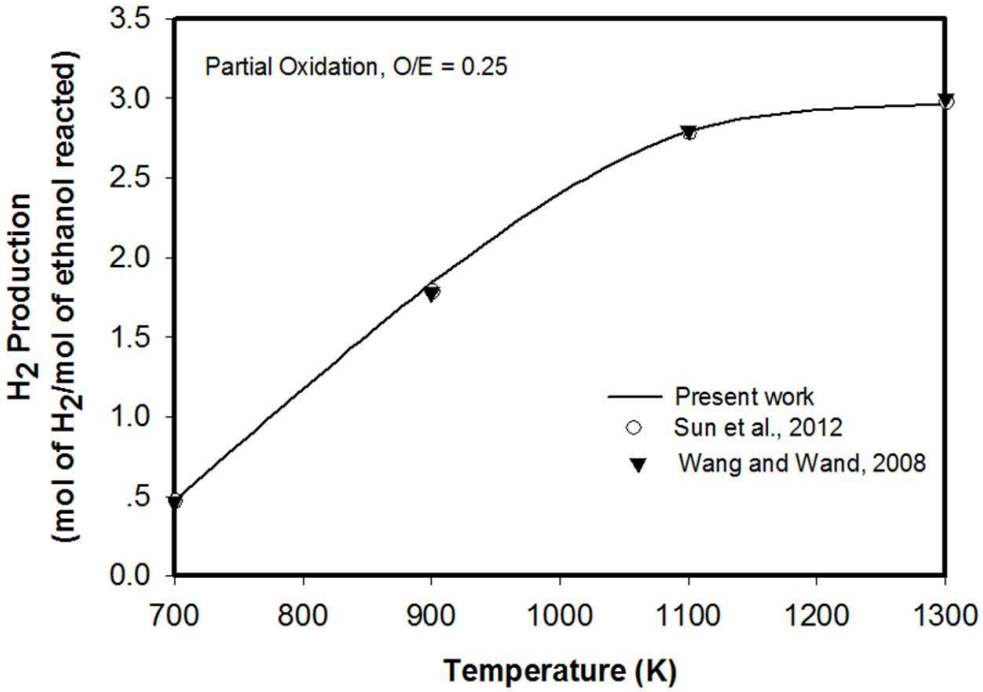

(c)

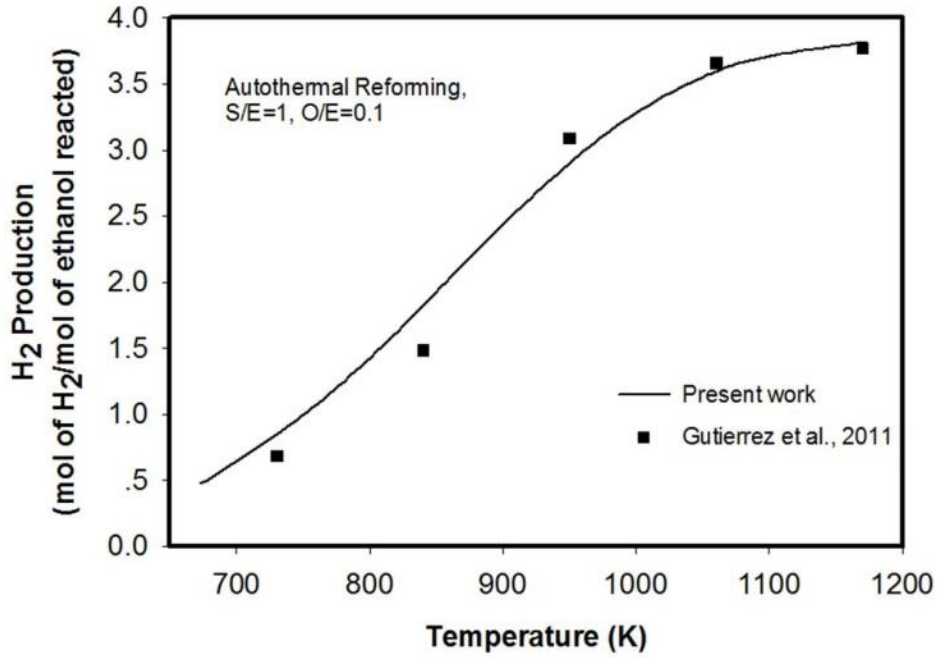

Figure 4.1 Comparison of hydrogen yield obtained from the model prediction and reported data in literatures: (a) steam reforming, (b) partial oxidation and (c) autothermal reforming.

As mentioned earlier, this study deals with different fuel processors. When ethanol is dehydrogenated to acetaldehyde in dehydrogenation unit and the yield of acetaldehyde in this simulation result is compared with experimental data of Deng et al., (1995) which reported by using Al_2O_3 membrane reactor as shown in Figure 4.2. The most errors made by a model prediction are below 10%. While the ethanol steam reformer added CaO sorbent have validated by comparing with Mahishi's work (Mahishi et al., 2008) as Figure 4.3.

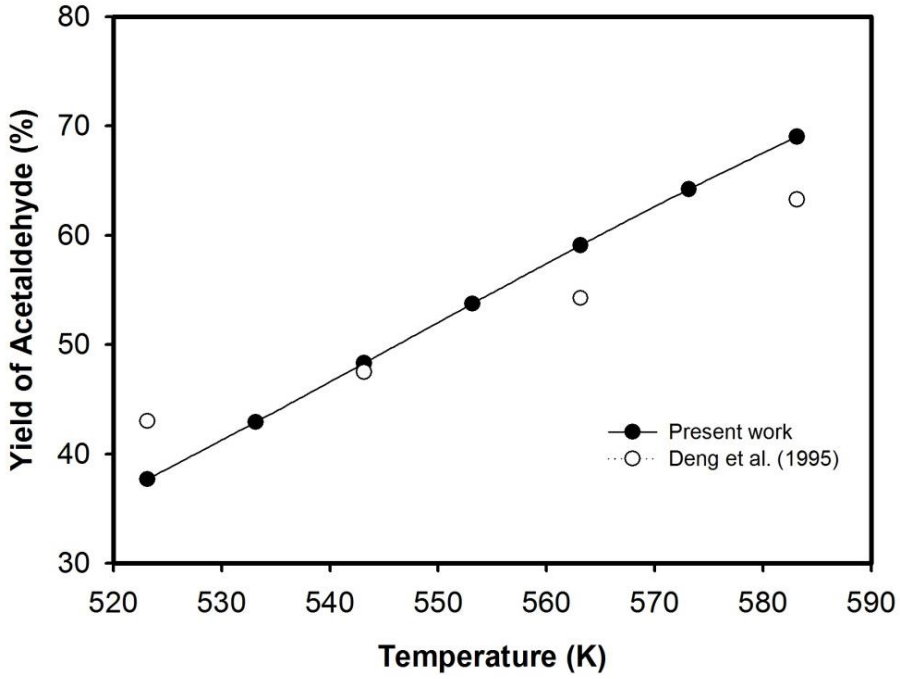

Figure 4.2 Comparison of ethanol dehydrogenation units between simulation results and experimental data (Deng et al., 1995).

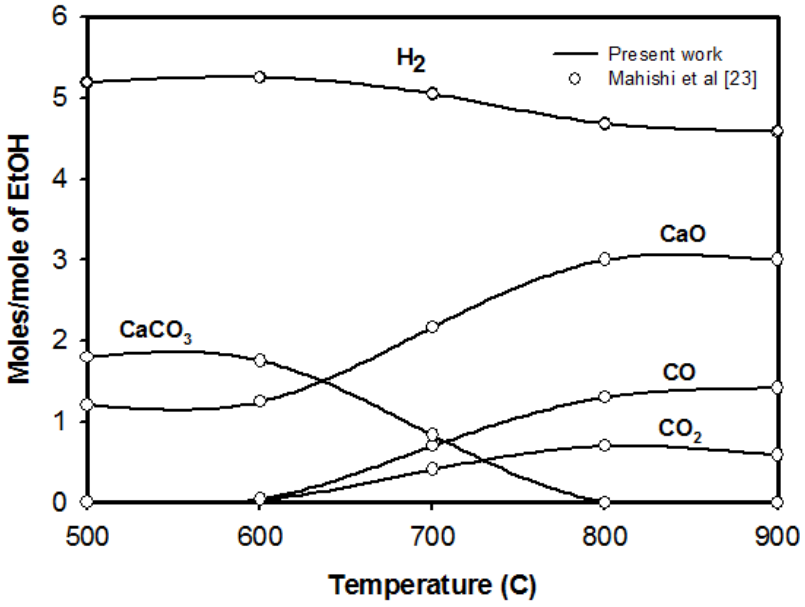

Figure 4.3 Comparison of sorption-enhanced ethanol steam reforming between this work and literature (Mahishi et al., 2008).

4.2 Solid oxide fuel cell

4.2.1 Model configuration

An SOFC stack is a power generating device that converts the chemical energy in fuel obtained from the reforming process into electrical power via an electrochemical reaction. The electricity that fuel cells generate is direct current (DC). If alternating current (AC) is needed, the DC output of the fuel cells must be converted through an inverter. In this integrated SOFC system, the recycling of the anode exhaust gas is considered to improve its performance as shown in Figure 4.4.

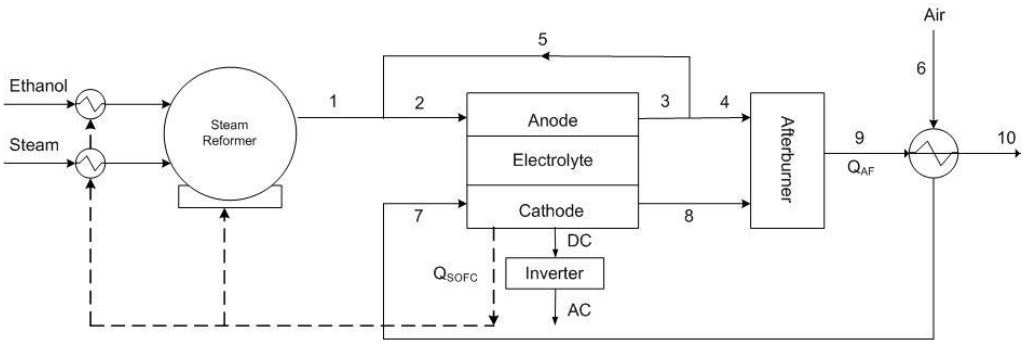

Figure 4.4 A solid oxide fuel cell configuration.

The simulation of an SOFC unit is performed by using the input parameters given in Table 4.2 at constant temperature and pressure operations.

The assumptions for this SOFC model are as follows (Colpan et al., 2007):

- Steady state and isothermal operation is considered.
- All gaseous components behave as an ideal gas.
- SOFC is configured to be planar.
- Both air and fuel flows have the same temperature at the inlet of the SOFC.
- Both air and fuel flows have the same temperature at the exit of the SOFC.
- The air entering the SOFC consists of 79% N_2 and 21% O_2.
- Only the electrochemical reaction of hydrogen is present.
- The gas mixture at the exit of the fuel channel is at chemical equilibrium.
- The radiation heat transfer between the gas channels and the solid structure is negligible.
- The contact resistances are negligible.
- Pressure drop is negligible.

The possibility of internal reforming of methane (CH_4) and carbon monoxide (CO) is located inside the fuel cell as follows:

$$CH_4 + H_2O \leftrightarrow CO + 3H_2 \tag{4.7}$$

$$CO + H_2O \leftrightarrow CO_2 + H_2 \tag{4.8}$$

and the overall reaction that occur within the solid oxide fuel cell to generate electricity is

$$H_2 + \frac{1}{2}O_2 \leftrightarrow H_2O \tag{4.9}$$

The model used to solve the equilibrium equations of the SOFC is based on a model developed by Aguiar et al., (2004), assuming the methane is fully converted. The molar conversion rates of Eqs. (4.7)–(4.9) are a, b and c, respectively. The molar flow rates of the reaction equations, Eq. (4.7)–(4.9), are derived and shown in Table 4.3. In the table, the variables $\dot{n}$, U_{f} and $U_{\mathrm{O_2}}$ are the molar flow rate, fuel utilization ratio and oxygen utilization ratio, respectively.

Table 4.2 Material properties and kinetic parameters for the SOFC stack (Petruzzi et al., 2003; Aguiar et al., 2004)

	Cathode	**Electrolyte**	**Anode**
Material	$La_{1-x}\ Sr_xMnO_3$	YSZ	Ni-YSZ
Layer thickness (μm)	50	20	500
Pre-exponential factor of exchange current density ($\Omega^{-1}m^{-2}$)	2.35×10^{11}	-	6.54×10^{11}
Activation energy of exchange current density (kJ mol^{-1})	137	-	140
Diffusion coefficient (m^2s^{-1})	1.37×10^{-5}	-	3.66×10^{-5}
Electronic conductivity ($\Omega^{-1}m^{-1}$)	8.4×10^3	-	80×10^3
Ionic conductivity ($\Omega^{-1}m^{-1}$)	-	33.4×10^3 exp(-10,300 T^{-1})	-

Table 4.3 The equilibrium number of moles for each composition.

$\dot{n}_{3,CH_4} = \dot{n}_{2,CH_4} - a$
$\dot{n}_{3,CO} = \dot{n}_{2,CO} + a - b$
$\dot{n}_{3,CO_2} = \dot{n}_{2,CO_2} + b$
$\dot{n}_{3,H_2} = \dot{n}_{2,H_2} + 3a + b - c$
$\dot{n}_{3,H_2O} = \dot{n}_{2,H_2O} - a - b + c$
$\dot{n}_3 = \dot{n}_2 + 2a$
$\dot{n}_{O_2,u} = c/2$
$\dot{n}_{7,O_2} = c/\left(2 \cdot U_{O_2}\right)$
$\dot{n}_{8,O_2} = c/2 \cdot \left(1/U_{O_2} - 1\right)$
$\dot{n}_{8,N_2} = 79/21 \cdot \left[c/\left(2 \cdot U_{O_2}\right)\right]$
$\dot{n}_{7,N_2} = \dot{n}_{8,N_2}$
$c = U_f \cdot \left(\dot{n}_{1,H_2O} + 3a + b\right)/\left(1 - r - r \cdot U_f\right)$

4.2.2 Electrochemical model

4.2.2.1 Actual cell voltage

A generalized steady state model is considered in order to investigate the performance of a SOFC system integrated with reforming process (Aguiar et al., 2004). The theoretical open-circuit cell voltage, which is the maximum voltage under specific operating conditions, can be calculated from the following equations:

$$E = E^0 + \frac{RT}{2F}\ln\left(\frac{P_{H_2}P_{O_2}^{0.5}}{P_{H_2O}}\right) \tag{4.10}$$

where E^0 is the reversible open-circuit potential at standard pressure and is a function of the operating temperature (Ni et al., 2007b) as:

$$E^0 = 1.253 - 2.4516\times10^{-4}T \tag{4.11}$$

The actual voltage is determined from the theoretical open-circuit voltage subtracted by the various voltage losses as:

$$V = E - \left(\eta_{act} + \eta_{ohmic} + \eta_{conc}\right) \tag{4.12}$$

4.2.2.2 Voltage losses

a) Activation Losses

Some voltage difference from equilibrium is needed to get the electrochemical reaction going. This is called activation losses. These losses happen at both anode and cathode; however, oxygen reduction causes higher activation losses because it is a much slower reaction than hydrogen oxidation. Activation losses are governed by the Butler-Volmer equation

$$i = i_{0,\text{electrode}} \left\{ \exp\left[\frac{\alpha n F}{RT} \left(V_{\text{act,electrode}} \right) \right] - \exp\left[-\frac{(1-\alpha) n F}{RT} \left(V_{\text{act,electrode}} \right) \right] \right\} \tag{4.13}$$

$$i_{0,\text{electrode}} = \frac{RT}{nF} k_{\text{electrode}} \exp\left(-\frac{E_{\text{electrode}}}{RT} \right), \text{electrode} \in \{\text{anode,cathode}\} \tag{4.14}$$

where i is current density (A/m^2), α is transfer coefficient, and i_0 is exchange current density (A/m^2).

b) Concentration Losses

Concentration losses occur when a reactant is rapidly consumed at the electrode by the electrochemical reaction so that concentration gradients are established. A relationship for voltage loss due to concentration polarization could be written:

$$\eta_{conc} = E_{OCV} - E_{OCV,TPB} \tag{4.15}$$

$$\eta_{conc} = \frac{RT}{2F} \ln\left(\frac{p_{H_2O,TPB} p_{H_2}}{p_{H_2O} p_{H_2,TPB}} \right) + \frac{RT}{4F} \ln\left(\frac{p_{O_2}}{p_{O_{2,TPB}}} \right) \tag{4.16}$$

Where the first term on the right-hand side of Eq. (4.16) refers to the anodic concentration overpotential, $\eta_{conc,a}$, and the second term refers to the cathodic concentration overpotential, $\eta_{conc,c}$, and $p_{H_2,TPB}$, $p_{H_2O,TPB}$, and $p_{O_2,TPB}$ represent the partial pressures of hydrogen, water, and oxygen at TPB respectively. Their diffusion transport in a porous electrode can be described by Fick's model as given by

$$p_{H_2,TPB} = p_{H_2} - \frac{RT\tau_{anode}}{2F\overline{D}_{eff,anode}} i \quad (4.17)$$

$$p_{H_2O,TPB} = p_{H_2O} + \frac{RT\tau_{anode}}{2F\overline{D}_{eff,anode}} i \quad (4.18)$$

$$p_{O_2,TPB} = P - (P - p_{O_2}) \exp\left(\frac{RT\tau_{cathode}}{4F\overline{D}_{eff,cathode}P} i \right) \quad (4.19)$$

The diffusion coefficients of the anode ($D_{eff,anode}$) and the cathode ($D_{eff,cathode}$) are 33.4 $\times 10^{-5}$ and 1.37 $\times 10^{-5}$ m^2s^{-1}, respectively as shown in Table 4.2.

c) Ohmic Losses

Ohmic losses occur because of resistance to the flow of ions in the electrolyte and resistance to the flow of electrons through the electrically conductive fuel cell components. These losses can be expressed by Ohm's law:

$$\eta_{ohm} = iR_{ohm} \quad (4.20)$$

where R_{ohm} is total cell internal resistance ($\Omega\,cm^2$). Here, R_{ohm} is calculated from the conductivity of the individual layers as given by:

$$R_{Ohm} = \frac{\tau_{anode}}{\sigma_{anode}} + \frac{\tau_{electrolyst}}{\sigma_{electrolyst}} + \frac{\tau_{cathode}}{\sigma_{cathode}} \quad (4.21)$$

where τ_{anode}, $\tau_{electrolyte}$ and $\tau_{cathode}$ represent the thickness of the anode, electrolyte, and cathode layers, respectively, σ_{anode} and $\sigma_{cathode}$ is the electronic conductivity of the anode and cathode, and $\sigma_{electrolyst}$ is the ionic conductivity of the electrolyte.

4.2.3 SOFC parameters and efficiency

The fuel utilization factor (U_f) is the ratio of the total fuel inlet used to produce electricity in the cell and the inlet fuel flow, and is defined by

$$U_{\mathrm{f}}(\%) = \left(\frac{\dot{m}_{\mathrm{f,in}} - \dot{m}_{\mathrm{f,out}}}{\dot{m}_{\mathrm{f,in}}} \right) \times 100 = \frac{\dot{m}_{\mathrm{f,consumed}}}{\dot{m}_{\mathrm{f,in}}} \times 100 \qquad (4.22)$$

where $\dot{m}_{\mathrm{f,in}}$ is the mass flow rate of fuel inlet and $\dot{m}_{\mathrm{f,out}}$ is the mass flow rate of fuel outlet.

The oxygen utilization factor is a very important process parameter for the design of the total system. It reflects the air excess which is supplied to the cell for cooling and retaining the cell temperature. Therefore, the oxygen utilization factor can be defined as

$$U_{\mathrm{O_2}}(\%) = \left(\frac{\dot{m}_{\mathrm{O_2,in}} - \dot{m}_{\mathrm{O_2,out}}}{\dot{m}_{\mathrm{O_2,in}}} \right) \times 100 = \frac{\dot{m}_{\mathrm{O_2,consumed}}}{\dot{m}_{\mathrm{O_2,in}}} \times 100 \qquad (4.23)$$

The SOFC efficiency (η_{SOFC}) is evaluated by the ratio of fuel cell power to the total energy that could be produced if hydrogen entering into the cell is completely burned:

$$\eta_{\mathrm{SOFC}}(\%) = \frac{\mathrm{Power}_{\mathrm{SOFC}}}{n_{\mathrm{C_2H_5OH,in}} \times \mathrm{LHV}_{\mathrm{C_2H_5OH}}} \times 100 \qquad (4.24)$$

where $\mathrm{Power}_{\mathrm{SOFC}}$ is the power output of the SOFC and $n_{\mathrm{C_2H_5OH,in}}$ and $\mathrm{LHV}_{\mathrm{C_2H_5OH}}$ are the inlet molar flow rate and the lower heating value of ethanol

4.2.4 Model validation

Figure 4.5 shows a comparison of the SOFC model prediction and experimental data (Zhao and Virkar, 2005) in term of the cell voltage at different current densities and operating temperatures. In their experiment, the inlet fuel consists of 97% H_2 and 3% H_2O and inlet oxidant comprises of 21% O_2. The thickness of anode, cathode, and electrolyte were 1000, 20 and 8 μm, respectively. It indicates that the model prediction shows good agreement with experimental data reported in literature with no results exceeding 7 % error. Although there are some discrepancies obtained at high current density operation, fuel cells are normally designed to operate at a cell voltage between 0.6-0.7 V (Aguiar et al., (2004). This range of operation is found at current density range of 0.2-1.5 A/cm^2 which the model presents more precise predictions.

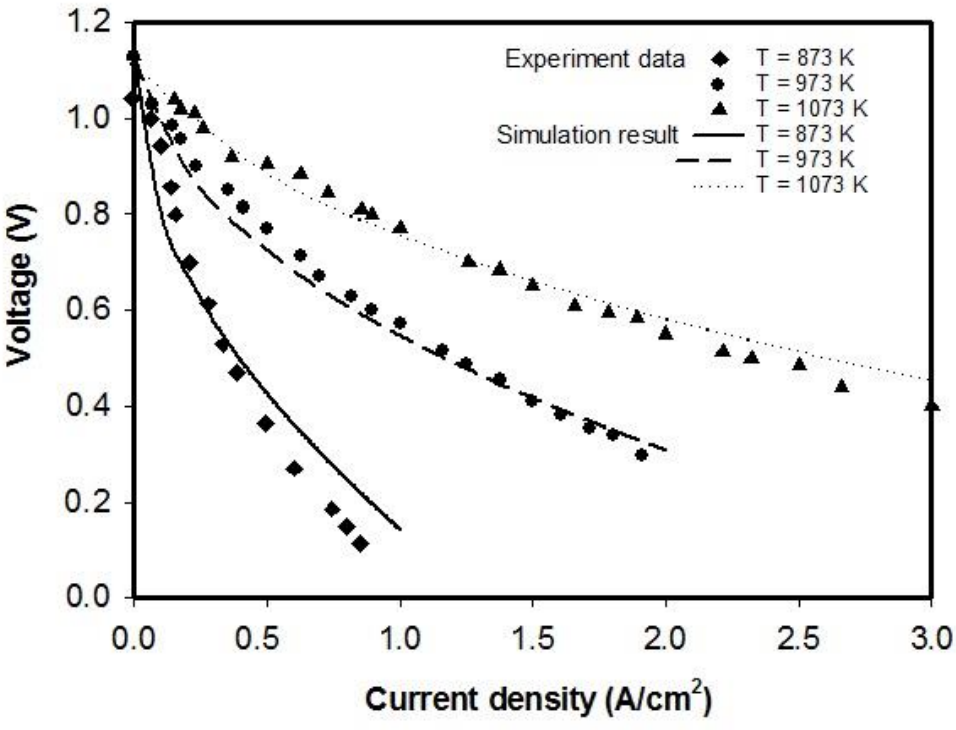

Figure 4.5 V-I curve obtained from the SOFC model and experimental data (Zhao and Virkar, 2005)

4.3 Auxiliary units

4.3.1 Afterburner

In general, the SOFC cannot electrochemically utilize 100% of the fuel. Because excess air is supplied and the assumption of perfect chemical equilibrium is a very good approximation to the overall real combustion process, the residual fuel and the excess air are assumed to combust in an afterburner completely in order to obtain extra useful heat at high temperatures. The equilibrium composition of the combustion process is determined by a stoichiometric approach. The combustion reaction occurring in afterburner is

$$\begin{aligned}&(y_{CH_4}CH_4 + y_{CO_2}CO_2 + y_{CO}CO + y_{H_2}H_2 + y_{H_2O}H_2O)\\&+a_s(y_{O_2}O_2 + y_{N_2}N_2) \rightarrow b_sCO_2 + c_sH_2O + d_sN_2\end{aligned} \tag{4.25}$$

where the parameters a_s, b_s, c_s and d_s are the coefficients for the stoichiometric reaction. The parameters y_{CH_4}, y_{CO_2}, etc. indicate the mole fractions of the components in the anode exhaust gas. The stoichiometric reaction, Eq. (4.25), is balanced by conserving the individual atoms. The balances of each atom provide:

C: $$y_{CH_4} + y_{CO_2} + y_{CO} = b_s \tag{4.26}$$

H: $$4y_{CH_4} + 2y_{H_2} + 2y_{H_2O} = 2c_s \tag{4.27}$$

O: $$2y_{CO_2} + y_{CO} + y_{H_2O} + 2a_s y_{O_2} = 2b_s + c_s \tag{4.28}$$

N: $$2a_s y_{N_2} = 2d_s \tag{4.29}$$

4.3.2 Heat exchanger

The hot flue gas from the afterburner flows through an air pre-heater to exchange the heat for air preheating in the heat exchanger and then passes the another heat exchanger called steam generator to transfer the heat to the feed water. The water is heated and converted into a superheated steam which is used to drive a double-effect absorption chiller.

The heat recovery from heat exchanger is calculated from enthalpy change between inlet and outlet of hot and cold stream as follows:

$$Q_{hot} = Q_{cold} \tag{4.30}$$

$$Q_{hot} = \sum \dot{m}_{in,hot} h_{in,hot} - \sum \dot{m}_{out,hot} h_{out,hot} \tag{4.31}$$

$$Q_{cold} = \sum \dot{m}_{in,cold} h_{in,cold} - \sum \dot{m}_{out,cold} h_{out,cold} \tag{4.32}$$

where $\dot{m}$ is the mass flow rate and h is the enthalpy.

The total heat recovered from hot stream is not actual value because there are some heat losses occurring in the heat exchanger. Therefore, the heat exchanger efficiency at 0.5 will be added to consider heat loss in the model.

4.3.3 Compressor and pump

To supply fuel for fuel processor and SOFC, a compressor and a pump are used as auxiliary units Therefore, the required power from the compressor and pump is taken into account for calculating the system efficiency.

The work powers for compressor and pump from pressure to are shown in Eq. (4.33) and (4.34).

$$W_{cop} = \frac{\dot{m} \cdot C_p \cdot T}{\eta_{cop}} \left[\left(\frac{P_2}{P_1} \right)^{\frac{k-1}{k}} - 1 \right] \quad (4.33)$$

$$W_{pump} = \frac{\dot{m} \cdot (P_2 - P_1)}{\eta_{pump} \cdot \rho} \quad (4.34)$$

where $\dot{m}$ is mass flow rate, C_p is specific heat capacity, T is temperature before compression, k is ratio of specific heat (for diatomic gases; k=1.4), ρ is density and η is efficiency which is defined to be 75% in this study.

4.4 Absorption chiller

4.4.1 Model configuration

The performance analysis applied to the double-effect absorption chiller is similar to that used by Herold et al., (1996). The key components of a double effect absorption chiller are an evaporator, an absorber, a low pressure generator, a high pressure generator, a condenser, two solution heat exchangers, two pump, and throttling valves as shown in Figure 4.6. The heat from superheated steam is supplied to the high pressure generator ($\dot{Q}_{HP,GE}$) to obtain the primary steam and a concentrated LiBr solution. The primary vapor released from the high pressure generator is condensed in the low pressure generator, transferring the heat of condensation to the concentrated solution ($\dot{Q}_{LP,GE}$) to generate a secondary steam. The secondary stream flows to the condenser, and the most concentrated solution, which flows to the absorber. In the condenser, the heat is rejected to the external circuit ($\dot{Q}_{CO}$) to change the steam to the liquid phase. After expansion, the condensed water continues to the evaporator where it is evaporated at low pressure, removing the heat of vaporization ($\dot{Q}_{EV}$). In the absorber, the vapor contacts the concentrated solution, from the low pressure generator through the solution heat exchanger 1, to reject its heat of absorption ($\dot{Q}_{AB}$). The diluted

working solution in the absorber is then pumped to the generators, passing through solution heat exchangers 1 and 2, to continuously repeat the thermodynamic cycle.

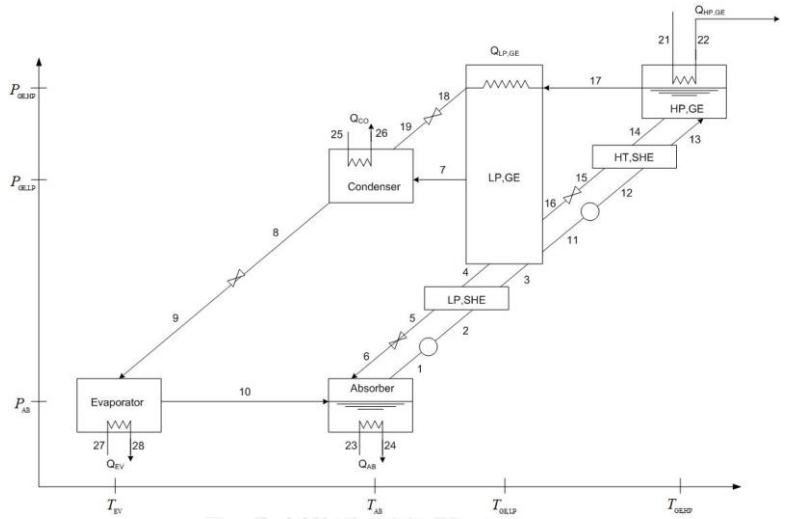

Figure 4.6 Schematic diagram of a double effect absorption chiller.

4.4.2 Mathematical models of the double effect absorption chiller

The developed model is based on the following assumptions:

- Pure water is used as a refrigerant.
- The liquid states are considered saturated liquid.
- The water from an evaporator is saturated vapor.
- The pressure in the low pressure generators and condenser are equivalent.
- The pressure in the evaporator and the absorber are equivalent.
- Heat losses and pressure drops in piping and the components are negligible.
- The expanding process in the throttling valves is isenthalpic.
- The H_2O-LiBr concentrations are zero in steam phase.

The components in the system are all defined as thermodynamic open systems, which allow mass to flow into/out of the system and exchange heat and/or work within the systems. Mass and energy balances for each component in the system with reference to Figure 4.6 are shown below under steady state condition.

Absorber

$$\dot{m}_{23} = \dot{m}_{24} \tag{4.35}$$

$$\dot{m}_1 = \dot{m}_{10} + \dot{m}_6 \tag{4.36}$$

$$\dot{m}_1 x_1 = \dot{m}_6 x_6 \tag{4.37}$$

$$\dot{m}_{10} h_{10} + \dot{m}_6 h_6 - \dot{Q}_{\mathrm{AB}} - \dot{m}_1 h_1 = 0 \tag{4.38}$$

$$\dot{Q}_{\mathrm{AB}} = \dot{m}_{23} c_{\mathrm{p}} (T_{24} - T_{23}) \tag{4.39}$$

$$UA_{\mathrm{AB}} = \dot{Q}_{\mathrm{AB}} / LMTD_{\mathrm{AB}} \tag{4.40}$$

$$LMTD_{\mathrm{AB}} = [(T_6 - T_{24}) - (T_1 - T_{23})] / \ln[(T_6 - T_{24}) / (T_1 - T_{23})] \tag{4.41}$$

Condenser

$$\dot{m}_{25} = \dot{m}_{26} \tag{4.42}$$

$$\dot{m}_8 = \dot{m}_7 + \dot{m}_{19} \tag{4.43}$$

$$\dot{Q}_{\mathrm{CO}} = \dot{m}_7 h_7 + \dot{m}_{19} h_{19} - \dot{m}_8 h_8 \tag{4.44}$$

$$\dot{Q}_{\mathrm{CO}} = \dot{m}_{25} c_{\mathrm{p}} (T_{26} - T_{25}) \tag{4.45}$$

$$UA_{\mathrm{CO}} = \dot{Q}_{\mathrm{CO}} / LMTD_{\mathrm{CO}} \tag{4.46}$$

$$LMTD_{\mathrm{CO}} = [(T_8 - T_{25}) - (T_8 - T_{26})] / \ln[(T_8 - T_{25}) / (T_8 - T_{26})] \tag{4.47}$$

Evaporator

$$\dot{m}_{27} = \dot{m}_{28} \tag{4.48}$$

$$\dot{m}_9 = \dot{m}_{10} \tag{4.49}$$

$$\dot{Q}_{\mathrm{EV}} = \dot{m}_9 (h_{10} - h_9) \tag{4.50}$$

$$\dot{Q}_{\mathrm{EV}} = \dot{m}_{27} c_{\mathrm{p}} (T_{27} - T_{28}) \tag{4.51}$$

$$UA_{\mathrm{EV}} = \dot{Q}_{\mathrm{EV}} \,/\, LMTD_{\mathrm{EV}} \tag{4.52}$$

$$LMTD_{\mathrm{EV}} = [(T_{27} - T_{10}) - (T_{28} - T_{9})] \,/\, \ln[(T_{27} - T_{10}) \,/\, (T_{28} - T_{9})] \tag{4.53}$$

High Pressure Generator

$$\dot{m}_{21} = \dot{m}_{22} \tag{4.54}$$

$$\dot{m}_{13} = \dot{m}_{14} + \dot{m}_{17} \tag{4.55}$$

$$\dot{m}_{13} x_{13} = \dot{m}_{14} x_{14} \tag{4.56}$$

$$\dot{Q}_{\mathrm{HP,GE}} = \dot{m}_{17} h_{17} + \dot{m}_{14} h_{14} - \dot{m}_{13} h_{13} \tag{4.57}$$

$$\dot{Q}_{\mathrm{HP,GE}} = \dot{m}_{21} c_{\mathrm{p}} (T_{21} - T_{22}) \tag{4.58}$$

$$UA_{\mathrm{HP,GE}} = \dot{Q}_{\mathrm{HP,GE}} \,/\, LMTD_{\mathrm{HP,GE}} \tag{4.59}$$

$$LMTD_{\mathrm{HP,GE}} = [(T_{21} - T_{14}) - (T_{22} - T_{17})] \,/\, \ln[(T_{21} - T_{14}) \,/\, (T_{22} - T_{17})] \tag{4.60}$$

Low Pressure Generator

$$\dot{m}_{17} = \dot{m}_{18} \tag{4.61}$$

$$\dot{m}_{3} + \dot{m}_{16} = \dot{m}_{4} + \dot{m}_{11} + \dot{m}_{7} \tag{4.62}$$

$$\dot{m}_{3} x_{3} + \dot{m}_{16} x_{16} = \dot{m}_{4} x_{4} + \dot{m}_{11} x_{11} \tag{4.63}$$

$$\dot{m}_{3} h_{3} + \dot{m}_{16} h_{16} + \dot{m}_{17} h_{17} = \dot{m}_{4} h_{4} + \dot{m}_{11} h_{11} + \dot{m}_{18} h_{18} + \dot{m}_{7} h_{7} \tag{4.64}$$

$$\dot{Q}_{\mathrm{LP,GE}} = \dot{m}_{17} (h_{17} - h_{18}) \tag{4.65}$$

$$UA_{\mathrm{LP,GE}} = \dot{Q}_{\mathrm{LP,GE}} \,/\, LMTD_{\mathrm{LP,GE}} \tag{4.66}$$

$$LMTD_{\mathrm{LP,GE}} = [(T_{18} - T_4) - (T_{18} - T_7)] / \ln[(T_{18} - T_4) / (T_{18} - T_7)] \quad (4.67)$$

High Temperature Solution Heat Exchanger

$$\dot{m}_{12} = \dot{m}_{13} \quad (4.68)$$

$$\dot{m}_{14} = \dot{m}_{15} \quad (4.69)$$

$$\dot{m}_{12} x_{12} = \dot{m}_{13} x_{13} \quad (4.70)$$

$$\dot{m}_{14} x_{14} = \dot{m}_{15} x_{15} \quad (4.71)$$

$$\dot{m}_{11}(h_{13} - h_{12}) = \dot{m}_{14}(h_{14} - h_{15}) \quad (4.72)$$

Low Temperature Solution Heat Exchanger

$$\dot{m}_2 = \dot{m}_3 \quad (4.73)$$

$$\dot{m}_4 = \dot{m}_5 \quad (4.74)$$

$$\dot{m}_2 x_2 = \dot{m}_3 x_3 \quad (4.75)$$

$$\dot{m}_4 x_4 = \dot{m}_5 x_5 \quad (4.76)$$

$$\dot{m}_1(h_3 - h_2) = \dot{m}_4(h_4 - h_5) \quad (4.77)$$

Lower Solution Expansion Valve

$$\dot{m}_5 = \dot{m}_6 \quad (4.78)$$

$$\dot{m}_5 x_5 = \dot{m}_6 x_6 \quad (4.79)$$

$$h_5 = h_6 \quad (4.80)$$

Upper Solution Expansion Valve

$$\dot{m}_{15} = \dot{m}_{16} \tag{4.81}$$

$$\dot{m}_{15} x_{15} = \dot{m}_{16} x_{16} \tag{4.82}$$

$$h_{15} = h_{16} \tag{4.83}$$

Lower Refrigerant Expansion Valve

$$\dot{m}_{8} = \dot{m}_{9} \tag{4.84}$$

$$\dot{m}_{8} x_{8} = \dot{m}_{9} x_{9} \tag{4.85}$$

$$h_{8} = h_{9} \tag{4.86}$$

Upper Refrigerant Expansion Valve

$$\dot{m}_{18} = \dot{m}_{19} \tag{4.87}$$

$$\dot{m}_{18} x_{18} = \dot{m}_{19} x_{19} \tag{4.88}$$

$$h_{18} = h_{19} \tag{4.89}$$

Lower Pump

$$\dot{m}_{1} = \dot{m}_{2} \tag{4.90}$$

$$\dot{m}_{1} x_{1} = \dot{m}_{2} x_{2} \tag{4.91}$$

$$Pump_{1} = \dot{m}_{1} v_{1} (P_{\mathrm{m}} - P_{\mathrm{l}}) \tag{4.92}$$

$$h_{2} = h_{1} + Pump_{1} / \dot{m}_{1} \tag{4.93}$$

Upper Pump

$$\dot{m}_{11} = \dot{m}_{12} \tag{4.94}$$

$$\dot{m}_{11} x_{11} = \dot{m}_{12} x_{12} \tag{4.95}$$

$$Pump_2 = \dot{m}_{11} v_{11} (P_{\mathrm{h}} - P_{\mathrm{m}}) \tag{4.96}$$

$$h_{12} = h_{11} + Pump_2 / \dot{m}_{11} \tag{4.97}$$

where $\dot{m}$ is mass flow rate, C_{p} is specific heat capacity of water, x is LiBr concentration fraction, P_{h}, P_{m}, P_{l} are high, medium and low pressures respectively, v is volume of substance per unit mass, $LMTD$ is log mean temperature difference and UA represents the heat exchanger size which is reported in Table 4.4.

Table 4.4 Input data for the double-effect absorption chiller

$UA_{\mathrm{HP,GE}}$	1.25 kW/K
$UA_{\mathrm{LP,GE}}$	0.5 kW/K
UA_{CO}	3.25 kW/K
UA_{EV}	4 kW/K
UA_{AB}	2.5 kW/K

4.4.2 Absorption chiller efficiency

Thermal Efficiency is measured in terms of cooling output. The evaporator cooling capacity ($\dot{Q}_{\mathrm{EV}}$) is calculated as Eq. (4.36). The cooling capacity of an absorption cycle is defined as the performance of the evaporator that removes heat from water to produce the chilled water.

$$\dot{Q}_{EV} = \dot{m}_{27}(h_{27} - h_{28}) \quad (4.98)$$

4.4.3 Model validation

The analysis of the double-effect absorption chiller was validated by Somers et al., (2011), as shown in Table 4.5. This Table details the model validation performed for the double effect cycle by comparing the significant parameters, including the heat duty of each component. The results are promising in that no parameter exceeds a 5% error, with most discrepancies below or near 1%.

Table 4.5 Double effect cycle verification using the literature of Somers et al. (2011)

Parameters	**Current Study**	**Somers et al. (2011)**	**Discrepancy[a] (%)**
Low pressure (kPa)	0.881	0.8805	0.06
Middle pressure (kPa)	4.178	4.1776	0.01
High pressure (kPa)	64.298	64.37	0.11
Concentration, LiBr strong solution (%)	52.76	52.72	0.08
Concentration, LiBr weak solution (%)	61.96	61.6	0.58
$\dot{Q}_{AB}$ (kW)	436	421.25	3.50
$\dot{Q}_{LP,GE}$ (kW)	192.68	189.86	1.49
$\dot{Q}_{CO}$ (kW)	185.62	188.58	1.57
$\dot{Q}_{EV}$ (kW)	354.2	354.37	0.05
$\dot{Q}_{HP,GE}$ (kW)	267.4	255.43	4.69
COP (–)	1.325	1.387	4.47

[a] Discrepancy (%) = $\frac{|\text{Current value} - \text{Published data}|}{\text{Published data}} \times 100\%$

4.5 Analysis tools

4.5.1 Energy and exergy analyses

Under the steady-state condition, a conservation balance equation around each unit operation in the reforming process can be written as follows (Cohce et al., 2011):
Mass balance:

$$\sum_{i=1}^{N} \dot{m}_{i,in} = \sum_{i=1}^{N} \dot{m}_{i,out} \tag{4.99}$$

Energy balance:

$$\dot{Q}_{cv} - \dot{W}_{cv} = \sum_{out} \dot{n}_i h_i - \sum_{in} \dot{n}_i h_i \tag{4.100}$$

where $\dot{n}_i$ and h_i represent the molar flow rate and specific molar enthalpy, respectively, of the flow stream into and out of each component in the system.

Unlike energy, exergy is not conserved. Exergy is defined as the maximum work that can be extracted from a system interacting with a reference environment. Exergy destruction is an important parameter in exergy analysis. It is formulated as the potential work lost as a

Exergy balance:

$$\dot{E}x_d = \sum \left(1 - \frac{T_0}{T}\right) \dot{Q}_{cv} - \dot{W}_{cv} + \sum_{in} \dot{n}_i ex_i - \sum_{out} \dot{n}_i ex_i \tag{4.101}$$

where ex_i is the specific molar flow exergy for each component of the inlet and outlet flow streams. The subscript i is the property value at state i, and the subscript 0 is the value of a property in the surroundings. The comparison of energy and exergy balances is shown in Figure 4.7.

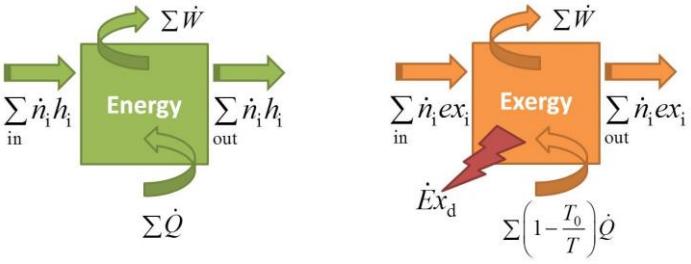

Figure 4.7 Comparison of energy and exergy balances.

The exergy can be defined by neglecting the kinetic and potential energy changes as follows:

$$ex_i = (h_i - h_0) - T_0(s_i - s_0) + ex_{ch} \tag{4.102}$$

The specific chemical exergy (ex_{ch}) of different species in a gas mixture is defined as

$$ex_{ch} = \sum y_i \cdot ex_{ch,i} + RT_0 \sum y_i \cdot \ln y_i \tag{4.103}$$

where $ex_{ch,i}$ is the specific molar chemical exergy of the flow streams and y_i is the molar fraction of the gas species i in the gas mixture. The standard molar chemical exergies of relevant substances are shown in Table 4.6. The enthalpy and entropy for each component of the gas are calculated using thermophysical property functions in Aspen Plus or EES (Engineering Equation Solver) as a function of the temperature and/or pressure. The equations used to calculate the efficiency of the system are presented in Table 4.7.

Table 4.6 The standard molar chemical exergy of selected substances at reference states (T0 = 298.15 K, P0 = 101.325 kPa) (Szargut et al., 1988).

Substance	**State**	**Exergy (kJ/kmol)**
C_2H_6O	g	1363900
	l	1357700
CH_4	g	831650
CO	g	275100
CO_2	g	19870
H_2	g	236100
H_2O	g	9500
	l	900
O_2	g	3970
N_2	g	720
C	s, graphite	410260

Table 4.7 Efficiency equations of the system (Al-Sulaiman F.A. et al., 2011).

Total energy in	$\dot{Q}_{in} = \dot{m}_{C_2H_5OH} \cdot \mathrm{LHV}_{C_2H_5OH}$
The net electrical power of the system	$\dot{W}_{net} = \eta_{inverter} \cdot \dot{W}_{SOFC,DC}$
The heating power	$\dot{Q}_h = \dot{m}_{HP} \cdot (h_{HP,2} - h_{HP,1})$
The cooling load of the evaporator	$\dot{Q}_c = \dot{m}_{EV} \cdot (h_{EV,1} - h_{EV,2})$
The electrical to heating ratio	$r_{el,h} = \dot{W}_{net} / \dot{Q}_h$
The electrical to cooling ratio	$r_{el,c} = \dot{W}_{net} / \dot{Q}_c$
Net electrical efficiency of the cycle	$\eta_{el} = \dot{W}_{net} / \dot{Q}_{in}$
The efficiency of the heating cogeneration	$\eta_{cog,h} = \frac{\dot{W}_{net} + \dot{Q}_h}{\dot{Q}_{in}}$
The efficiency of the cooling cogeneration	$\eta_{cog,c} = \frac{\dot{W}_{net} + \dot{Q}_c}{\dot{Q}_{in}}$
The efficiency of trigeneration	$\eta_{tri} = \frac{\dot{W}_{net} + \dot{Q}_h + \dot{Q}_c}{\dot{Q}_{in}}$
the fuel chemical exergy	$\dot{E}x_f = \dot{n}_{C_2H_5OH} \cdot Ex_{C_2H_5OH}$
The net electrical exergy efficiency	$\psi_{el} = \dot{W}_{net} / \dot{E}x_f$
The heating-cogeneration exergy efficiency	$\psi_{cog,h} = \frac{\dot{W}_{net} + \left(1 - \left(\frac{T_0}{T_{HP}}\right)\right) \cdot \dot{Q}_h}{\dot{E}x_f}$
The exergy efficiency of the cooling cogeneration	$\psi_{cog,c} = \frac{\dot{W}_{net} + \left(1 - \left(\frac{T_0}{T_{EV}}\right)\right) \cdot \dot{Q}_c}{\dot{E}x_f}$
The trigeneration exergy efficiency	$\psi_{tri} = \frac{\dot{W}_{net} + \left(1 - \left(\frac{T_0}{T_{HP}}\right)\right) \cdot \dot{Q}_h + \left(1 - \left(\frac{T_0}{T_{EV}}\right)\right) \cdot \dot{Q}_c}{\dot{E}x_f}$

4.5.2 Exergoenvironmental analysis

Energy conversion processes should be designed by reducing an environmental impact, resulting in the improved process performance. Because CO_2 emission is a significant issue, a reduction in this greenhouse gas in the afterburner of the SOFC system can lead to the improvement of the cycle. The normalized CO_2 emissions of the trigeneration system can be expressed as follows:

$$Emi(\mathrm{CO_2}, \mathrm{tri}) = \frac{\dot{m}_{\mathrm{CO_2}}}{(\dot{W}_{\mathrm{SOFC}} + \dot{Q}_{\mathrm{h}} + \dot{Q}_{\mathrm{c}})} \tag{4.104}$$

To achieve sustainability, energy conversion processes must be employed indicators that define and quantify the subsystems involved in the process. For the properties which are not directly measurable, it should be used assessment tools in order to obtain their indicators. The exergy analysis is an example of these tools, very useful in the evaluation of energy conversion processes, being a strong indicator, namely exergy destruction. Finally it is necessary to relate this indicator in order to express the overall process in a single value through a sustainability index which is used to relate the exergy with environmental impact as:

$$SI = \frac{1}{D_{\mathrm{P}}} \tag{4.105}$$

where D_{P} is the depletion number, which is defined as the exergy destruction/input exergy. This relation demonstrates how reducing a system's environmental impact can be achieved by reducing its exergy destruction (Rosen et al., 2008; Dincer and Naterer, 2010).

CHAPTER V

COMPARISON OF HYDROGEN PRODUCTION FROM ETHANOL REFORMING PROCESSES

This chapter presents the application of a thermodynamic concept to identify a suitable reforming process for an ethanol-fueled solid oxide fuel cell (SOFC). Three different reforming technologies, i.e., steam reforming, partial oxidation and autothermal reforming, are considered. The first and second laws of thermodynamics are employed to determine an energy demand and to describe how efficiently the energy supplied to the reforming process and to identify the best ethanol reforming process for SOFC applications.

5.1 Introduction

As mentioned earlier, ethanol is a very attractive green fuel as it is produced by fermentation of agricultural products and easy to handle as a liquid fuel (Cardona and Sánchez, 2007). There are several methods to produce hydrogen rich gas from ethanol. A steam reforming is among the widely used processes due to its high hydrogen yield; however, this process involves a highly endothermic reaction and requires high energy supply. To minimize the external heat input, partial oxidation and autothermal reforming are alternative routes for hydrogen production (Rabenstein and Hacker, 2008). Because SOFC is operated at high temperatures and a waste heat recovery is generally included in the SOFC system to enhance its performance, a selection of appropriate fuel processing technology should be also takes an efficient energy usage into account.

In this study, the first and second laws of thermodynamics are applied to analysis of an ethanol reforming process to produce hydrogen fuel. Three different reforming methods, i.e., steam reforming, partial oxidation and autothermal reforming, are considered. Effects of key operating parameters, such as reactant feed ratio and operating reforming temperatures, on the equilibrium composition of reforming

products are also presented. The performance assessment of each ethanol reforming process in terms of product yield, carbon-free operational region and energy usage is carried out in detail with the aim to optimize the process operation. Based on the second law of thermodynamics, the comprehensive analysis of an exergy destruction in different ethanol reforming processes is also discussed. Finally, the application of the ethanol reforming to produce hydrogen for SOFC is also commented.

5.2 Methodology

In order to find the optimal operating conditions of the ethanol reforming, thermodynamic analysis of ethanol reforming processes is performed based on steady-state. The equilibrium composition of the reforming products was determined by the minimization of a total Gibbs free energy as mentioned in section 4.1.1. To provide the highest SOFC performance without facing a carbon formation problem, an analysis of the effect of key design parameters on the reformer performance is first performed. Table 5.1 shows a range of operating conditions under consideration in this study (Rabenstein and Hacker, 2008; Sun et al., 2012).

Table 5.1 Range of operating conditions for different ethanol reforming processes.

Ethanol Reforming Processes	Temperature (K)	S/E	O/E
Steam Reforming	700-1200	0-10	-
Partial Oxidation	700-1400	-	0-3
Autothermal Reforming	700-1200	0-10	0-3

Energy and exergy efficiencies are evaluated as a ratio of products to inputs. For the overall electrical efficiency, the energy efficiency η is evaluated as:

$$\eta = \frac{\text{net energy output with electricity}}{\text{energy input}} \tag{5.1}$$

and the exergy efficiency ψ as:

$$\psi = \frac{\text{net exergy output with electricity}}{\text{exergy input}} \tag{5.2}$$

5.3 Results and discussion

5.3.1 Effect of temperature and reactant ratios on product distribution

Effects of reforming temperatures, steam-to-ethanol (S/E) ratio and oxygen-to-ethanol (O/E) ratio on the product yields of the ethanol reforming processes, i.e., steam reforming, partial oxidation and autothermal reforming, are given in Figure 5.1 (a)-(c), respectively. A carbon free region of reformer operation is also presented in the figure, so that it will be easy to choose the reforming operational conditions without the formation of carbon. The results clearly indicate that the carbon formation is prone to be occurred when the reformer is operated at low ratio of the reforming reagents for all operating temperatures. It is noted that the intermediate by-products, such as acetaldehyde and ethylene, appears to be a very low content compared with other reforming products.

For the ethanol steam reforming process, H_2 yield increases with the increased temperature and S/E ratio. Severe operating conditions are required to avoid the carbon formation. At temperatures higher than 800 K, CH_4 is nearly converted to other reforming products, whereas CO, one of the carbon promoters, is not present in the reforming products at low-temperature operation as a result of the exothermicity of the water gas shift reaction. In order to maximize the SOFC performance, the optimal operating conditions for the reformer is chosen to give high hydrogen fraction without the formation of carbon. When considering the partial oxidation of ethanol, the maximum H_2 and CO yields are found at high operating temperatures (T = 1200-1400 K) and low oxygen-to-ethanol ratio operation (O/E < 0.5); however, the formation of carbon is unavoidable under these conditions. Thus, it seems that the partial oxidation of ethanol is not a suitable process for hydrogen production. In case of the ethanol autothermal reforming process, oxygen is introduced to the reformer at the oxygen-to-ethanol ratio of 0.61, according to the stoichiometric ratio of the reaction (Eq. (3.12)) in section 3.3.3. Figure 5.1 (c) shows that the product distribution of the autothermal

reforming process is similar to that of the steam reforming process and the maximum H_2 yield is obtained under the operating temperature above 900 K and the S/E higher than 6; however, high CO_2 is observed under these conditions. A promising advantage of this process is a lower carbon formation activity. When the operating temperature is higher than 1100 K, there is no carbon formation.

(a)

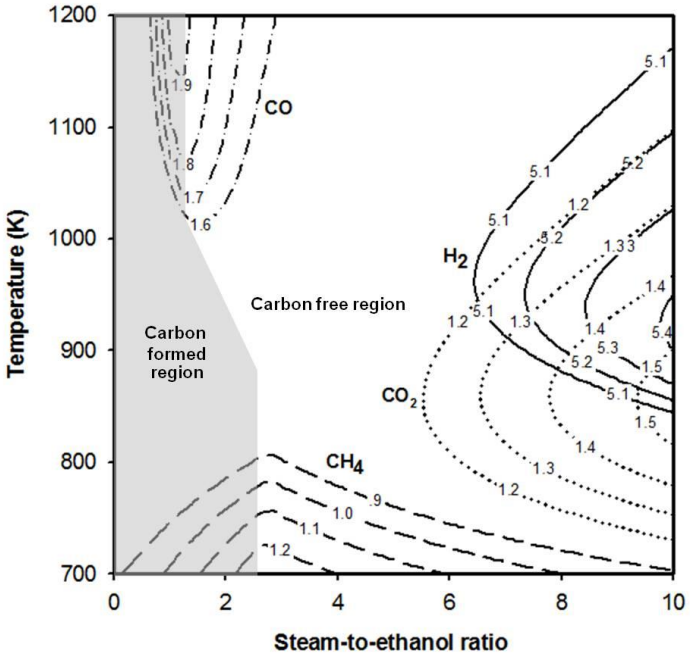

(b)

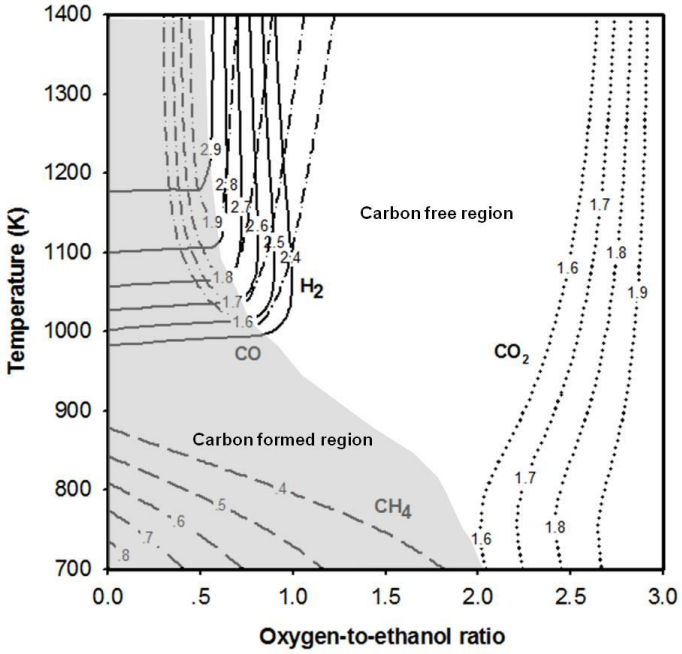

(c)

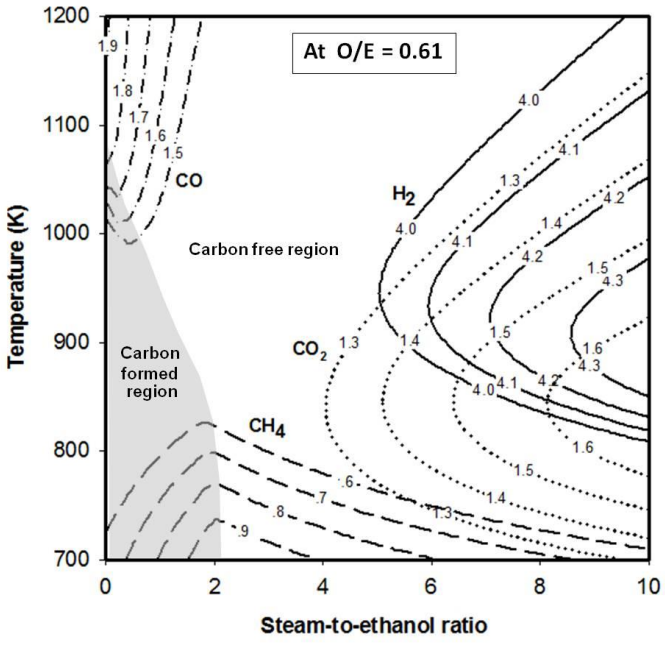

Figure 5.1 Effect of temperatures and feed ratio on the product yields: (a) steam reforming, (b) partial oxidation and (c) autothermal reforming (grey area is the carbon formed region and a number on the line is the amount of gaseous products (mole/mole of ethanol feed)).

5.3.2 Effect of temperature and reactant ratios on SOFC efficiency and heat duty

Figure 5.2 shows the effects of feed ratio of ethanol to reforming reagents and operating temperatures on the SOFC efficiency and heat duty required by the reformer. It shows that an increase in the reforming reagents (i.e., H_2O and/or O_2) degrades the efficiency of SOFC because the excess of water causes a fuel dilution effect and the presence of more oxygen enhances the CO oxidation, leading to a decrease in hydrogen fuel. The steam reforming process operated at high temperatures requires more heat duty (Figure 5.2(a)). To achieve the maximum SOFC efficiency ($\approx$67.5%), the steam reformer should be operated at temperatures higher than 1000 K and S/E ratio of 1.5; however, under these conditions, the system needs the high level of energy input and faces the carbon formation problem. Thus, the reformer is suggested to be run at a lower temperature (T = 980 K) and more steam input is required (S/E = 1.8) to move the operating point to a carbon free region (star symbol in Figure 5.2(a)). Regarding the partial oxidation process as shown in Figure 5.2(b), the reformer heat duty depends on the quantity of O_2 feed. If the oxygen-to-ethanol ratio increases, high heat will be released due to the exothermicity of the partial oxidation reaction. However, the SOFC fed by the synthesis gas from the partial oxidation reactor generates less electricity power than that from other reforming processes. When considering the performance of SOFC and the avoidance of carbon formation in the reactor, the partial oxidation reformer is selected to be operated at the temperature of 1150 K and the O/E ratio of 0.6. Figure 5.2(c) shows effect of the amount of reforming agents, i.e., steam and oxygen, on the heat duty of the autothermal reformer (operated at 1000 K) and the efficiency of SOFC. The SOFC efficiency is enhanced when less oxygen is introduced to the autothermal reformer. In general, a heat duty of the autothermal reforming is a key operational factor for this process. The results indicate that the endothermic steam reforming and the exothermic partial oxidation can be balanced by adjusting oxygen feed to reach a thermal-neutral operation, which an external heat input is unnecessary. To achieve the maximum efficiency while minimizing the energy demand, the autothermal reformer should be operated at temperature of 1000, S/E ratio of 1.5 and O/E ratio of 0.5 and thus, the SOFC efficiency of 56% is obtained. The selected operating conditions of different ethanol reforming processes are summarized in Table 5.2.

(a)

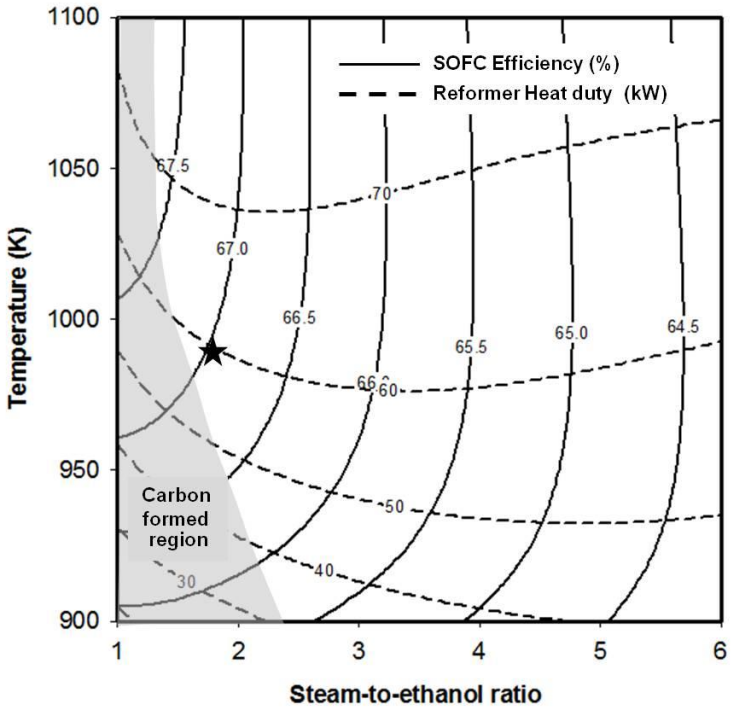
SOFC Efficiency (%)
Reformer Heat duty (kW)
Temperature (K)
Steam-to-ethanol ratio
Carbon formed region
67.5
67.0
66.5
66.0
65.5
65.0
64.5
70
60
50
40
30
1100
1050
1000
950
900
1
2
3
4
5
6

(b)

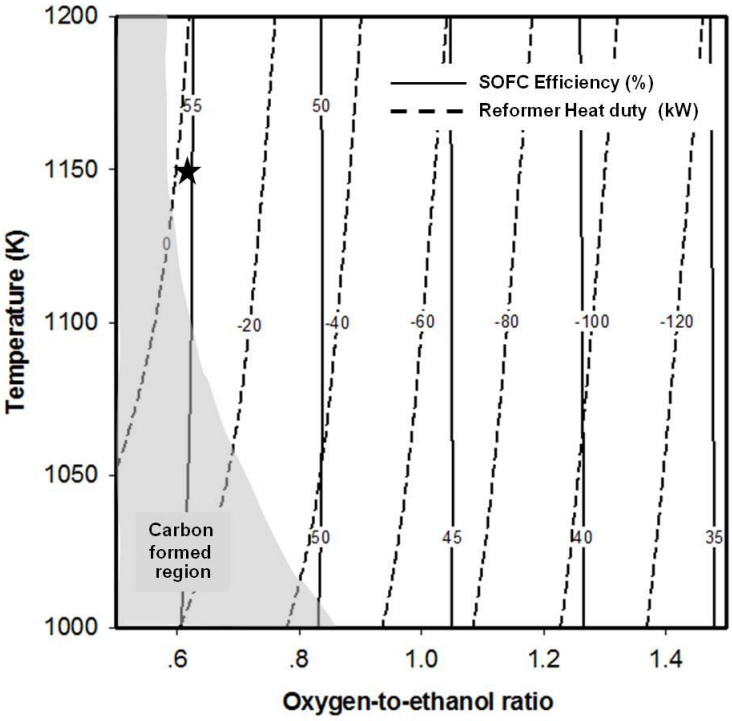
SOFC Efficiency (%)
Reformer Heat duty (kW)
Temperature (K)
Oxygen-to-ethanol ratio
Carbon formed region
55
50
45
40
35
0
-20
-40
-60
-80
-100
-120
1200
1150
1100
1050
1000
.6
.8
1.0
1.2
1.4

(c)

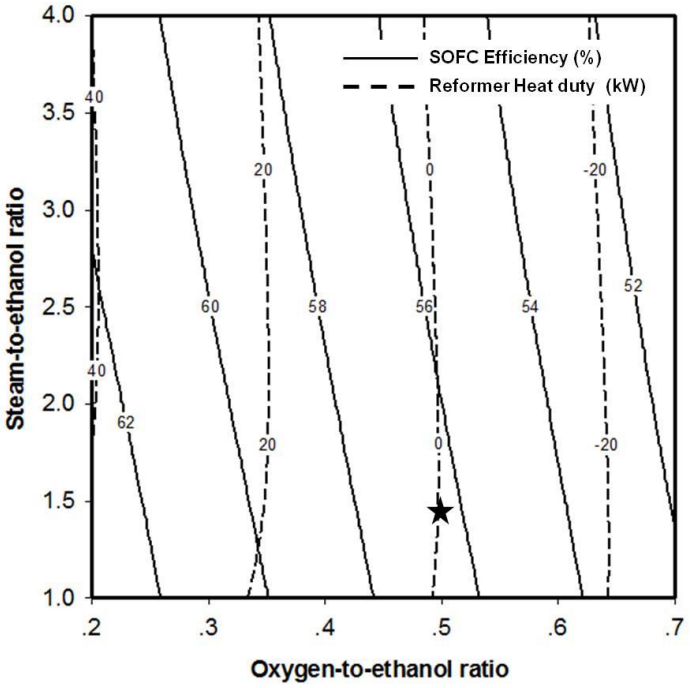

Figure 5.2 Effect of temperatures and feed ratio on SOFC efficiency and reformer heat duty: (a) steam reforming, (b) partial oxidation and (c) autothermal reforming.

Table 5.2 Optimal conditions for each ethanol reforming process

Ethanol Reforming Processes	T (K)	S/E	O/E	SOFC Efficiency (%)	Reformer Heat Duty (kW)
Steam Reforming (SR)	980	1.8	-	66.89	61.20
Partial Oxidation (POX)	1150	-	0.6	55.60	-7.22
Autothermal Reforming (ATR)	1000	1.5	0.5	56.36	-0.32

5.3.3 Energy and exergy analyses

A comparison of the energy demand for the ethanol reforming processes operated at their optimal conditions is shown in Figure 5.3(a). It is found that the steam reforming of ethanol requires the highest energy consumption process because of extremely endothermic operation, whereas the partial oxidation process needs the lowest one. In the partial oxidation process, the heater is a unit that needs the highest energy because preheating air requires high amount of energy. However, the heat requirement in the evaporator is lower than the other two reforming processes because only liquid ethanol is evaporated. When considering the total energy demand of the fuel processor including the evaporator, heater and reformer, the partial oxidation process seems to be operated at a thermoneutral condition. A steam requirement of the steam reforming and autothermal reforming processeses causes a higher heat load in the evaporator.

Figure 5.3(b) shows the exergy destruction in each unit of the ethanol reforming processes. In general, a process unit involved chemical reactions affects the overall process irreversibility because chemical reactions are related to the motion of electrons during forming and breaking chemical bonds between atoms. High frequency of molecular collisions causes an increase in entropy within the system, resulting in high exergy destruction. For the reforming processes to produce hydrogen, the ethanol reformer dominates the total rate of exergy destruction. The partial oxidation reactor is the unit that causes the highest exergy destruction because its flow of exergy is associated with a large difference in heat transfer between reactant feed (input) and synthesis gas product (output). In other words, exothermic or combustion processes lose more the exergy of heat. In addition, the partial oxidation is operated at higher temperature than other processes. For this reason, reactant and product gases will spread quickly and collide with each other frequently, so the entropy is more generated and then destroys some exergy. On the other hand, the steam reformer can maintain the quality of energy as shown in a reformer part of the steam reforming process (Figure 5.3(b)). The results also indicate that in the evaporator, high value of the energy demand turns into an excellent exergetic performance. The total exergy destruction in the ethanol reforming processes follows in order: partial oxidation > autothermal reforming > steam reforming.

(a)

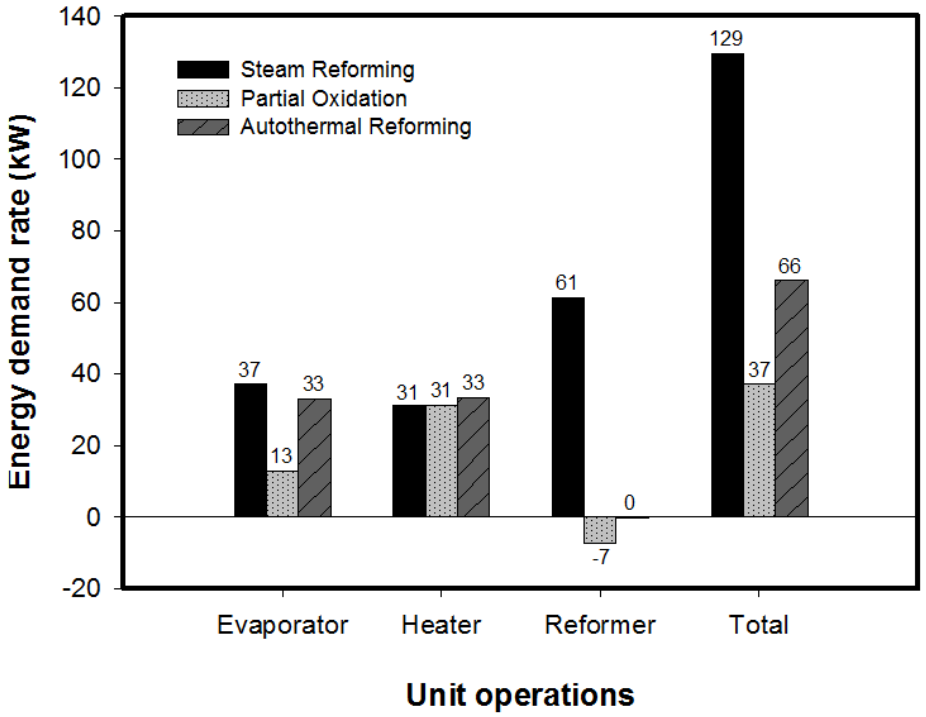

(b)

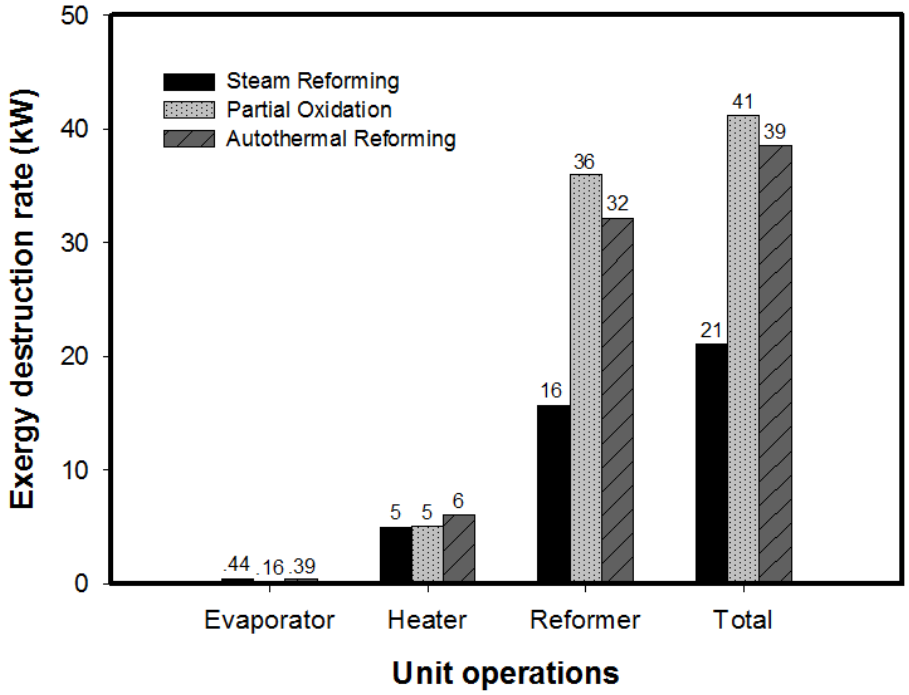

Figure 5.3 Comparison of (a) energy demand and (b) exergy destruction in different ethanol reforming processes at the optimal operating conditions.

Table 5.3 Energy and exergy efficiencies of ethanol reforming processes and their exergy destruction in the SOFC system

Ethanol Reforming Processes	**Efficiency (%)**		**Exergy destruction**
	Energy	Exergy	(kW)
Steam Reforming (SR)	66.89	60.60	21.11
Partial Oxidation (POX)	55.60	50.37	41.24
Autothermal Reforming (ATR)	56.36	51.06	38.58

5.3.4 Ethanol reforming process for solid oxide fuel cell applications

Based on the thermodynamic analysis, an implementation of the ethanol reforming processes for SOFC applications is addressed from a practical point of view. It is found that the ethanol steam reforming process requires high energy consumption and thus its integration with the SOFC is preferable as the high quality of an exhaust gas from the anode and afterburner can be employed in the steam reforming process, e.g., evaporation and heating units, as shown in Figure 5.4. The SOFC system consists of three main parts: (1) fuel processor where ethanol is converted into hydrogen-rich gases, (2) SOFC where electricity is generated from the electrochemical reaction of hydrogen and oxygen and (3) afterburner where the residual fuel from the SOFC is combusted in order to generate useful heat for other heat requiring parts of the SOFC system. The autothermal reforming process can be managed without the need for external heat sources, leading to a simpler design and higher reforming efficiency. Therefore, it would be more suitable for automobile, residential and portable applications (Lin et al., 2007; Dawes et al., 2009). From the thermodynamic viewpoint, the partial oxidation of ethanol is not a good option for hydrogen production. Although, this process requires less energy demand, its exergetic efficient is low due to the high-temperature operation. In addition, it generates the reformate gas with high CO content and thus, needs a purification process to give more pure hydrogen. It is noted that the autothermal reforming and the partial oxidation of ethanol have lower energy and exergy efficiencies, even though exhaust gases from the anode and afterburner are used in evaporation and heating units. Table 5.3 summarizes the energy and exergy

efficiencies of the ethanol reforming processes and their exergy destruction in the SOFC system.

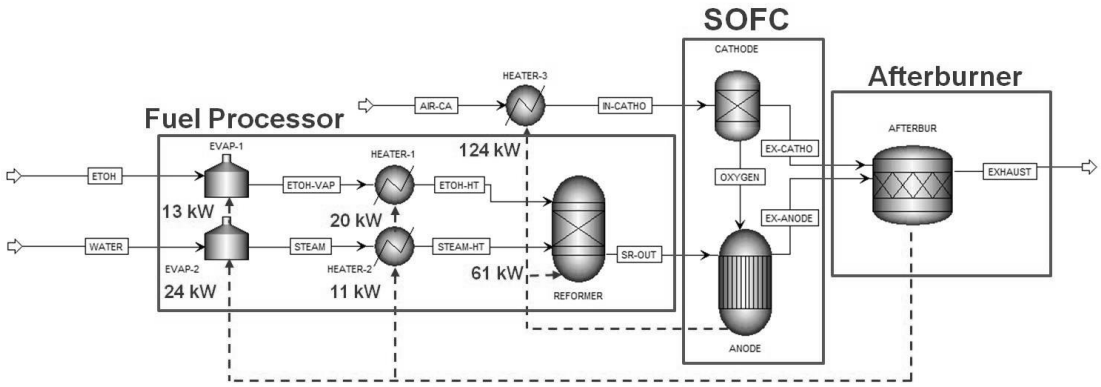

Figure 5.4 Ethanol steam reforming integrated with solid oxide fuel cell system.

5.4 Conclusions

Thermodynamic analysis of different ethanol reforming processes was performed. The optimal operating conditions of each reforming process to maximize the SOFC efficiency were identified. Energy and exergy analysis were also carried out to find the best ethanol reforming process. Although the steam reforming process provides the highest hydrogen yield, it is the highest energy requiring process. The exergy analysis showed that the highest exergy destruction is found in the partial oxidation process. The integration of ethanol steam reformer operated at temperature of 980 K and steam-to-ethanol ratio of 1.8 and solid oxide fuel cell provides the best energetic and exergetic performances.

CHAPTER VI

A TWO-STEP ETHANOL STEAM REFORMING FOR CARBON-FREE HYDROGEN PRODUCTION

This chapter presents the use of a two-step ethanol steam reforming, which consists of ethanol dehydrogenation and steam reforming, as a fuel processor to replace a conventional ethanol steam reforming (single step steam reforming) for carbon-free hydrogen production. The effect of intermediates, the number of reforming steps, the dehydrogenation temperatures, the reforming temperatures and feed ratios on product yield and carbon formation is studied. The carbon-free hydrogen production in the two-step ethanol steam reforming system is analyzed, and the optimal operating conditions are discussed.

6.1 Introduction

Fuel cells utilize hydrogen as an important energy carrier to convert chemical energy into electricity via an electrochemical reaction. Hydrogen does not exist by itself on Earth; however, it can be produced from a wide variety of sources, e.g., natural gas, coal, oil, and water, by using several modern process technologies (Parthasarathy and Narayanan, 2014). Currently, the most commonly used and economically competitive method for hydrogen production is the steam reforming of natural gas (Angeli et al., 2014; De Falco et al., 2014). However, natural gas is a limited and non-renewable fossil fuel. Therefore, it is interesting to explore the production of hydrogen from other renewable resources.

Ethanol presents several advantages compared with other fuels, such as methanol, gasoline, LPG and methane, due to its natural availability, storage and handling safety, high heat of vaporization and low photochemical reactivity. Bio-ethanol can be produced renewably by biomass fermentation. Carbon dioxide produced in the process is consumed by biomass growth, and thus, the reforming of biomass-derived ethanol does not contribute to global warming. Saebea et al., (2013) showed

that ethanol is a suitable fuel for solid oxide fuel cell system because of lower CO_2 emission, compared to the use of other fuels, such as, glycerol and biogas. Moreover, it is observed from our previous work that the ethanol steam reforming process operated with a fuel cell also provides the best energetic and exergetic performances (Tippawan and Arpornwichanop, 2014). Although the steam reforming process is widely used in the chemical industry, steam reforming of ethanol for hydrogen production involves a complex multiple reaction system, and thus, the purity of hydrogen product is affected by many undesirable by-products. This factor causes the hydrogen yield to depend on a complex manner of process variables, such as pressure, temperature and ratio of reactants. To maximize the yield of hydrogen, it is necessary to determine the effect of these variables on the product composition (Fishtik et al., 2000).

For the complete ethanol steam reforming reaction, ethanol reacts with steam in the most desirable way, and only hydrogen and CO_2 are produced, as shown in Eq. (6.1). However, there are several reaction pathways that could occur in the ethanol/water system, depending on the catalysts used. Various types of intermediate by-products, such as acetaldehyde and ethylene, usually form, and the main problems during the ethanol steam reforming involve catalyst coking and formation of undesirable products (Freni S. et al., 2000). Ethanol can be transformed to ethylene through the dehydration reaction, as shown in Eq. (6.2). In addition, it is well known that carbon formation increases dramatically in the presence of ethylene via polymerization, as shown in Eq. (6.3). Lima da Silva et al., (2009) studied the thermodynamic conditions of carbon deposition in ethanol steam reforming and observed that ethanol is preferentially converted into ethylene, which promotes carbon deposition through ethylene polymerization. Considering this problem, it is reasonable to first convert ethanol into species with lower coking activities and only then convert these species into hydrogen-rich gas. Acetaldehyde is one of the desired species that can be easily produced from ethanol dehydrogenation and is favored during relatively low temperature operations (Freni S. et al., 2000; Nishiguchi et al., 2005).

$$C_2H_5OH + 3H_2O \rightarrow 6H_2 + 2CO_2 \qquad (6.1)$$

$$C_2H_5OH \rightarrow C_2H_4 + H_2O \quad (6.2)$$

$$C_2H_4 \rightarrow \text{polymer} \rightarrow 2H_2 + 2C \quad (6.3)$$

Therefore, the objective of this study is to thermodynamically analyze the ethanol steam reforming reaction mechanisms for carbon-free hydrogen production. In this approach, the ethanol steam reforming process is divided into two steps: dehydrogenation and steam reforming. First, ethanol is dehydrogenated to acetaldehyde in the dehydrogenation unit, which is not in the presence of the water stream. Second, the gas product from the first unit is fed into the steam reforming environment to produce more hydrogen and reduce the amount of reactants for carbon formation (methane and carbon monoxide) by methane steam reforming and water-gas shift, respectively. The effect of operating conditions on equilibrium compositions, carbon formation boundary is studied and discussed.

6.2 Methodology

6.2.1 Thermodynamic analysis

A thermodynamic analysis of ethanol steam reforming process was performed by using the commercial software Aspen Plus® to investigate the effect of reaction mechanisms and operating parameters, such as the dehydrogenation and steam reforming temperatures and the steam-to-ethanol molar ratio (S/E), on the carbon formation of hydrogen production. The minimization of total Gibbs free energy is a common method to determine the equilibrium compositions of hydrogen-rich gas. The equation of state used in the calculation was the Peng-Robinson method. The species considered in the calculations throughout this study depended on the reaction pathways as shown in Table 6.1. However, acetaldehyde is considered to be a desirable intermediate compound during ethanol reforming to avoid the carbon formation. From thermodynamic point of view, it is assumed that carbon formed is elemental or in the graphitic form. In this study, the results of carbon formation were compared with the different pathways. Furthermore, the dehydrogenation temperature, reforming temperature, and steam-to-ethanol molar ratio (S/E) are varied to find its optimal operating condition and to investigate the energy usage.

6.2.2 Possible pathways in the ethanol steam reforming system

There are four reaction pathways that can be feasible in ethanol/water environment. Conventional pathway has the all of general species of ethanol steam reforming process. To focus on the carbon formation via intermediates, other pathways have different species of ethylene or acetaldehyde. However, in the last case it is need to show the ethanol steam reforming via acetaldehyde as the intermediate into two steps because ethanol favors dehydrogenation in the absence of water stream. Possible pathways and their considered compositions are shown in Table 6.1

Table 6.1 Possible pathways in the ethanol steam reforming system.

Possible pathways	Considered compositions
Conventional 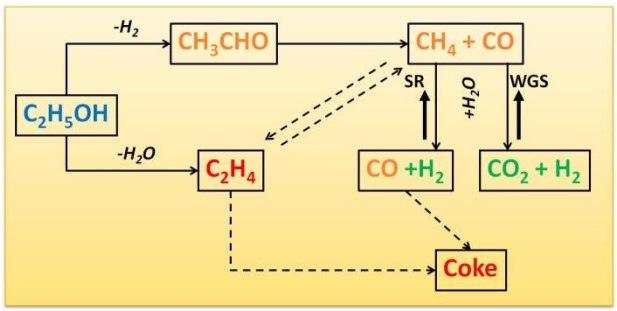	C_2H_5OH, H_2O, CH_3CHO, C_2H_4, H_2, CH_4, CO_2, CO, C
Via Ethylene 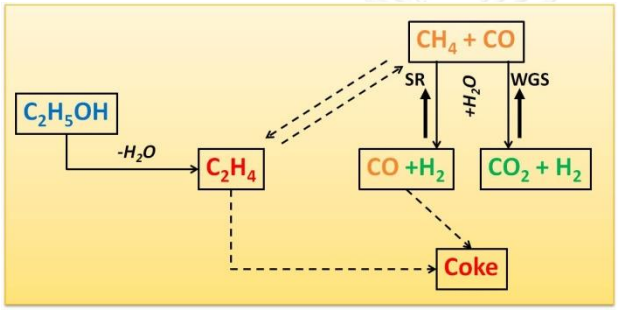	C_2H_5OH, H_2O, C_2H_4, H_2, CH_4, CO_2, CO, C
Via Acetaldehyde 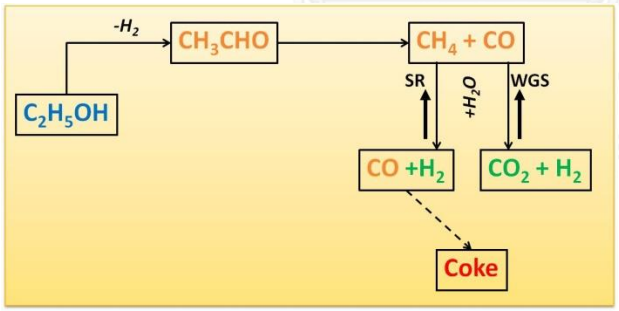	C_2H_5OH, H_2O, CH_3CHO, H_2, CH_4, CO_2, CO, C
Via Acetaldehyde in two step reforming 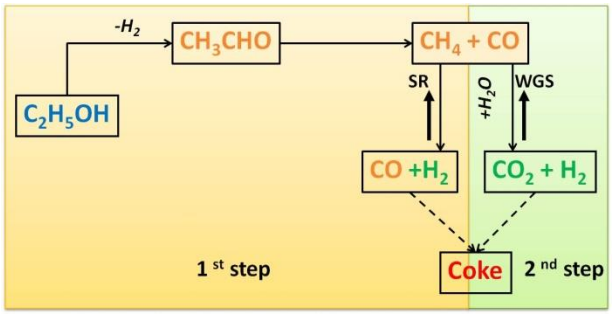	1st step: C_2H_5OH, CH_3CHO, H_2, CH_4, CO_2, CO, C 2nd step: C_2H_5OH, H_2O, CH_3CHO, H_2, CH_4, CO_2, CO, C

6.3 Results and discussion

6.3.1 Effect of intermediates on carbon formation

Acetaldehyde and ethylene are important intermediates that have roles in ethanol reforming process. The maximum possibilities of the carbon formation region from different coking mechanisms pathways are shown in Figure 6.1. When ethanol is fully dehydrated to be ethylene, the process of polymerization will certainly occur, and then carbon will unavoidably form. Ethylene is clearly a major cause of the carbon formation problem. Using acetaldehyde as an intermediate instead of ethylene through the ethanol dehydrogenation reaction can reduce the carbon formation possibility to 24%. Because four reactions of carbon formation (Eqs. (6.4-6.7)) are involved, carbon still forms in the dehydrogenation of ethanol under some operating conditions.

$$2CO \leftrightarrow CO_2 + C \quad (6.4)$$

$$CH_4 \leftrightarrow 2H_2 + C \quad (6.5)$$

$$CO + H_2 \leftrightarrow H_2O + C \quad (6.6)$$

$$CO_2 + 2H_2 \leftrightarrow 2H_2O + C \quad (6.7)$$

Equilibrium of coke via the Boudouard reaction (Eq. (6.4)), hydrogenation of carbon monoxide (Eq. (6.6)), and hydrogenation of carbon dioxide (Eq. (6.7) become less favored as the temperature increases, while carbon formation via methane decomposition (Eq. (6.5) becomes increasingly important at higher temperatures. However, from the thermodynamic point of view, to avoid the carbon formation ethanol steam reforming is assured by using acetaldehyde as an intermediate.

Fortunately, ethanol does not dehydrate into ethylene only. Ethylene, acetaldehyde, methane, carbon monoxide, carbon dioxide, hydrogen and water are the combination of conventional ethanol decomposition gases. In the absence of steam, the amount of carbon formation from conventional pathway is compared to that of pathway via acetaldehyde as shown in Figure 6.2. At low temperature, ethanol thermodynamically favors decomposed to carbon but it is not in the same way when

the system is forced to reform via acetaldehyde. Ethanol dehydrogenation shows the lower amount of carbon formation in all ranges of temperature.

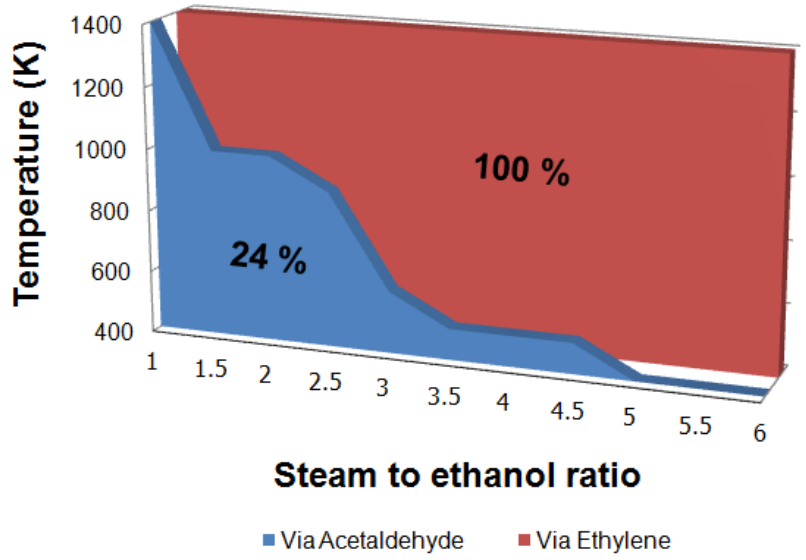

Figure 6.1 Maximum possibilities of the carbon formation region from different pathways

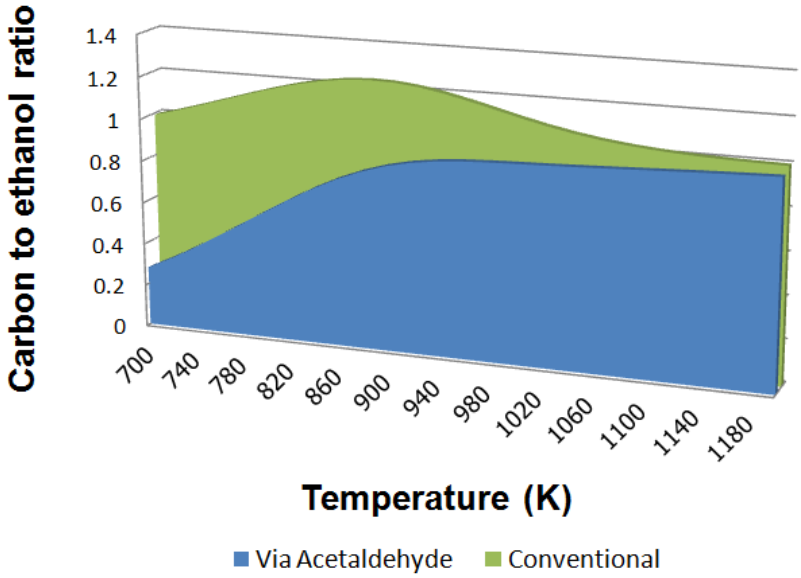

Figure 6.2 The amount of carbon formation from different pathways of ethanol decomposition.

To assure that acetaldehyde is a significant intermediate of ethanol reforming, there are several works focusing on the dehydrogenation reaction of ethanol. Iwasa and Takezawa, (1991) concluded that the dehydrogenation of ethanol to acetaldehyde occurs much more rapidly than its decomposition to ethyl acetate and acetic acid, and it is the intermediate product in the steam reforming environment. Freni S. et al., (2000) studied a two-layer fixed-bed reactor for hydrogen-rich gas production with the first layer composed of a Cu-based catalyst for ethanol dehydrogenation at 370 ˚C and the second one composed of a Ni-based catalyst under steady-state conditions at 650 ˚C. In addition, Nishiguchi et al., (2005) studied steam reforming of ethanol over CuO/CeO_2. They revealed that acetaldehyde and hydrogen are mainly produced at low temperatures (260 ˚C). In this study, when ethanol is dehydrogenated to acetaldehyde in dehydrogenation unit, the yield of acetaldehyde in this simulation result is compared with experimental data of Deng et al., (1995) which reported by using Al_2O_3 membrane reactor as shown in Figure 6.3.

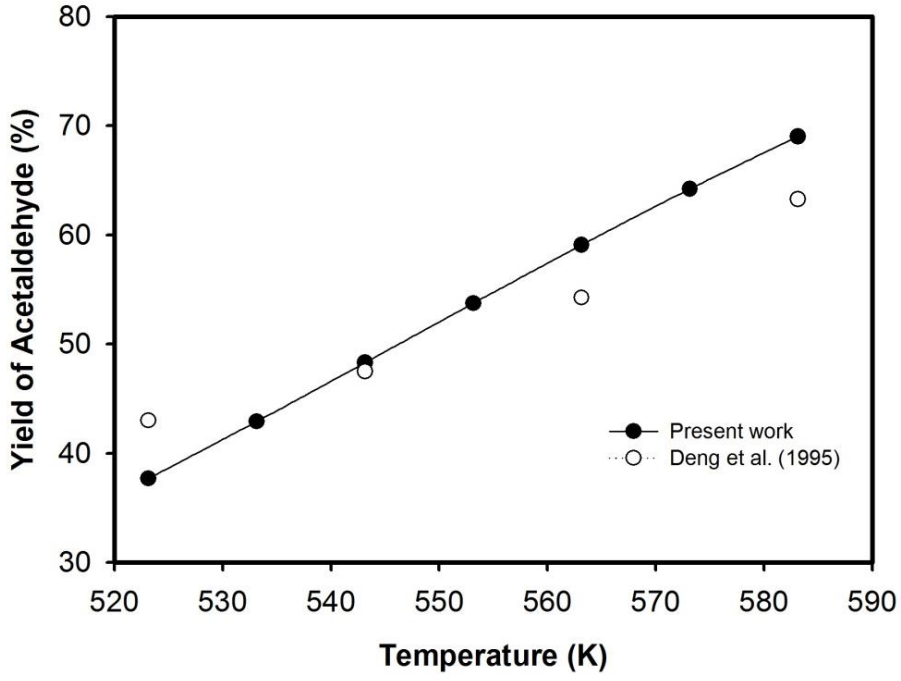

Figure 6.3 Comparison of ethanol dehydrogenation units between simulation results and experimental data (Deng et al., 1995).

6.3.2 Effect of the number of reforming steps on carbon formation

Water is the reforming agent in steam reforming process. Generally, ethanol and water are mixed in a suitable ratio to avoid the carbon formation and to reach high hydrogen yield. However, feeding the mixture of ethanol and water to reforming in single step cannot control the presence of acetaldehyde as an intermediate. Water leads to ethanol dehydration and forms ethylene in conventional pathway. And in single step via acetaldehyde water also leads to early methanation and water gas shift that may cause the unfavorable carbon formation too. Instead, the two-step ethanol steam reforming is recommended. Firstly, ethanol is fed into the dehydrogenation reactor without steam. Secondly, the gas mixture from the first step is mixed with steam and fed into the steam reformer. From this way, the carbon-free hydrogen rich gas is produced as shown in Figure 6.4. Nevertheless, it is important to note that Figure 6.4 is presented on steam to ethanol of 1.8. At other feed ratios the amount of carbon is changed according to multiple complex reactions system.

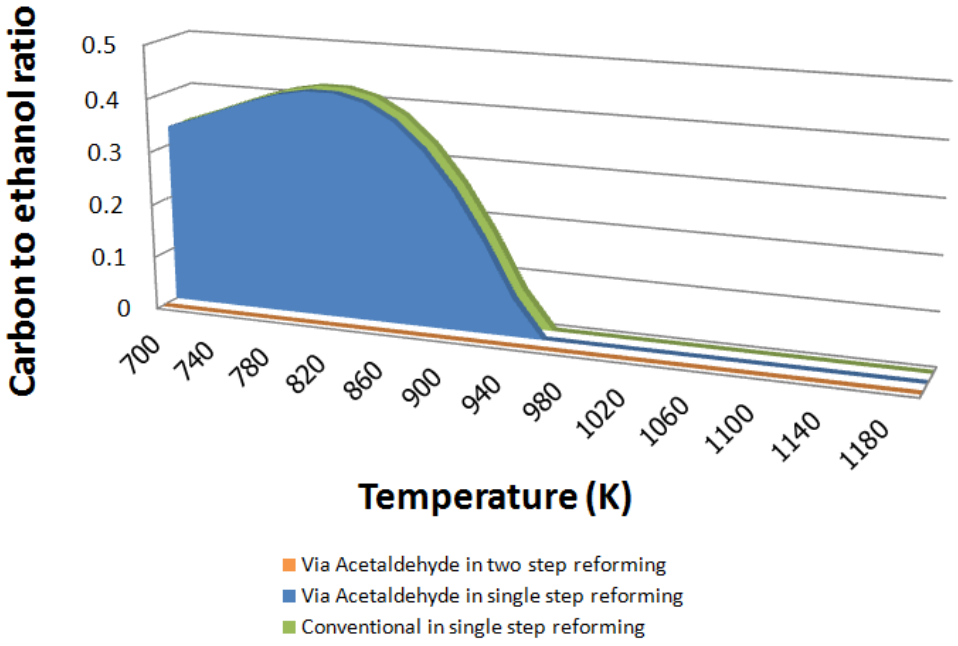

Figure 6.4 The amount of carbon formation from different pathways of ethanol steam reforming.

6.3.3 Effect of dehydrogenation temperature on product yields

In the first step, the yields of the dehydrogenation reactor are in various products. Figure 6.5 illustrates the amount of many species that can be occurred when ethanol is heated in the temperature ranges of 400 K to 1200 K. From the simulation results, the trace of ethanol and acetaldehyde is found. It can be predicted that ethanol is easily dehydrogenated to acetaldehyde and acetaldehyde is not too stable to stay its form. Acetaldehyde is decomposed to methane and carbon monoxide quickly. The amount of carbon monoxide is enough to form carbon by Boudouard reaction at low temperature. Increasing temperature leads to methane decomposition that mainly causes the carbon formation at high temperature. The effect of dehydrogenation temperature on the conversion of ethanol is considered in this study. From the simulation results, it can be seen from Table 6.2 that at any temperatures ethanol can be totally conversed without the presence of steam. However, it is essential to know that ethanol can dehydrogenate at quite low temperature and dehydrogenation reactor presents the exothermic heat at operating temperature between 400 K to 500 K. This information is enough to select the dehydrogenation temperature to close the thermo neutral zone.

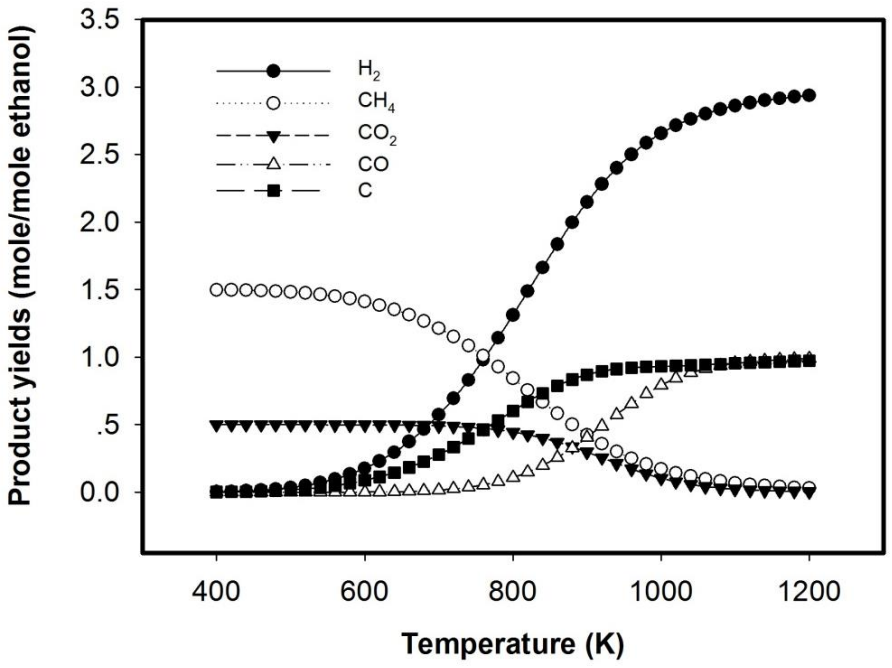

Figure 6.5 The effect of dehydrogenation temperature on product yields.

Table 6.2 The effect of dehydrogenation temperature on ethanol conversion, product yields and heat duty of reactor.

Temperature (K)	Ethanol conversion (%)	Product yields (mole/mole ethanol)					Heat duty (kW)
		H_2	CH_4	CO_2	CO	C	
400	100	0.003	1.498	0.500	0	0.002	-6.247
500	100	0.035	1.483	0.500	0	0.017	-3.476
600	100	0.177	1.412	0.499	0.001	0.088	0.909
700	100	0.573	1.214	0.492	0.016	0.278	9.004
800	100	1.313	0.844	0.446	0.108	0.602	23.589
900	100	2.148	0.426	0.297	0.406	0.871	44.812

6.3.4 Effect of reforming temperature and feed ratio on product yields

The effects of reforming temperature and feed ratio in the steam reformer on product yields and carbon formation are investigated. To compare the prediction of carbon formed, Figure 6.6 (a) presents the grey area that shows the carbon formed region but Figure 6.6 (b) does not. The two-step of ethanol steam reforming has the crucial benefit of carbon-free hydrogen production. It can be noticed that the trend of methane and carbon monoxide lines is changed from the conventional pathway. Through hydrogen and carbon dioxide yields do not change apparently, the two-step reforming via acetaldehyde has the higher amount of methane with no carbon formation at low temperature and feed ratio.

(a)

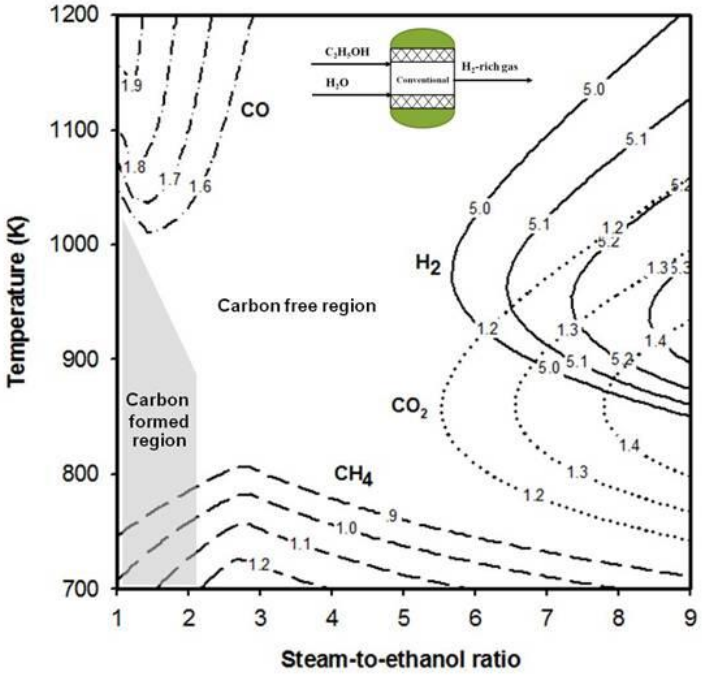

(b)

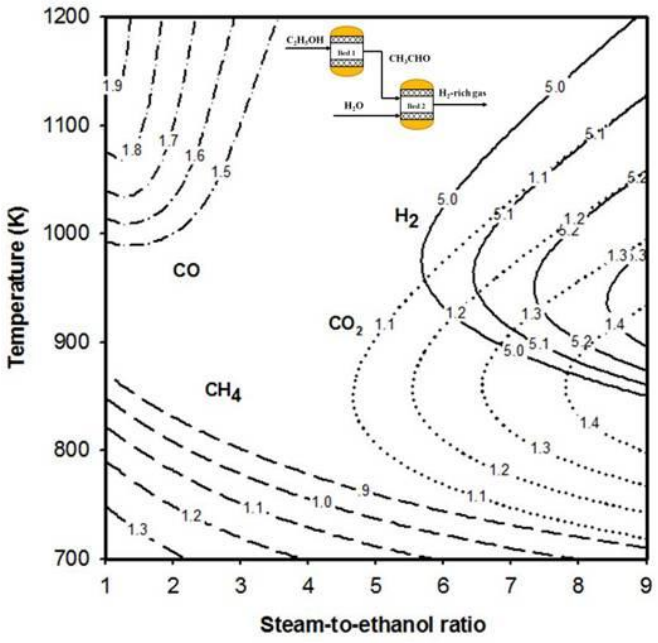

Figure 6.6 Effect of temperatures and feed ratio on the product yields: (a) conventional pathway and (b) via acetaldehyde in two step reforming (grey area is the carbon formed region and a number on the line is the amount of products (mole/mole of ethanol feed))

6.4 Conclusions

The thermodynamic analysis of a two-step ethanol steam reforming for carbon-free hydrogen production is investigated by using Gibbs free energy minimization method. The main advantage of our proposed reaction pathway is to avoid ethylene and carbon formation by dehydrogenating ethanol to acetaldehyde before being fed into the steam reformer. The effect of intermediates, the number of reforming steps, the dehydrogenation temperatures, the reforming temperatures and feed ratios on product yield and carbon formation have been studied at isothermal conditions. Using acetaldehyde as an intermediate instead of ethylene can reduce the carbon formation possibility from 100% to 24%. The two-step reforming is necessary to control the pathway via acetaldehyde. Based on the thermodynamic calculations, ethanol totally converts to hydrogen and acetaldehyde which then decomposes to methane and carbon monoxide spontaneously. Dehydrogenation reactor performs nearly thermo neutral condition and presents low carbon formed at temperature of 500 K. In the steam reformer, the carbon-free hydrogen rich gas is produced even at low temperature and feed ratio.

CHAPTER VII

PERFORMANCE IMPROVEMENT OF ENHANCED ETHANOL STEAM REFORMING AND SOFC INTEGRATED SYSTEMS

This chapter presents the effect of removing CO_2 and steam from the reforming gas on the SOFC performance. The addition of CaO to capture CO_2 and the installation of a dehumidifier to remove steam in the reformer are proposed to improve hydrogen production efficiency. Efficiency of the steam reformer and SOFC integrated system with and without an enhancement unit is compared and analyzed with respect to key operating parameters.

7.1 Introduction

Nowadays a steam reforming is the most commonly used process for hydrogen production from ethanol. However, the steam reforming is limited by chemical equilibrium reactions which typically produce more dilute products such as CO_2 and water. For this reason the removal of CO_2 and excess steam in the reforming environment is an interesting alternative to enhance the purity of hydrogen-rich gas.

Using CaO sorbent for CO_2 capture (Elzinga et al., 2011; Cormos and Simon, 2013) is believed to be thermodynamically the best candidate among metal oxides for CO_2 capture in zero emission power generation systems. Upon reaction of carbon dioxide (CO_2) and the solid sorbent (CaO), CO_2 is converted to a solid carbonate. Regenerating the sorbent results in releasing CO_2 suitable for storage. The carbonation/calcination (or adsorption/desorption) equilibrium reaction is written as in Eq. (7.1):

$$CO_2 + CaO \leftrightarrow CaCO_3 \tag{7.1}$$

Schematic diagram of the ethanol-fuelled SOFC system integrated with a sorption-enhanced reforming process is shown in Figure 7.1. Additionally, to attain high hydrogen yield, the addition of more steam to the steam reformer is generally

needed to promote the steam reforming reactions; typically methane steam reforming and water gas shift reaction, as shown in Eq. (7.2) and (7.3) respectively:

$$CH_4 + H_2O \leftrightarrow CO + 3H_2 \quad (7.2)$$

$$CO + H_2O \leftrightarrow CO_2 + H_2 \quad (7.3)$$

However, excess steam will dilute the hydrogen product stream, thereby degrading the fuel cell performance. Therefore, it is reasonable to remove steam from the reformate gas before it is fed to a cell stack by using a dehumidifier. In this study, the dehumidifier is conceptually designed and is employed to keep the humidity of the synthesis gas product at a desired limit. Schematic diagram of the ethanol-fuelled SOFC system integrated with a dehumidifier is shown in Figure 7.2.

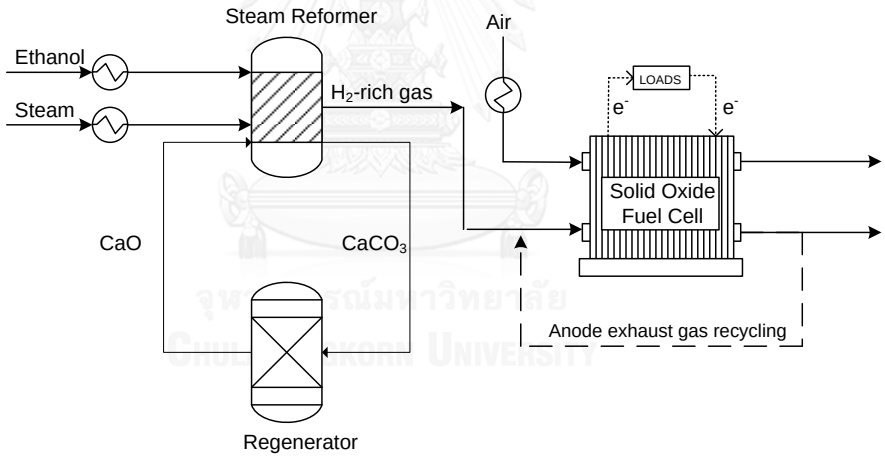

Figure 7.1 Schematic diagram of the ethanol-fuelled SOFC system integrated with a sorption-enhanced reforming process.

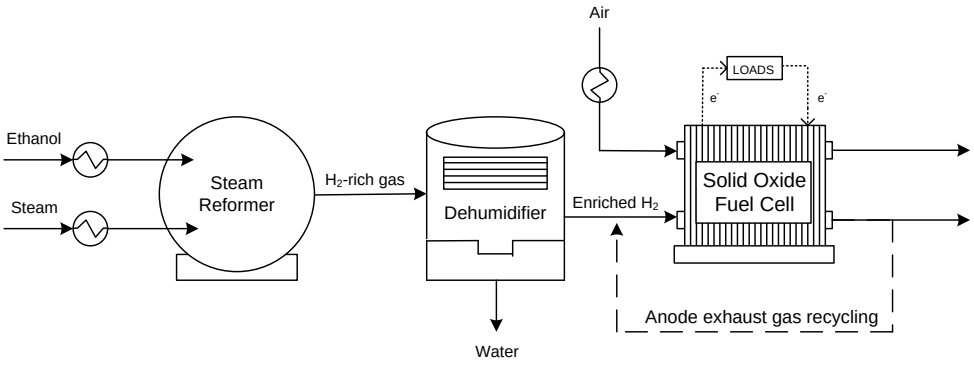

Figure 7.2 Schematic diagram of the ethanol-fuelled SOFC system integrated with a dehumidifier.

7.2 Methodology

In CO_2 capture study, an equilibrium reactor module in Aspen Plus, which is based on the minimization of total Gibbs free energy, is employed to predict the equilibrium composition of the outlet gas from the reforming process. The thermodynamic properties of involved substances are determined by the Peng-Robinson equation of state. The species considered in the calculations include C_2H_5OH, H_2O, CH_3CHO, C_2H_4, H_2, CH_4, CO_2, CO ,C, CaO and $CaCO_3$. To analyze the formation of coke from a thermodynamic point of view, it is assumed that carbon formed is elemental, in the graphitic form. The reforming with CO_2 capture is studied and discussed in terms of SOFC performance.

In steam removal study, the dehumidification ratio (DR) is defined as the ratio of steam removed from the gas product to the total amount of steam in the synthesis gas feed. The simulation of the ethanol steam reformer is also performed based on the minimization of total Gibbs free energy. But the concerned compositions are different. CaO and $CaCO_3$ are not taken into account. To investigate its performance with respect to key operating parameters, a model of the SOFC integrated system is developed and employed to study its electrical and thermal energy performance. High-quality by-product heat form anode exhaust gas is recovered to be used in all requiring heat units.

The SOFC integrated system with and without the dehumidifying unit is compared and analyzed in terms of electrical and thermal efficiencies by using Aspen Plus®.

7.3 Results and discussion

7.3.1 Enhancement of hydrogen production by using sorption-enhanced reforming

The performance of CaO to capture CO_2 as a function of operating reforming temperatures is shown in Figure 7.3. At low temperature operation, most CO_2 can be removed; however, the efficiency of CaO decreases at high temperatures due to the exothermicity of the carbonation reaction. The amount of steam fed to the reformer seems to have a stronger effect on the H_2 yield than the operating temperatures. The addition of more steam can enhance the production of H_2; however, high energy input is required to generate steam. In addition, the excess steam can dilute the H_2 product stream, which costs a dehydration process. Therefore, the reforming condition at temperature of 900 K and steam-to-ethanol ratio of 5 providing 93% CO_2 capture and 5.6 moles H_2/1 mole of ethanol is chosen to be the operating condition of ethanol reforming processor.

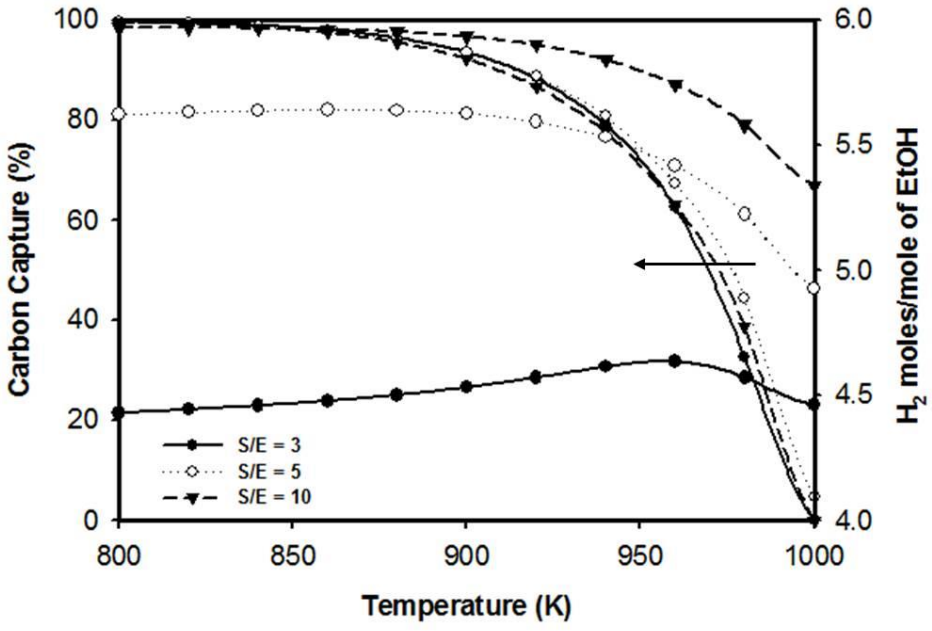

Figure 7.3 Effect of temperature on CO_2 capture and H_2 yield at different steam-to-ethanol ratios (CaO/C_2H_5OH = 3).

To demonstrate the benefit of the CO_2 removal using CaO sorbent in the reforming process, the performance of the SOFC run on the reformate gas derived from the steam reforming without and with CaO is compared as shown in Figure 7.4. The SOFC is operated at the fuel utilization of 70% and temperatures of 973 K, 1023 K and 1073 K. The results show a significant improvement of the SOFC in terms of the cell voltage and power density generation when the reformate gas from the steam reforming with CaO is fed to the SOFC. In addition, the limiting current density of the SOFC system combined with CO_2 capture is expanded, especially at high-temperature operation. Figure 7.5 shows the percentage of performance improvement of the combined SOFC and the steam reforming with CO_2 capture process. Compared with the performance of the SOFC and steam reforming process without CaO, it can be seen that at the operating current density of 3 A/cm^2 and the temperature of 1073 K, the power density of the SOFC run on the reformate gas from the process with CO_2 capture increases by 13.46%.

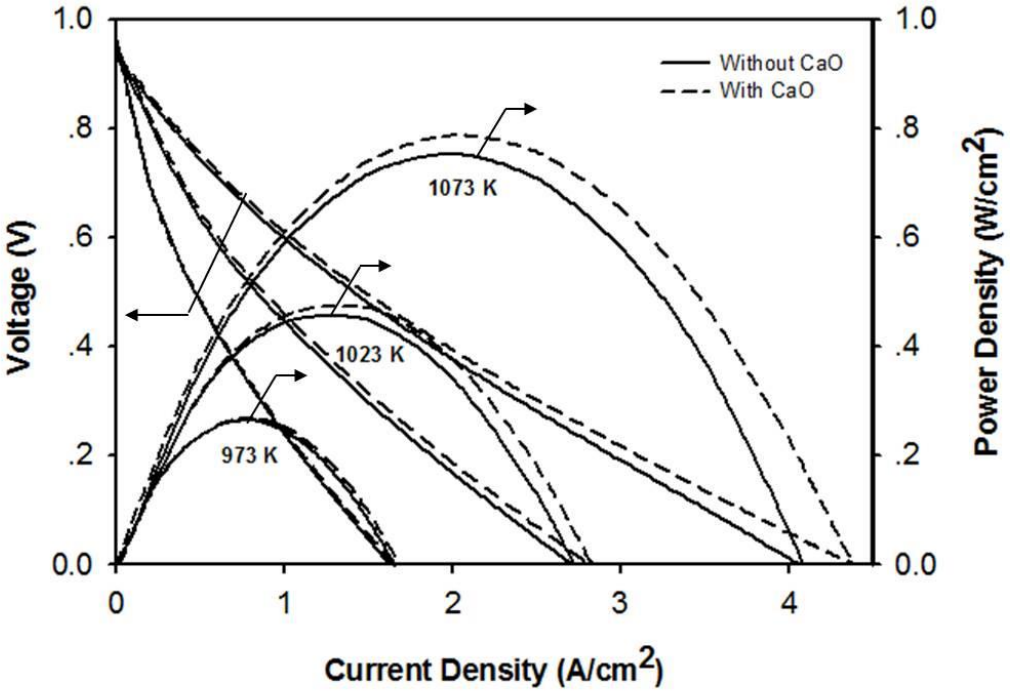

Figure 7.4 Cell voltage and power density as a function of current density at T = 973 K, 1023 K, and 1073K (70% fuel utilization)

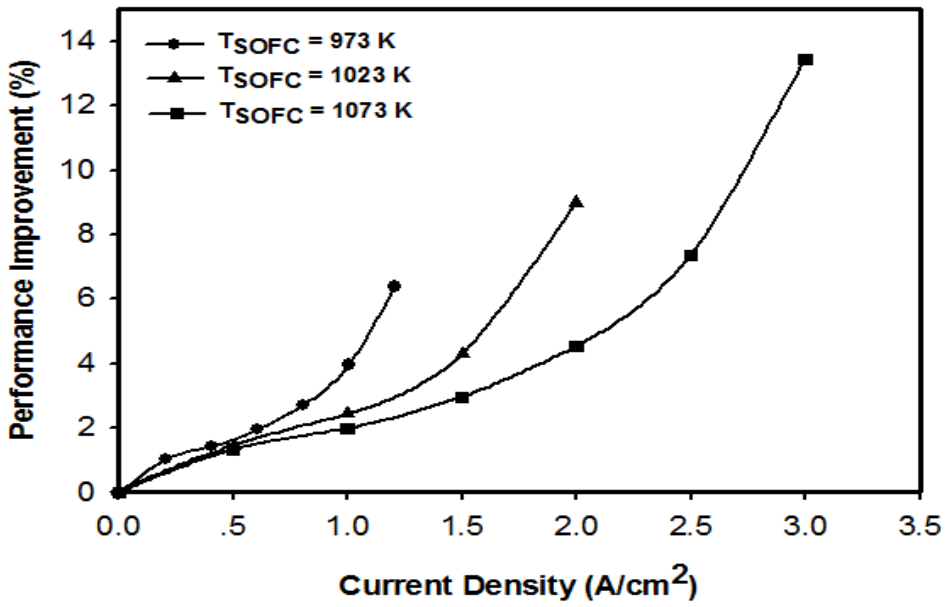

Figure 7.5 Performance improvement of the steam reforming with CO_2 capture and SOFC integrated system.

7.3.2 Enhancement of hydrogen production by using dehumidification

Simulation of the ethanol steam reforming process is performed to investigate the effect of key operating parameters, such as, temperature and steam-to-ethanol ratio (S/E). For each water feed ratio, the hydrogen yield reaches the highest value when the reforming temperature is in the range of 900-1,000 K. However, the more steam feed the more hydrogen production can be enhanced. For example, when the reformer is operated at the steam-to-ethanol ratio of 10, the highest hydrogen yield of 5.4 mole/mole ethanol is obtained. It is noted that in practice, the reformer can be run at a lower S/E ratio to save energy demand because the remaining CH_4 and CO can be used as fuel in SOFC; at low S/E ratio, these reforming products are more produced under the thermodynamic control. A carbon formed region under the reformer operation is also presented in the Figure 7.6, so that it will be easy to choose the reforming operational conditions without facing the carbon formation problem. Effect of temperatures on the H_2 and H_2O compositions at different steam-to-ethanol ratios is shown in Figure 7.7. The results show that the concentration of H_2 increases with the

increased temperature and is kept content when the reforming temperature is higher than 980 K. Under this operating temperature, the synthesis gas obtained contains H_2 around 45-60 %, depending on the amount of steam used. Significantly, it can be noticed that the more steam fed the more hydrogen-rich gas will be diluted.

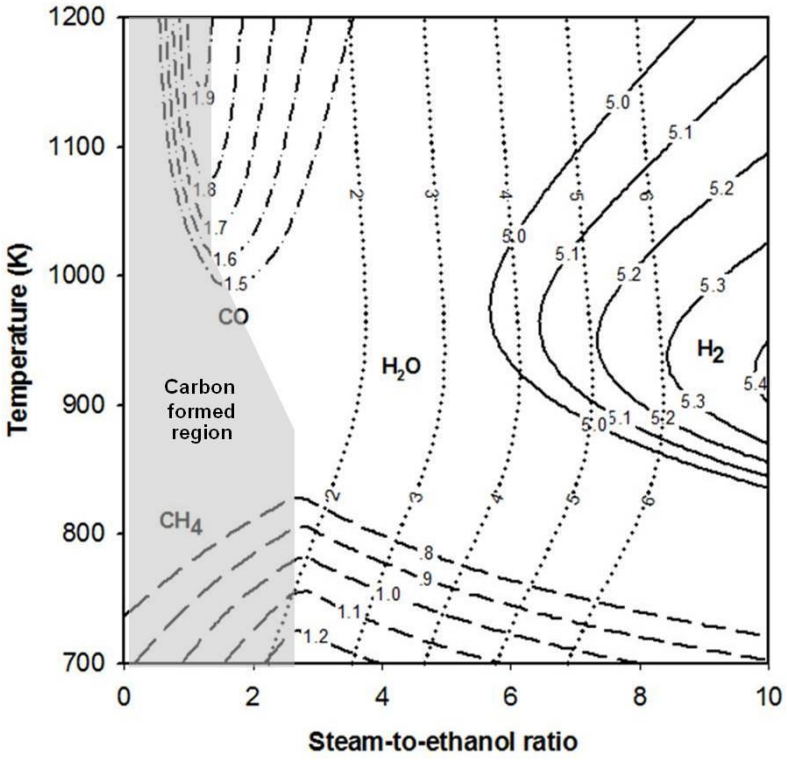

Figure 7.6 Effect of temperature and steam-to-ethanol ratio on the product yields (a number on the line is the amount of gaseous products (mole/mole of ethanol feed))

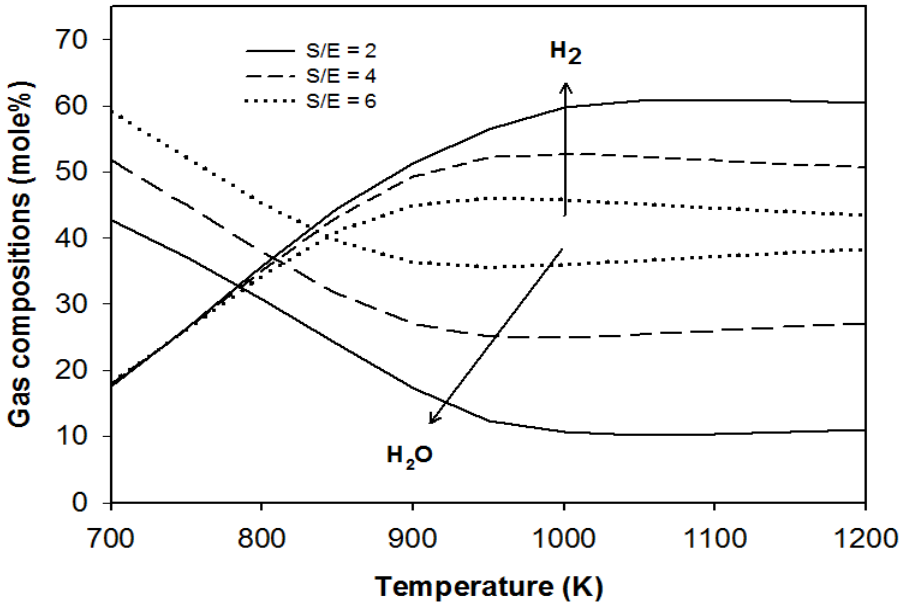

Figure 7.7 Effect of reforming temperature on product gas composition at different steam-to-ethanol ratios.

The dehumidification ratio (DR) is a parameter that is used to determine the ratio of steam removal. The SOFC system is simulated based on design specification and model given in section 4.2. The results show that the DR affects the SOFC performance in term of cell voltage as shown in Figure 7.8. An increase in DR increases the voltage of the SOFC. High removal of steam improves the quality of hydrogen feed to SOFC and the electrochemical reaction in the SOFC is more pronounced along with the decreased concentration loss.

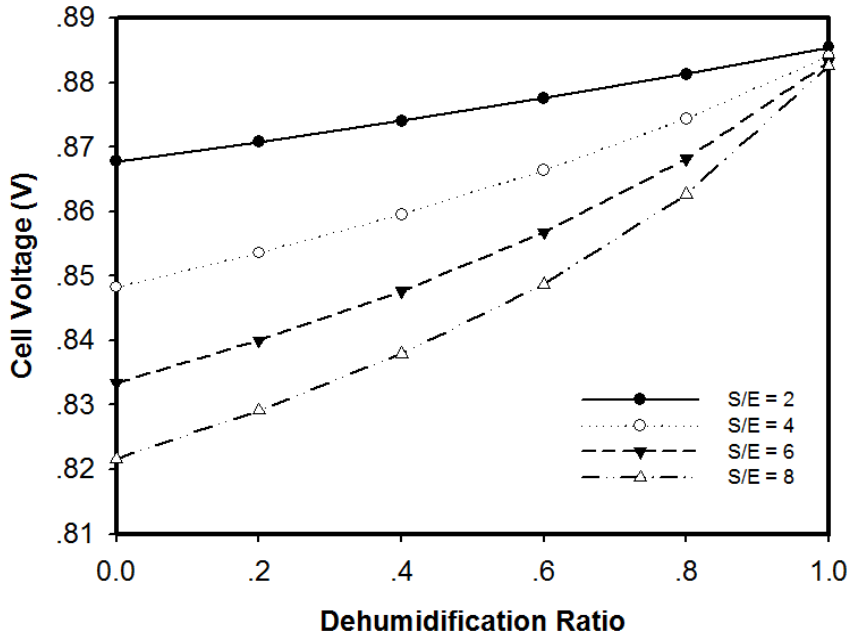

Figure 7.8 Effect of dehumidification ratio (DR) on the fuel cell voltage at different steam-to-ethanol ratios.

The comparison of the SOFC efficiencies with and without a dehumidifier is analysed at various steam-to-ethanol ratios as shown in Figures 7.9 and 7.10. It is found that the electrical performance of the SOFC system without the dehumidifier decreases when increasing the steam-to-ethanol feed ratio. This can be explained by a dilution of the fuel fed to the SOFC. When the steam and ethanol are fixed at the ratio of 8, the electrical efficiency of the SOFC system with 100 % dehumidification is 58.2 %, which is higher than that without the dehumidifier (54.1 %) as shown in Figure 7.9. However, it is observed that the SOFC system without the dehumidifier unit can achieve its high efficiency when it is operated at a lower steam-to-ethanol ratio. Moreover, it is better if the least amount of water is added to the reformer in order to keep its high thermal efficiency as shown in Figure 7.10. When the SOFC system is run at low steam-to-ethanol ratio, heat obtained from the anode gas is higher than that required by the reformer and heaters. To further improve the system efficiency, the remaining useful heat can be applied to other heat requiring components in cogeneration or trigeneration applications. Figure 7.10 also shows that the addition of the dehumidifier in the SOFC system has less impact on its thermal efficiency.

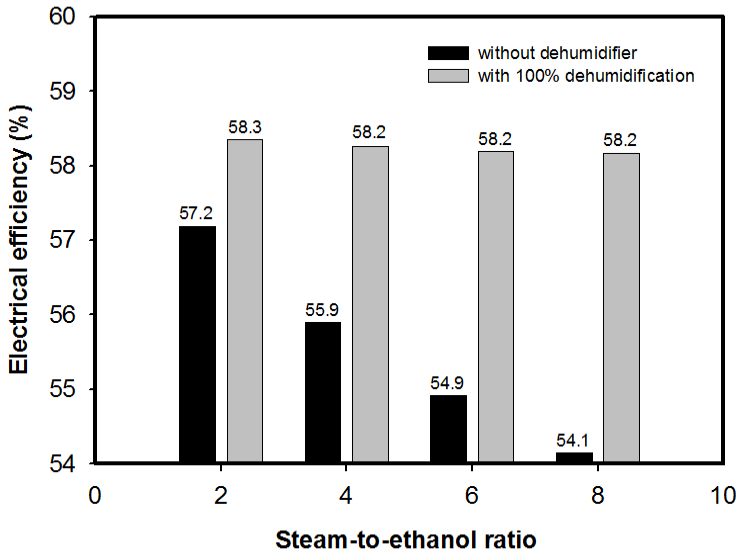

Figure 7.9 Electrical efficiency of the SOFC systems with and without dehumidifier at different steam-to-ethanol ratios

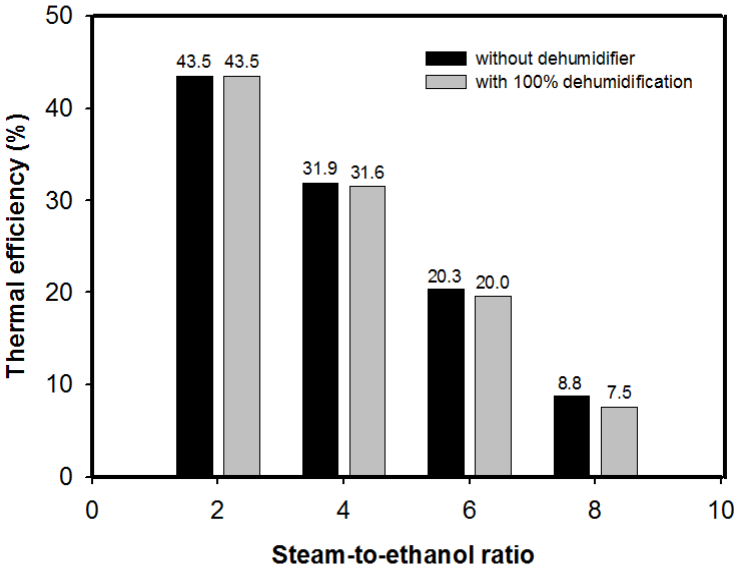

Figure 7.10 Thermal efficiency of the SOFC systems with and without dehumidifier at different steam-to-ethanol ratios

7.4 Conclusions

In this study, the performance of an ethanol-fuelled SOFC system integrated with a sorption-enhanced reforming process and dehumidifier were analyzed. Simulation of the ethanol steam reformer was first performed to study the effect of key operating parameters on product distribution. The result demonstrates that high hydrogen yield is found with high CO_2 content. When a carbon dioxide capture is considered, the steam reforming with CO_2 capture process outperforms the conventional steam reforming process as a high purity of H_2 is obtained. At constant current density, the use of reformate gases from the ethanol steam reformer added CaO has a higher actual cell voltage. However, the addition of the regenerator and fresh absorbent influences the economic consideration.

For the study of dehumidification, it was found that the highest hydrogen yield can be achieved when operating the ethanol steam reformer at the operating temperature of 980 K with any steam-to-ethanol ratios. Although increasing steam feed can enhance the hydrogen yield, excess steam dilutes the fuel and directly affects the SOFC efficiency. From this study, the results show that the installation of the dehumidifier at the outlet of the ethanol steam reformer to eliminate unnecessary steam can enrich the hydrogen fuel and improve the actual cell voltage and electrical efficiency. However, low steam feeding is more recommended because the operation of the reformer at low level of steam with the dehumidification provides few percentages of SOFC performance improvement. Moreover, the use of the dehumidifier has less effect on the thermal system efficiency.

CHAPTER VIII

ANALYSIS OF A SOLID OXIDE FUEL CELL SYSTEM COMBINED WITH A TWO-STEP REFORMING PROCESS USING CO_2 SORBENT

This chapter the two-step ethanol steam reforming, which consists of ethanol dehydrogenation and steam reforming, is used as a fuel processor to replace a conventional ethanol steam reforming (single step steam reforming) for solid oxide fuel cell applications. Performance of the SOFC integrated with the two-step steam reforming of ethanol is analyzed under thermally self-sufficient condition. The addition of CaO to capture CO_2 in the reformer is proposed to improve hydrogen production efficiency. The economic analysis is also provided in this chapter.

8.1 Introduction

The concept of a two-step ethanol steam reforming is proposed in order to produce only desired species in the first step of a dehydrogenation unit, and then convert these species into hydrogen-rich gas in a reformer. However, the steam reforming of acetaldehyde in the second step is limited by chemical equilibrium reactions, e.g., acetaldehyde decomposition, steam reforming of acetaldehyde, methane steam reforming and water gas shift reaction (Eqs.(8.1)-(8.4)).

$$CH_3CHO \leftrightarrow CH_4 + CO \quad (8.1)$$

$$CH_3CHO + H_2O \leftrightarrow 2CO + 3H_2 \quad (8.2)$$

$$CH_4 + H_2O \leftrightarrow CO + 3H_2 \quad (8.3)$$

$$CO + H_2O \leftrightarrow CO_2 + H_2 \quad (8.4)$$

The removal of CO_2 in the reforming environment is an interesting alternative to enhance the reforming efficiency and deal with environmental concerns by reducing greenhouse gas emission.

To improve the ethanol reforming process for hydrogen production, performing the two-step reforming reactions via acetaldehyde as an intermediate coupled with the removal of CO_2 by absorbents is an interesting combined methods in this study. However, the addition of the second reformer, fresh absorbent and even regenerator leads to the energy consumption concerns and establishes a sound costly framework. Therefore, the aim of this study is not only to show the hydrogen production performance but also to manage the energy inside the whole systems to operate under thermo-neutral conditions. Getting along with the economic aspects, a preliminary economic analysis is also carried out.

8.2 Methodology

In this study, three different ethanol reforming processes are considered as followings:

(i) conventional steam reforming (CSR);
(ii) two-step steam reforming (TSR);
(iii) two-step steam reforming with CO_2 capture (TSR&C).

In the CSR process, ethanol and steam are directly fed into the single-step steam reformer whereas the TSR and the TSR&C fuel processors consist of a dehydrogenation reactor and a steam reformer; ethanol is firstly dehydrogenated to acetaldehyde, which is then reformed with steam to produce hydrogen-rich gas. Similar to the previous studies, an equilibrium reactor module in Aspen Plus, which is based on the minimization of total Gibbs free energy, is employed to predict the equilibrium composition of the outlet gas from the reforming process. The thermodynamic properties of involved substances are determined by the Peng-Robinson equation of state.

When the fuel processor with different configurations (i.e., CSR, TSR, and TSR&C) is integrated with the SOFC, the exhaust gas of the SOFC is sent to an afterburner and the generated heat is used to supply to the fuel processor. In this work, the outlet gas temperature of the afterburner is considered the primary parameter for adjusting the SOFC system to achieve the self-sustain operation ($\dot{Q}_{net} = 0$). The other parameters are kept constant for economical comparison. The total net energy of the system ($\dot{Q}_{net}$) is defined as following:

$$\dot{Q}_{net} = \sum_{i=1}^{n} \dot{Q}_i = 0 \tag{8.5}$$

8.3 Results and discussion

8.3.1 Effect of temperature and steam-to-ethanol ratio on the product gas compositions

The effect of temperatures and feed ratio on the product yields in different ethanol processors is shown in Figure 8.1. It clearly shows that carbon is generated in the CSR when operated at low steam-to-carbon ratios under the temperature range of the study (Figure 8.1(a)), whereas the use of the two-step reforming of ethanol (TSR and TSR&C) can avoid the carbon formation (Figure 8.1(b) and (c)). In the dehydrogenation reactor, it is important to note that the temperature of 500 K is chosen to perform the analysis for the last two cases (TSR and TSR&C) with almost 100% ethanol conversion. In the steam reformer of the two-step ethanol reforming, acetaldehyde occurred from the dehydrogenation of ethanol can be easier decomposed to CH_4 and CO than reacted with water to produce hydrogen. For the TSR, although the effect of carbon formation is suppressed, the presence of CO_2 at the operating condition which gives high H_2 yield can dilute the reformate gas and turn into adversely affect on the SOFC performance. This difficulty can be overcome by introducing CaO as a CO_2 adsorbent to the steam reformer (TSR&C). Figure 8.1(c) shows the reforming products in the TSR&C process. High hydrogen product can be obtained at lower temperatures and lower steam-to-ethanol ratios, compared to the TSR process and in

addition, the produced CO_2 is decreased. A removal of CO_2 by CaO can shift the reforming reaction to the H_2 product side.

(a)

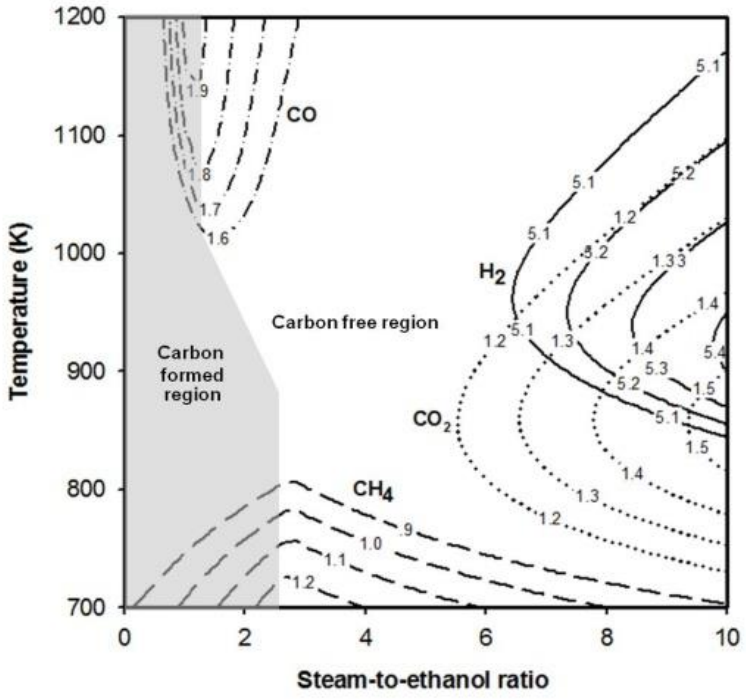

(b)

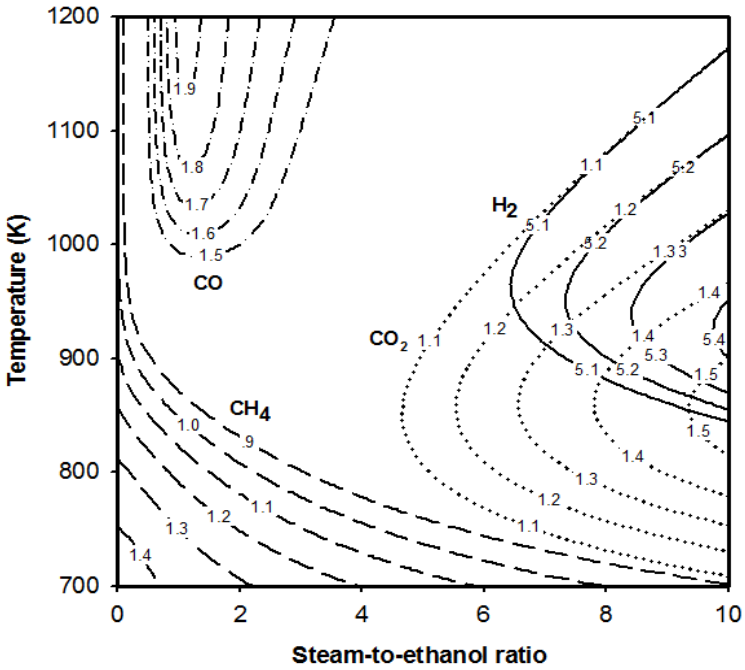

(c)

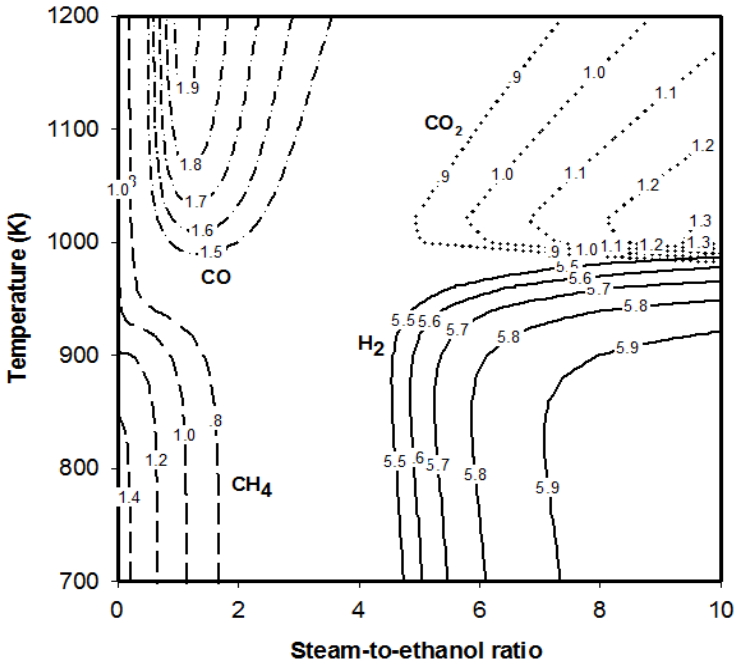

Figure 8.1 Effect of temperatures and feed ratio on the product yields: (a) conventional steam reforming (CSR), (b) two-step steam reforming (TSR) and (c) two-step steam reforming using CaO sorbent (TSR&C) ($CaO/C_2H_5OH = 3$)

8.3.2 System under a thermally auto-sustainable condition

Next, the SOFC systems are performed under a thermally auto-sustainable condition. First, the heat duty of each unit inside the system, in which the conditions of each configuration are operated as shown in Figure 8.2, is determined. And then the afterburner temperature is adjusted to balance the total heat generation and the total heat consumption. From Figure 8.2, it is found that all configurations can follow the benefits of heat supply and utilization equality. However, it can be noticed that the afterburner temperature in the TSR&C system, can be reduced to a lower temperature compared to CSR and TSR cases.

(a)

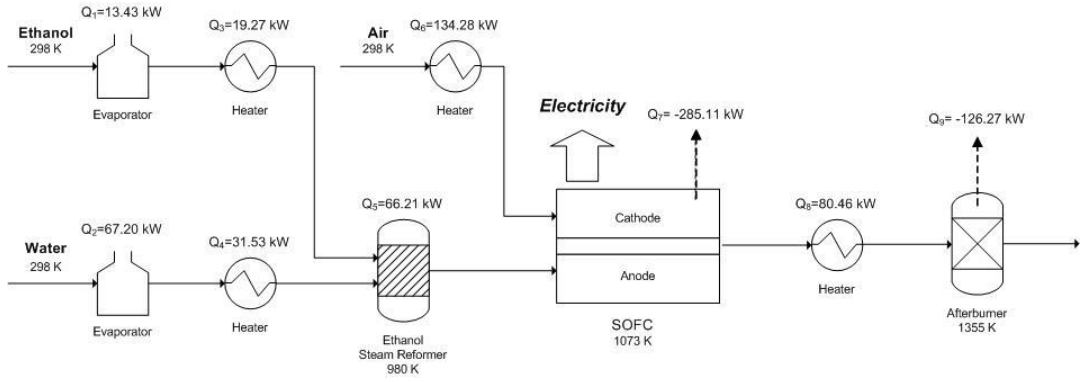

(b)

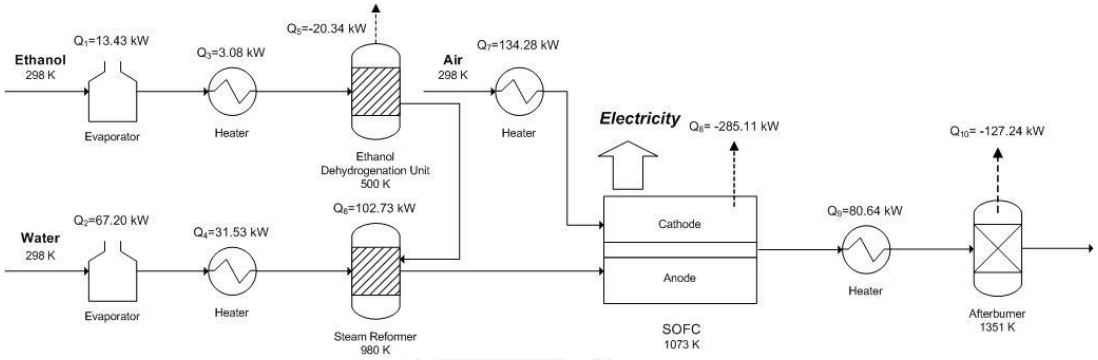

(c)

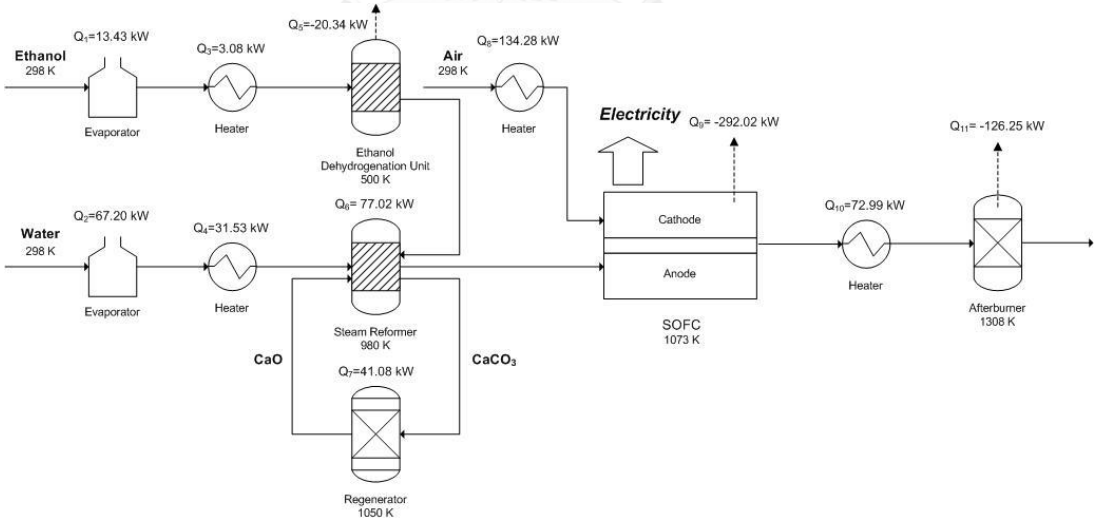

Figure 8.2 The configuration of the SOFC systems at a thermally auto-sustainable condition with: (a) CSR, (b) TSR and (c) TSR&C (ethanol feed rate = 1 kmol/hr)

8.3.3 Economic analysis

In this section, a preliminary economic analysis of the SOFC integrated with different ethanol steam reforming configurations for 1 MW of electrical power generation is performed. Two parameters, i.e., capital and raw material costs, are used to determine the economic feasibility for the investment decision making. Table 8.1 summarizes the costing model and economic parameters used in this analysis. For the capital costs, the SOFC stack and the fuel processors; including a dehydrogenation reactor, a steam reformer, and a regenerator, are calculated according to the considered case. However, it is assumed that in all cases the costs of the other units, such as evaporators, heaters and the afterburner, do not change much and are not considered in the economical calculations because they are used in the same size and the same material.

Table 8.1 Costing models and economic parameters used in the economic analysis.

Costing model			**Reference**
Fuel Processor	Reactor volume (ft^3)	$V_{\text{Reactor}} = 2[F_L \tau / \rho_L]$	(Biegler et al., 1997)
	Reactor Diameter (ft)	$D = \sqrt[3]{V_{\text{Reactor}} / \pi}$	
	Reactor Height (ft)	$L = 4D$	
	Reactor Cost ($)	$C = 1000\left(L/4\right)^{0.81}\left(D/3\right)^{1.05a}$	
	Material and Pressure Factor	$\text{MPF} = F_{\text{m}} F_{\text{p}}$	
	Updated Reactor cost ($)	$\text{UC} = (\text{UF}\cdot\text{C})\left(\text{MPF} + \text{MF} - 1\right)$	

SOFC	Cell cost ($)	$C_{cell} = A_{single\ cell} \times 0.1442$[b]	(Piroonlerkgul et al., 2010)
	Number of cells	$N_{cell} = A_{total} / A_{single\ cell}$	
	Number of stacks	$N_{stack} = N_{cell} / 100$	
	Fuel cell stack cost ($)	$C_{stack} = 2.7[(C_{cell} \times N_{cell}) + (2 \times N_{stack} \times A_{single\ cell} \times 0.46425)]$	

Economic parameters

Ethanol Feed Cost ($/L)	0.371	(Lopes et al., 2012)
Liquid hold up time; τ (min)	5	
Guthrie Material Factor; F_m	3.67 (Stainless 316)	
Guthrie Pressure Factor; F_p	1 (Atmospheric pressure)	
Module Factor; MF	4.23	
Update Factor; UF	4.7826 (assume present cost index= 550)	
CaO sorbent ($/ton)	60	(Piroonlerkgul et al., 2010)

[a] All reactors is in vertical fabrication.

[b] A single cell area is fixed at 200 cm^2.

The results of the economical analysis of the SOFC system based on the two-step steam reforming process under thermally auto-sustainable operation is summarized in Table 8.2. At the chosen operating condition, the use of the two-step steam reforming process with CO_2 capture (TSR&C) can reduce the SOFC stack size by 6.2%, comparing to the conventional steam reforming (CSR), because of a higher electrical power of the SOFC run on the reformate gas from the TSR&C; the power density of the SOFC system with TSR&C is increased by 6.61%. As a consequence, using the TSR&C in the SOFC system can save the total capital cost approximately 4.18 % even though it has three reactors inside.

Considering the raw material use and obtained product from different fuel processors, at the same net electrical power generation, the fuel feed cost of the CSR system is higher than that of the TSR and TSR&C systems. This result is because the CSR-SOFC system requires a higher amount of ethanol to produce the same amount of H_2 for the SOFC. It is noted that although the fuel feed cost of the TSR is almost equal to that of the CSR but the TSR has a benefit of no carbon formation possibility in the reformer. Based on the fuel feed costs and fuel processor capital costs, the use of the TSR process might not be a good alternative fuel processor in the SOFC system. However, the TSR process can remarkably return to be a promising candidate when CaO sorbent is added to a reformer (TSR&C process). The results in Table 8.2 show that the TSR&C process leads to the net saving cost of 13.08%.

Table 8.2 Economical comparison of the SOFC system with different fuel processors.

	Conventional steam reforming	Two-step steam reforming process	
		No CO_2 Capture	With CO_2 capture
Carbon formed region	Yes	No	No
Net electricity produced (MW)	1	1	1
Operating Voltage (Volt)	0.7	0.7	0.7
Ethanol feed rate (liter/hour)	341.35	341.31	276.55
% Fuel utilization	70	70	70
Power density (W/cm^2)	0.44745	0.44747	0.47701
Improvement of power density (%)	-	0.0056	6.6182
SOFC efficiency (%)	49.681	49.685	56.020
SOFC active area (m^2)	223.49	223.47	209.62
Improvement in SOFC area (%)	-	0.0078	6.2069
Capital cost of fuel processor ($)	21,159	37,585	37,943
Capital cost of SOFC ($)	870,156	870,088	816,146
SUM	891,315	907,673	854,089
Fuel feed cost ($/year)	2,691,240	2,690,886	2,180,302
CaO feed cost ($/year)	-	-	79,580
Saving capital cost (%)	-	- 1.83	4.18
Saving of raw material (%)	-	0.01	16.03
Net cost saving[a] (%)	-	- 0.45	13.08

[a] The net cost saving (%) = $\frac{(\text{total cost from CSR - total cost of process})}{(\text{total cost from CSR})} \times 100\%$

8.4 Conclusions

Performances of two main fuel processors: conventional steam reforming (CSR) and two-step steam reforming (TSR), are investigated in the ethanol-fuelled SOFC system under the thermally auto-sustainable condition at which an external energy input is unnecessary. The result demonstrates that the two reforming processes give similar product distribution; high hydrogen yield is found with high CO_2 content. However, a carbon formation can be avoided in the TSR process. When a CO_2 capture is considered, the TSR&C process outperforms the TSR process as a high purity of H_2 is obtained. This factor improves the performance of the SOFC in terms of high power density and cell stack efficiency. From the economic point of view, based on 1 MW power generation, the use of the TSR&C process in the SOFC system gives larger net saving cost than other processes. Thus, the TSR&C fuel processor which does not contribute to the economic problem is an attractive hydrogen production method for the SOFC system.

CHAPTER IX

ENERGY AND EXERGY ANALYSES OF AN ETHANOL-FUELED SOLID OXIDE FUEL CELL FOR A TRIGENERATION SYSTEM

This chapter presents an integrated solid oxide fuel cell (SOFC) system with an absorption chiller that uses heat recovery of the SOFC exhaust gas for combined cooling, heating, and power production (trigeneration) through energy and exergy analyses. The system consists of an ethanol reformer, SOFCs, an air pre-heater, a steam generator and a double-effect $LiBr/H_2O$ absorption chiller. To assess the system performance and determine the irreversibilities in each component, a parametric study of the effects of changing the current density, SOFC temperature, fuel utilization ratio and SOFC anode recirculation ratio on the net electrical efficiency and the efficiency of heating cogeneration, cooling cogeneration and trigeneration is presented.

9.1 Introduction

In addition to being environmentally friendly, a main objective of power generation is to design more efficient power generating plants that can provide multiproduct capabilities (Ahmadi et al., 2013). The solid oxide fuel cell (SOFC) is considered to be a potential technology that is characterized by its high efficiency, low CO_2 emissions and high quality by-product heat generation for cogeneration or trigeneration applications. Trigeneration is defined as the simultaneous production of combined cooling, heating, and power (CCHP) from the same energy source. This process utilizes the waste heat from an SOFC system to improve overall thermal performance because the heat can be recovered not only for heating by directly feeding to heat-demanding devices but also for cooling by driving an absorption chiller. Furthermore, there is a study confirmed that the near future integrated energy system will be reached by incorporating the demand for mobility, as well as the expansion of cogeneration and trigeneration system by adding the facility to produce hydrogen or ethanol from waste (Blarke and Lund, 2008).

The primary objective of this research is to improve understanding, by performing thermodynamic modeling of an integrated ethanol-fueled solid oxide fuel cell and a double-effect water/lithium bromide absorption chiller for a trigeneration system and analyzing it in detail through energetic and exergetic approaches. Comprehensive thermodynamic models have been developed by using the Engineering Equation Solver (EES) software (Klein, 2014) under steady-state operating conditions. The possibility of such an integrated system is also investigated under different operating conditions and parameters considering the process's abilities to handle with ethanol as a fuel.

9.2 System description

A general configuration of the integrated system is shown in Figure 9.1. The system considered herein consists of an SOFC stack, an ethanol reformer, an afterburner, an air pre-heater, a steam generator, and a double-effect water-lithium bromide absorption chiller.

Ethanol fuel is externally reformed with steam to produce a hydrogen-rich gas in the ethanol reformer before being fed into the SOFC anode, and the air is pre-heated and fed into the SOFC cathode. In the SOFC, the electrochemical reaction occurs at the interface of the electrolytes and anodes, in which electricity is generated through the electrochemical reaction of electrons flowing through the anode and an external circuit to the interconnection and cathode, from which SOFC exhausted heat ($\dot{Q}_{\mathrm{SOFC}}$) is also produced. In general, the SOFC cannot electrochemically utilize 100% of the fuel. The residual fuel and the excess air are combusted in the afterburner to obtain extra heat ($\dot{Q}_{\mathrm{AF}}$) at high temperature. Subsequently, the hot flue gas flows to exchange the heat for air preheating in the heat exchanger and then passes the steam generator, where it transfers the heat to the feed water, which is heated and converted into superheated steam used to drive the double-effect absorption chiller.

The key components of a double effect absorption chiller are an evaporator, an absorber, a low pressure generator, a high pressure generator, a condenser, two solution

heat exchangers, two pumps, and throttling valves as shown in Figure 9.1. The heat from superheated steam is supplied to the high pressure generator ($\dot{Q}_{HP,GE}$) to obtain the primary steam and a concentrated LiBr solution. The primary vapor released from the high pressure generator is condensed in the low pressure generator, transferring the heat of condensation to the concentrated solution ($\dot{Q}_{LP,GE}$) to generate a secondary steam. The secondary stream flows to the condenser, and the most concentrated solution, which flows to the absorber. In the condenser, the heat is rejected to the external circuit ($\dot{Q}_{CO}$) to change the steam to the liquid phase. After expansion, the condensed water continues to the evaporator where it is evaporated at low pressure, removing the heat of vaporization ($\dot{Q}_{EV}$). In the absorber, the vapor contacts the concentrated solution, from the low pressure generator through the solution heat exchanger 1, to reject its heat of absorption ($\dot{Q}_{AB}$). The diluted working solution in the absorber is then pumped to the generators, passing through solution heat exchangers 1 and 2, to continuously repeat the thermodynamic cycle.

The analysis of the components in the system (Figure 9.1) is modeled by balanced equations of mass, energy, entropy and exergy. The following assumptions were used: atmospheric air was considered an ideal gas with the composition of 21% oxygen and 79% nitrogen; all flow steams were assumed ideal gases; no pressure losses were considered in the flow paths; ambient temperature and pressure were constant; and a steady-state operation was assumed.

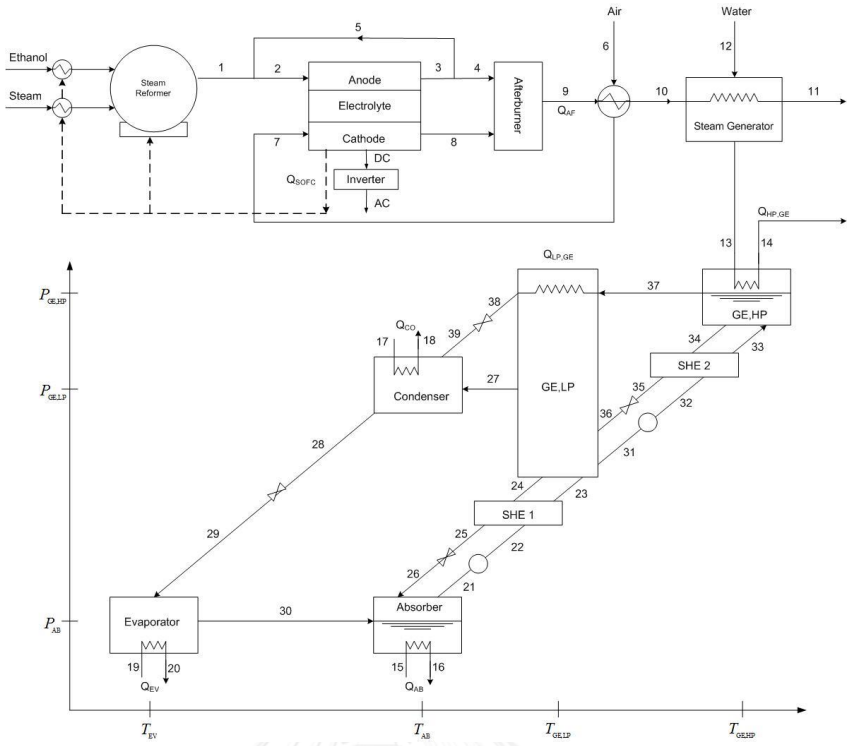

Figure 9.1 Schematic diagram of an SOFC system integrated with a double-effect absorption chiller

9.3 Results and discussion

A comprehensive energy and exergy analyses of the trigeneration system has been performed and results are presented here. The proposed guidance system allows for the sustainable production of electricity as long as an appropriate thermal heat source is available for ethanol steam reforming, air pre-heating, and even steam generating processes. Using the assumptions stated above where i = 0.5 A/cm^2, T =1073 K and U_f = 0.85, integrating energy of the available heat from SOFC by applying to the heat requiring units can boost the energy efficiency of the system to be 88 % instead of the normal which is 45 %. This is remarkable mainly because no additional external hot utilities are need. Moreover, the exergy analysis is accomplished to determine that the ruins of energy quality can be avoided by fitting the location of equipment. In this case the hot flue gas from afterburner should deliver to exchange the heat for air pre-heating in the heat exchanger before passing through steam generator. Such a proper configuration presents exergetic performance improvement resulting in

a 67 % and 25 % reduction in the exergy destruction of air pre-heater and steam generator respectively compared with the values when twisting the position of these two devices. This integrated power system is part of the success under energy and exergy analyses.

To investigate the performance variation of the trigeneration system in term of energy and exergy efficiencies, exergy destruction and the amount of product proportion, certain design parameters such as current density, SOFC temperature, fuel utilization ratio and SOFC anode circulation ratio are varied. These design parameters plays an important role in the system output. The variations of these parameters are discussed in detail below.

9.3.1 Energy and exergy analyses

9.3.1.1 Effect of current density of the SOFC on energy and exergy efficiencies, exergy destruction rate and electrical to heating and cooling ratios

The effect of changing the current density of the SOFC on the energy efficiency, exergy efficiency, exergy destruction rate and electrical to heating and cooling ratios is shown in Figure 9.2 (a)-(d) under a constant SOFC temperature of 1073 K, 85% fuel utilization and no anode exhaust gas circulation. In these figures, the current density increase from 0.2 to 0.9 A/cm^2 is considered. Figure 9.2 (a) and (b) show that all efficiencies decrease as the current density increases. The drop in the efficiency is attributed to the decrease in the cell voltage. As the efficiency of the SOFC decreases with increasing current density, the waste heat from the SOFC increases. However, both energy and exergy efficiencies of co- and trigeneration still decrease because the reduction of net SOFC power mainly dominates the heating and cooling products. The highest net electrical efficiency is 53%, which is obtained at a current density of 0.2 A/cm^2, whereas the lowest net electrical efficiency is 37% at 0.9 A/cm^2. The energy efficiency of the cooling cogeneration exhibited a 6% gaining in the net electrical energy efficiency; however, the cooling cogeneration exergy efficiency averaged 2% higher than the net electrical exergy efficiency. This small difference in gain is a result of the small amount of cooling energy to electrical energy in the cycle, which is

approximately 4-12% of the electrical energy. The maximum cooling energy efficiency is 59% whereas the maximum cooling exergy efficiency is 55%. Alternatively, the maximum heating energy and exergy efficiencies are 79% and 64%, respectively. It can be observed that when trigeneration is used, the energy efficiency significantly increases by at least 32% from the net electrical efficiency. The influence of the current density on the exergy destruction rate of the different components of the system is presented in Figure 9.2 (c). It can be observed that all of the exergy destruction components increase as the current density increases. This study reveals that although the current density has a slight effect on the absorption chiller, the reformer, and the air heat exchanger, the current density is one of the operating parameters modified inside the SOFC stack and directly affects the amount of SOFC exhaust heat that enters to the afterburner. Therefore, the change in the exergy destruction rate with current density is significantly increased for the afterburner and SOFC. The amount of the change in the exergy destruction reaches 1622 kW. The effect of the current density on the electrical to heating and cooling ratios is presented in Figure 9.2 (d). In this figure, the electrical to heating ratio changes from 2 to 0.9, whereas the electrical to cooling ratio changes from 8.5 to 25 with the change in the current density. The electrical to cooling ratio sharply increases when the SOFC system is operated at a high current density because of the reduced cooling capacity compared to the power output of the system.

(a)

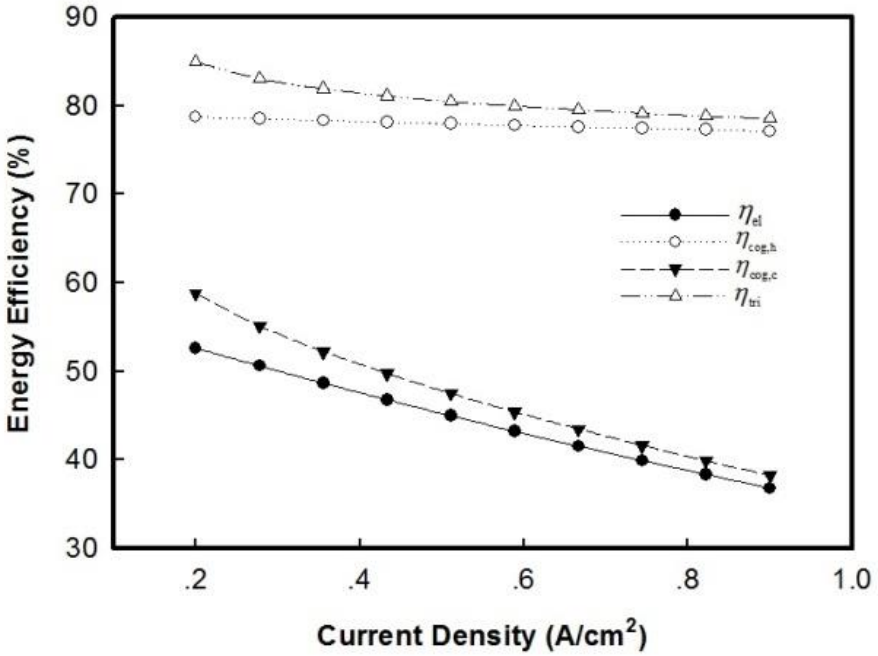
Energy Efficiency (%)
90
80
70
60
50
40
30
.2
.4
.6
.8
1.0
Current Density (A/cm²)
η_{el}
$\eta_{cog,h}$
$\eta_{cog,c}$
η_{tri}

(b)

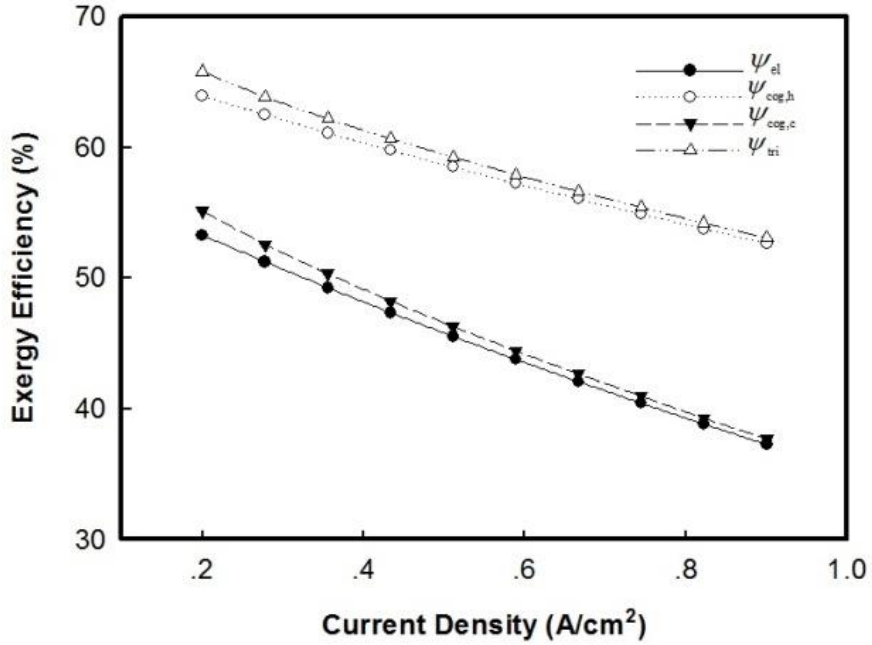
Exergy Efficiency (%)
70
60
50
40
30
.2
.4
.6
.8
1.0
Current Density (A/cm²)
ψ_{el}
$\psi_{cog,h}$
$\psi_{cog,c}$
ψ_{tri}

(c)

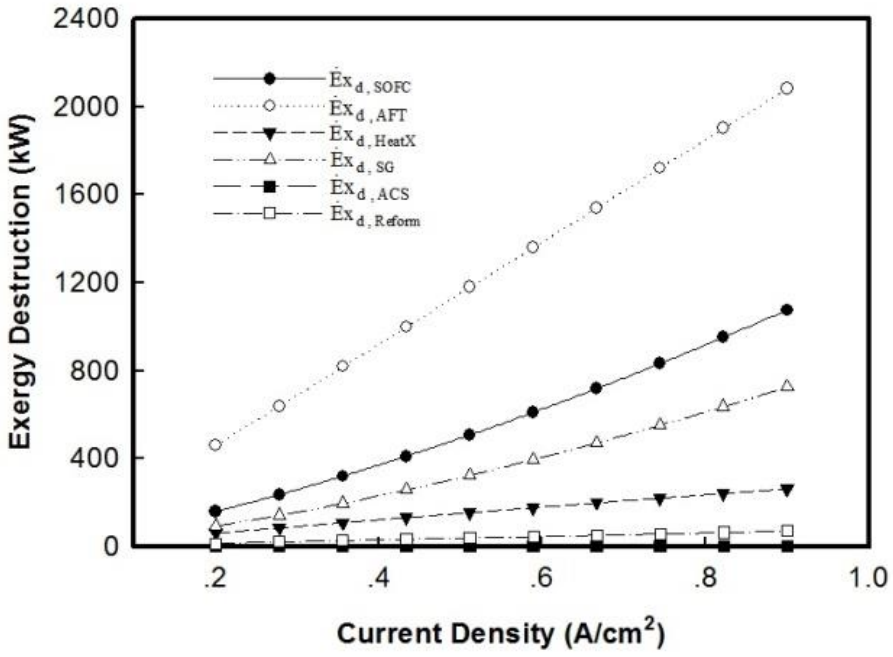

(d)

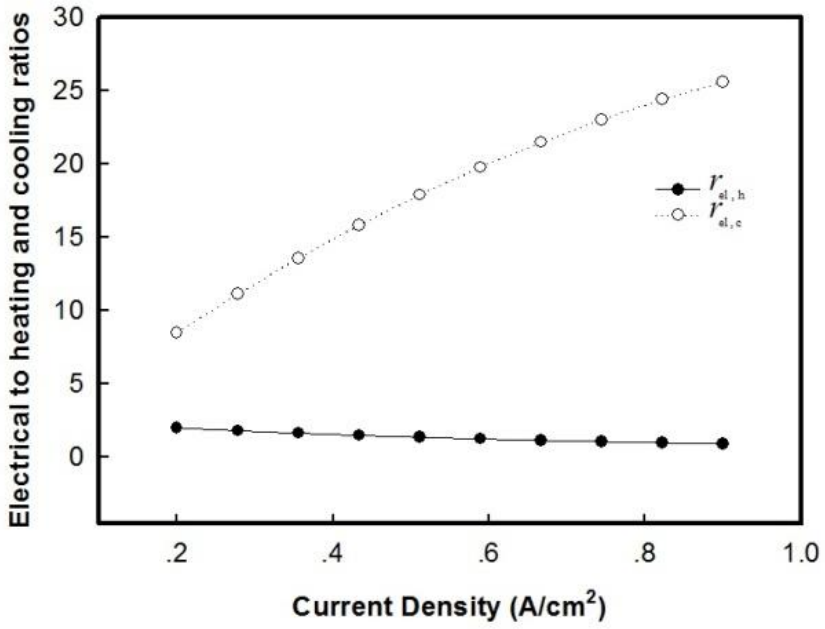

Figure 9.2 Effect of current density on (a) energy efficiency, (b) exergy efficiency, (c) exergy destruction rate and (d) electrical to heating and cooling ratios at T_{SOFC} = 1073 K and r = 0, U_f = 0.85.

9.3.1.2 Effect of SOFC temperature on energy and exergy efficiencies, exergy destruction rate and electrical to heating and cooling ratios

The variation of the energy efficiency, exergy efficiency, exergy destruction rate and electrical to heating and cooling ratios at different operating SOFC temperatures is shown in Figure 9.3 (a)-(d), respectively. The effect of changing the SOFC temperature was studied from 973 to 1173 K under a constant current density of 0.5, 85% fuel utilization and no anode exhaust gas circulation. The following results were obtained by performing a reverse behavior of the change in the current density. This is attributed to the fact that the internal reforming and electrochemical reactions in the SOFC are favored during operation at high temperatures: the increase in produced hydrogen promotes the electrochemical reaction in the SOFC stack. The voltage losses of the SOFC will be considerably decreased as the operating temperature increases, resulting in the increase of actual cell voltage and the generation of more SOFC electrical power. It is for this reason that the efficiency is enhanced as the SOFC temperature increases. Figure 9.3 (a)shows that the energy efficiencies reach their maximum at the maximum temperatures considered. The maximum energy efficiencies of the cooling and heating cogeneration and the trigeneration are 52%, 94%, and 96%, respectively. The cooling cogeneration efficiency has a similar trend compared with the net electrical efficiency, which has an approximate 3% gain in the net electrical energy efficiency. Figure 9.3 (b) reveals that the temperature at which the exergy efficiency is the highest is the same temperature at which the energy efficiency performs. The maximum exergy efficiencies of the cooling and heating cogeneration and the trigeneration are 51%, 61%, and 62%, respectively. Figure 9.3 (c) shows the effect of changing the SOFC temperature on the exergy destruction rate of different components of the system. This figure shows that the afterburner, SOFC, steam generator, and air heat exchanger exhibit a lot of change in the exergy destruction rates compared to the reformer and absorption cooling system. Specifically, at a high temperature of the SOFC, the exergy destruction of the afterburner is considerable. This result is because even the increase in SOFC temperature drops the net anode exhaust heat and depletes the useful gas, there is a high exergy value of hot gas fed to the afterburner and then a huge exergy of heat loss occurs when the heat of combustion is released. Figure 9.3 (d) shows the effect of changing the temperature of the SOFC on the electrical to heating

and cooling ratios, both of which exhibit their highest values at a temperature of 1084 K.

(a)

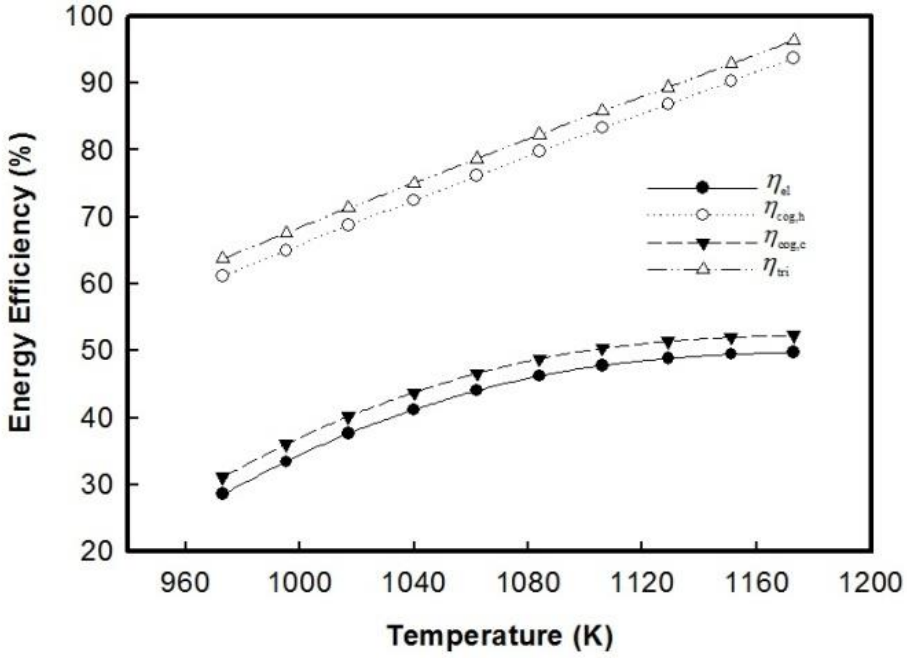

(b)

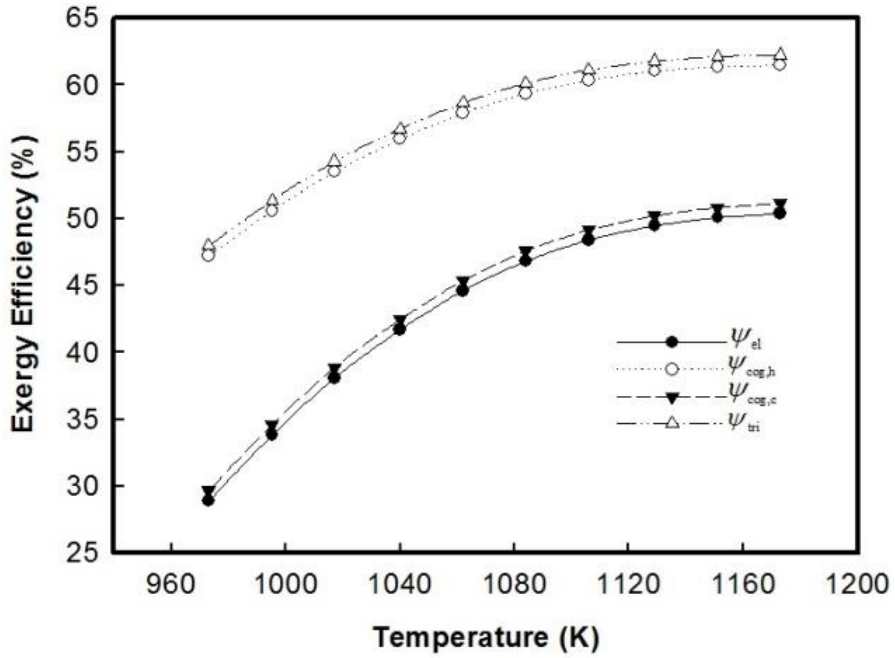

(c)

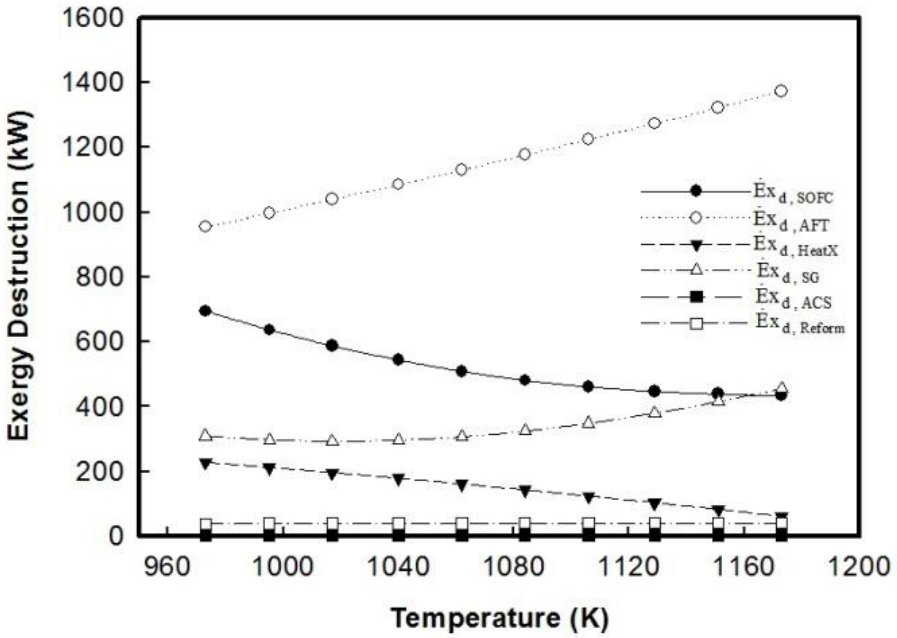

(d)

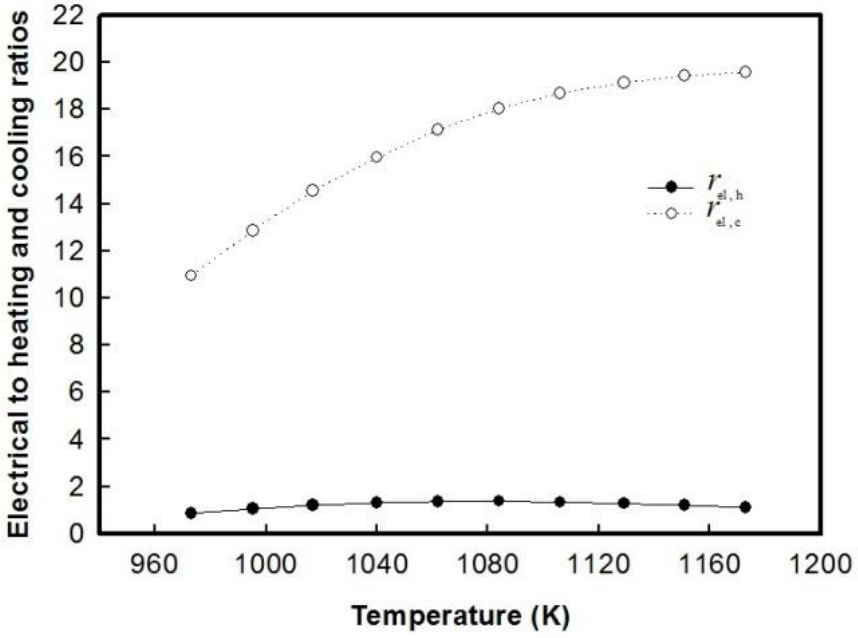

Figure 9.3 Effect of SOFC temperature on (a) energy efficiency, (b) exergy efficiency, (c) exergy destruction rate and (d) electrical to heating and cooling ratios at i = 0.5 A/cm^2 and r = 0, U_f = 0.85

9.3.1.3 Effect of fuel utilization ratio on energy and exergy efficiencies, exergy destruction rate and electrical to heating and cooling ratios

The increase in fuel utilization results in an increase in the hydrogen consumed in the SOFC stack and the production of electricity. Figure 9.4 (a) and (b) show that the energy and exergy efficiencies increase with the increasing fuel utilization ratio because of the improvement of the SOFC performance in terms of electrical efficiency. In both energy and exergy analyses, the change in the net electrical efficiency and cooling cogeneration efficiency is slightly lower than the heating cogeneration and trigeneration because the fuel utilization also indicates the electrochemical reaction and the amount of SOFC exhaust heat. The more the fuel utilization ratio increases, the more heat will be generated by the SOFC. The highest net electrical efficiency of 47% was obtained with a fuel utilization ratio of 0.93, whereas the lowest net electrical efficiency of 39% was obtained at a fuel utilization ratio of 0.73. The trigeneration cycle has maximum energy and exergy efficiencies higher than the power cycle at 37% and 17%, respectively. Figure 9.4 (c) shows that the exergy destruction in the afterburner strongly decreases with increasing fuel utilization because the amount of exergy gradient in the flow decreases with increasing amounts of heat. However, the trends of the electrical to heating and cooling ratios, as shown in Figure 9.4 (d), are unlike the previous two cases shown in Figure 9.2 (d) and Figure 9.3 (d). When the fuel utilization ratio increases, the electrical to cooling ratio decreases, whereas the electrical to heating ratio increases. This result is because at higher fuel utilization ratios, the heat generation rate from the SOFC is higher compared to the increase in power generation, whereas the cooling product increases in a lower value.

(a)

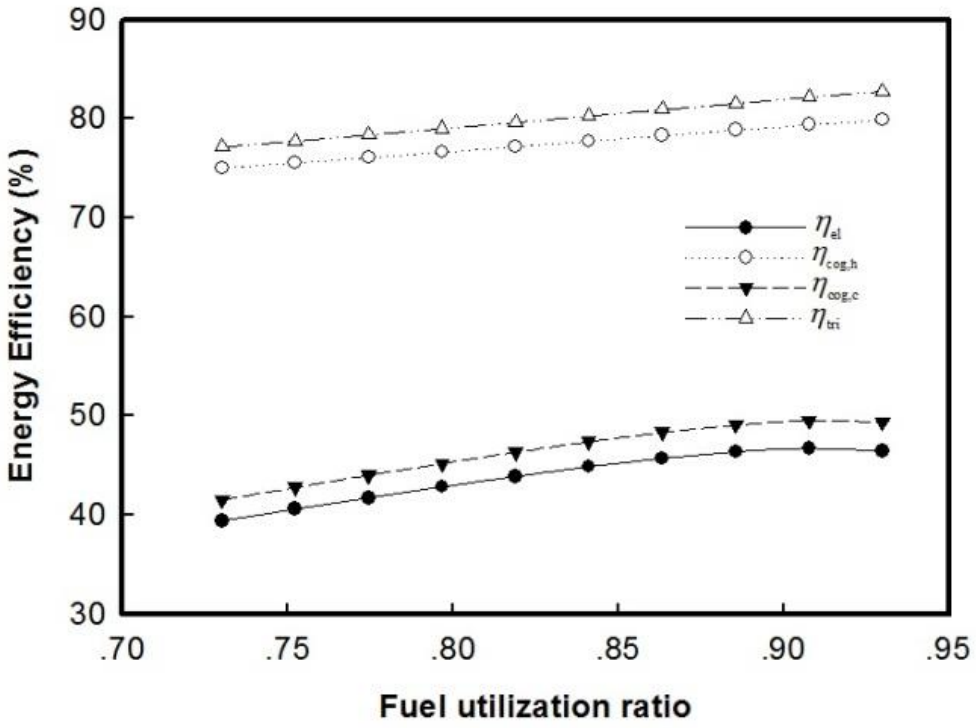
Energy Efficiency (%)
90
80
70
60
50
40
30
.70
.75
.80
.85
.90
.95
Fuel utilization ratio
η_{el}
$\eta_{cog,h}$
$\eta_{cog,e}$
η_{tri}

(b)

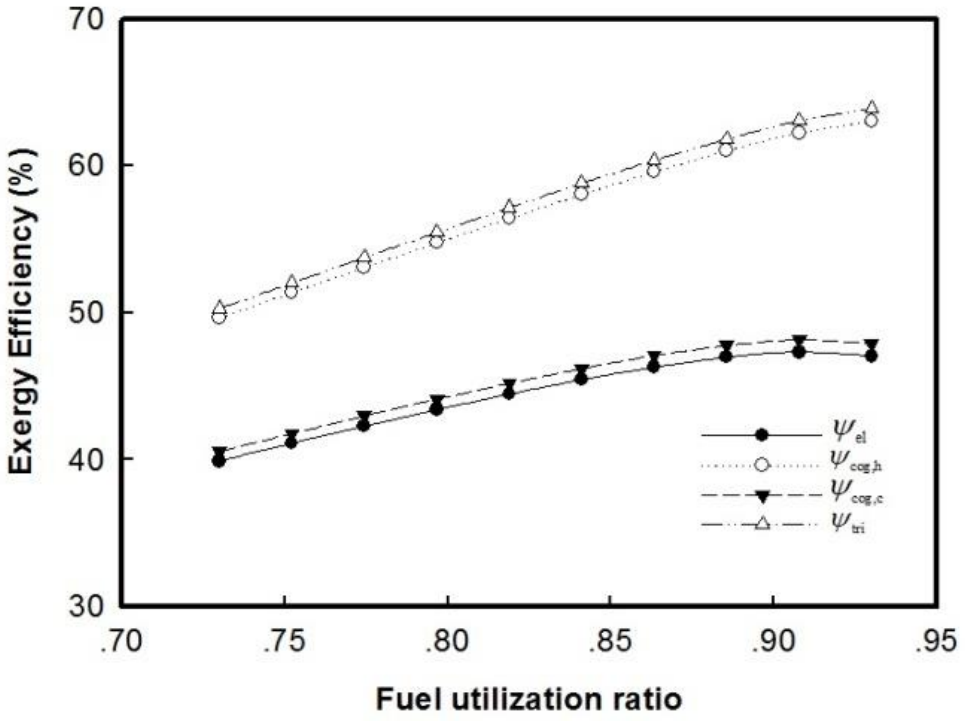
Exergy Efficiency (%)
70
60
50
40
30
.70
.75
.80
.85
.90
.95
Fuel utilization ratio
ψ_{el}
$\psi_{cog,h}$
$\psi_{cog,e}$
ψ_{tri}

(c)

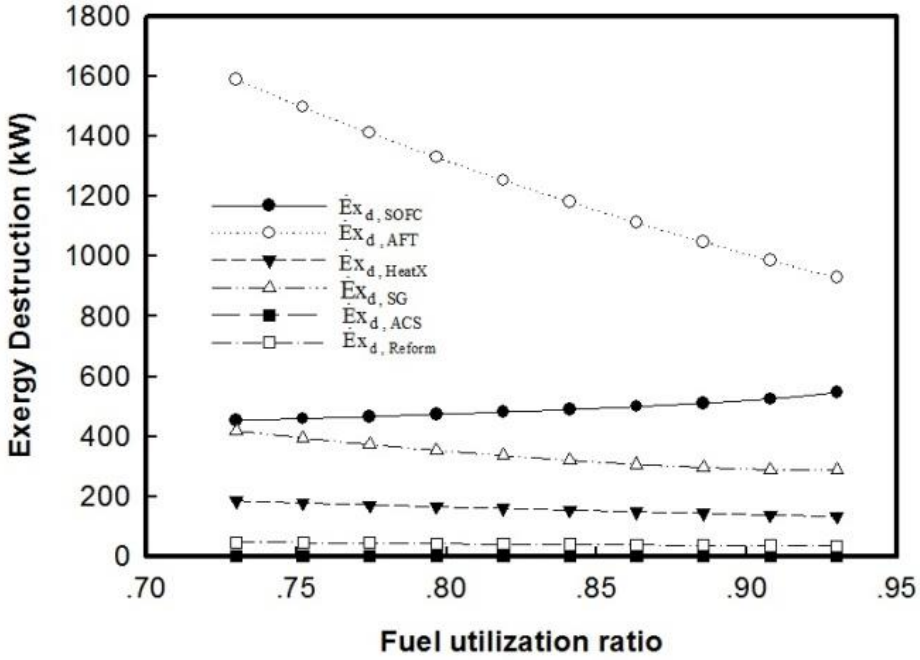

(d)

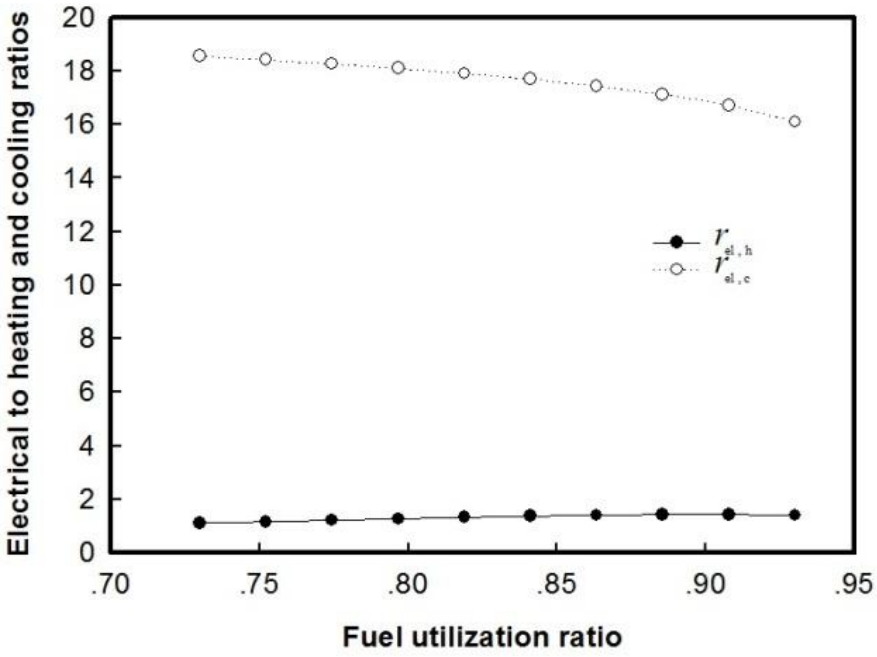

Figure 9.4 Effect of fuel utilization ratio on (a) energy efficiency, (b) exergy efficiency (c) exergy destruction rate and (d) electrical to heating and cooling ratios at i = 0.5 A/cm^2, T_{SOFC} = 1073 K, and r = 0.

9.3.1.4 Effect of SOFC anode circulation ratio on energy and exergy efficiencies, exergy destruction rate and electrical to heating and cooling ratios

The effect of the circulation ratio of the anode exhaust gas on the energy efficiency, exergy efficiency, exergy destruction and electrical to heating and cooling ratios is presented in Figure 9.5 (a)-(d), respectively. In these figures, the circulation ratio was varied from 0.2 to 0.5, which was shown to have a minimal effect on the efficiencies and the electrical to heating and cooling ratios. It was determined that the variation of the net electrical energy efficiency and cooling cogeneration energy efficiency was within 1%, which is similar to what was found for the exergy efficiency. The electrical efficiency is nearly constant because the useful fuel in the anode recycle stream is depleted by previous reactions in the SOFC. The residual gas exiting the SOFC anode was found to dilute the fuel-fed SOFC more than enhance the SOFC power. However, Figure 9.5 (c) shows that the exergy destruction of the afterburner decreases with increasing circulation ratio, as with the changing of the fuel utilization ratio; however, the change in exergy destruction of the SOFC was lower with increasing fuel utilization ratio. Considering the electrical to heating and cooling ratios shown in Figure 9.5 (d), when the SOFC is operated at any circulation ratio, the results do not change significantly. The electrical to heating and cooling ratios remain constant, which implies that the SOFC circulation ratio has less of an impact on the amount of power, heating and cooling compared to other parameters.

(a)

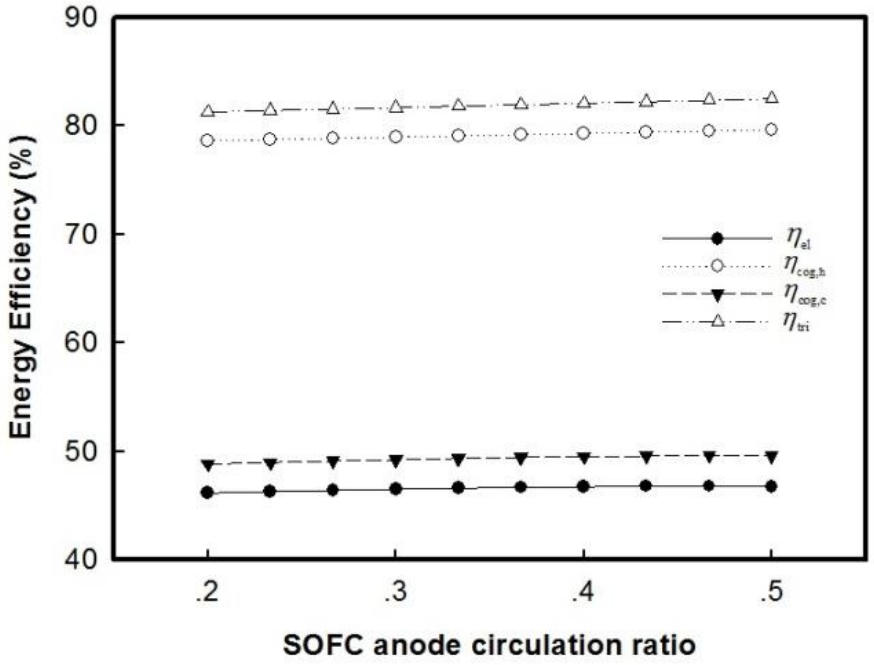
90
80
70
60
50
40
Energy Efficiency (%)
.2
.3
.4
.5
SOFC anode circulation ratio
η_{el}
$\eta_{cog,h}$
$\eta_{cog,c}$
η_{tri}

(b)

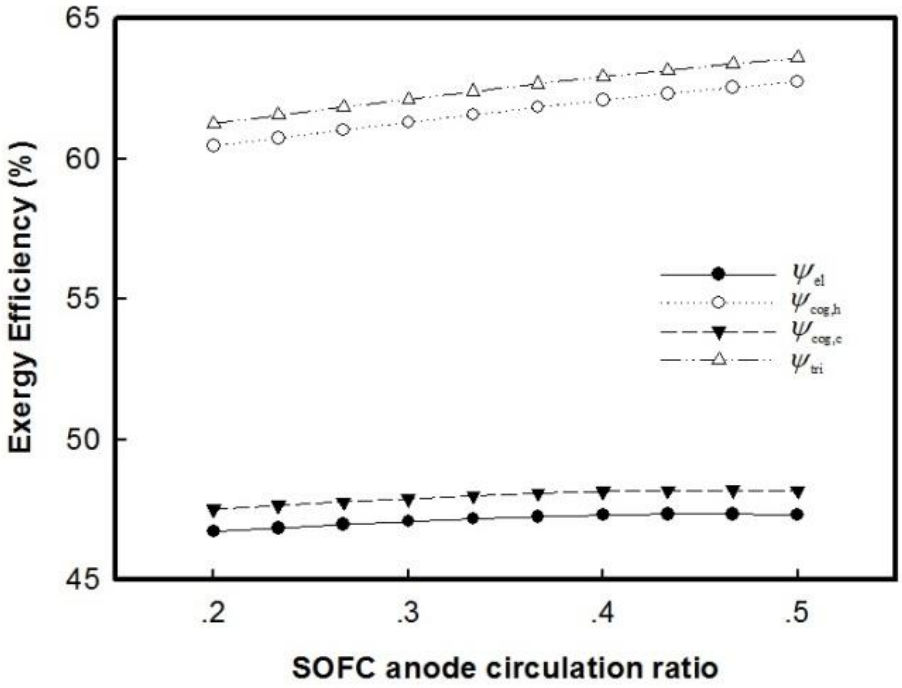
65
60
55
50
45
Exergy Efficiency (%)
.2
.3
.4
.5
SOFC anode circulation ratio
ψ_{el}
$\psi_{cog,h}$
$\psi_{cog,c}$
ψ_{tri}

(c)

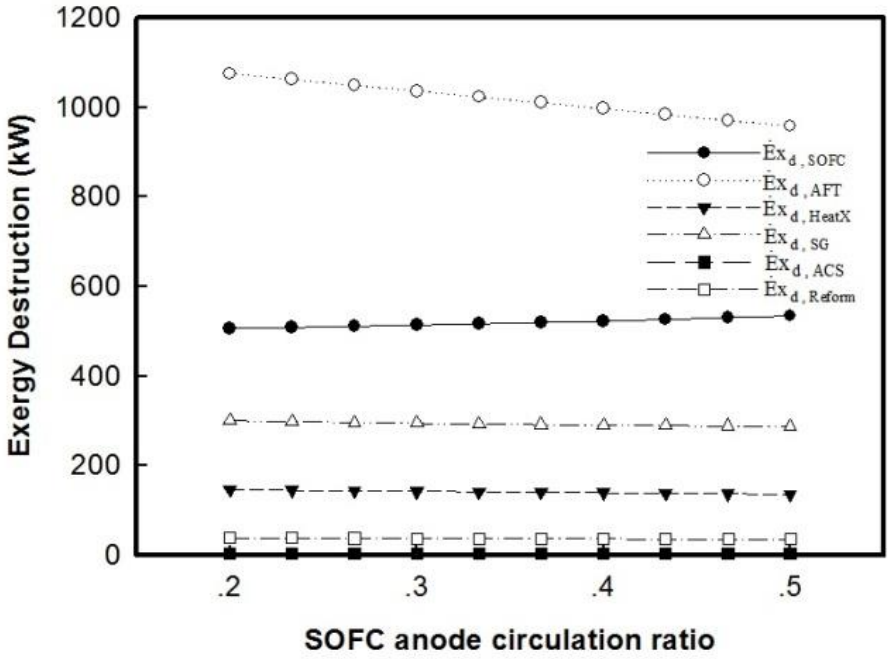

(d)

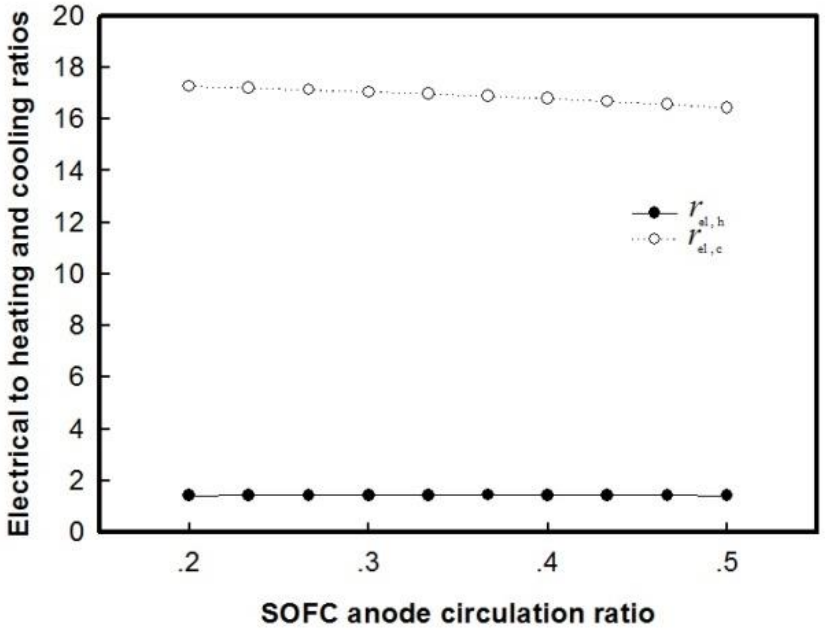

Figure 9.5 Effect of SOFC anode circulation ratio on (a) energy efficiency, (b) exergy efficiency (c) exergy destruction rate and (d) electrical to heating and cooling ratios at i = 0.5 A/cm^2, T_{SOFC} = 1073 K, and U_f = 0.85.

9.3.2 Exergoenvironmental analysis

9.3.2.1 Effect of current density on CO_2 emission and sustainability index.

The sustainability index decreases with increased current density as shown in Figure 9.6. It implies that the destruction of exergy mainly dominates the increase of exergy from input. Figure 9.6 also shows that increasing current density increases CO_2 emission due to the increase of the mass flow rate injected from the afterburner.

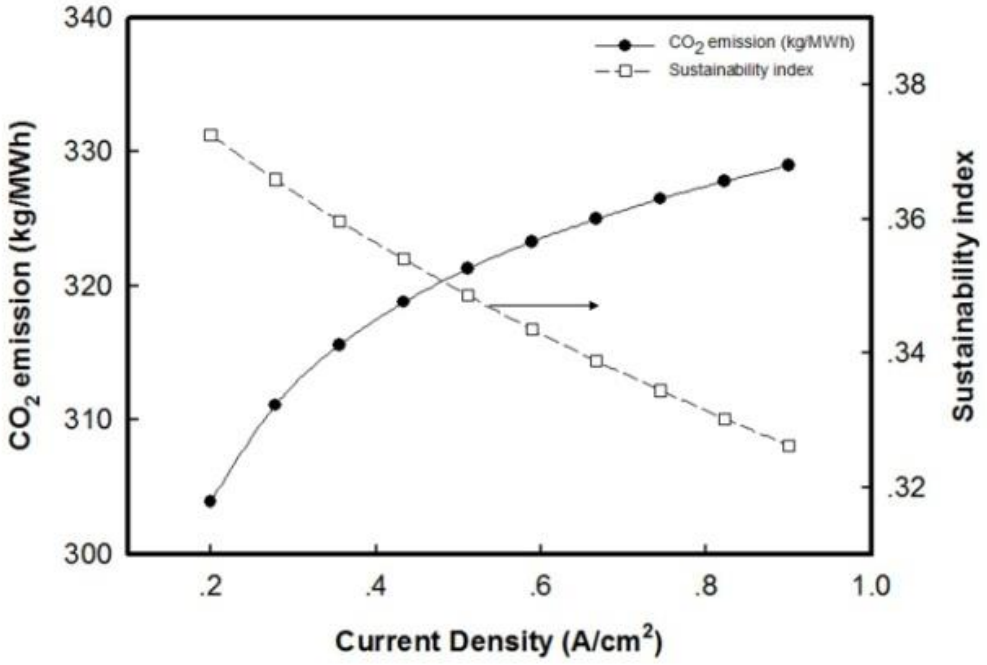

Figure 9.6 Effect of current density on CO_2 emission and sustainability index.

9.3.2.2 Effect of SOFC temperature on CO_2 emission and sustainability index.

On the other hand, increasing the SOFC temperature enhances the efficiencies and the exergy destruction decreases as presented in Figure 9.3. This is attributed to the fact that the increase of temperature promotes the electrochemical reaction in the SOFC stack to generate more electrical power. The optimum values of the SOFC temperature are shown in Figures 9.7. At the optimum temperature, a decrease in the exergy destruction of SOFC is higher than an increase in the exergy destruction of afterburner.

Consequently, the total exergy destruction is minimized and sustainability index reaches the maximum value.

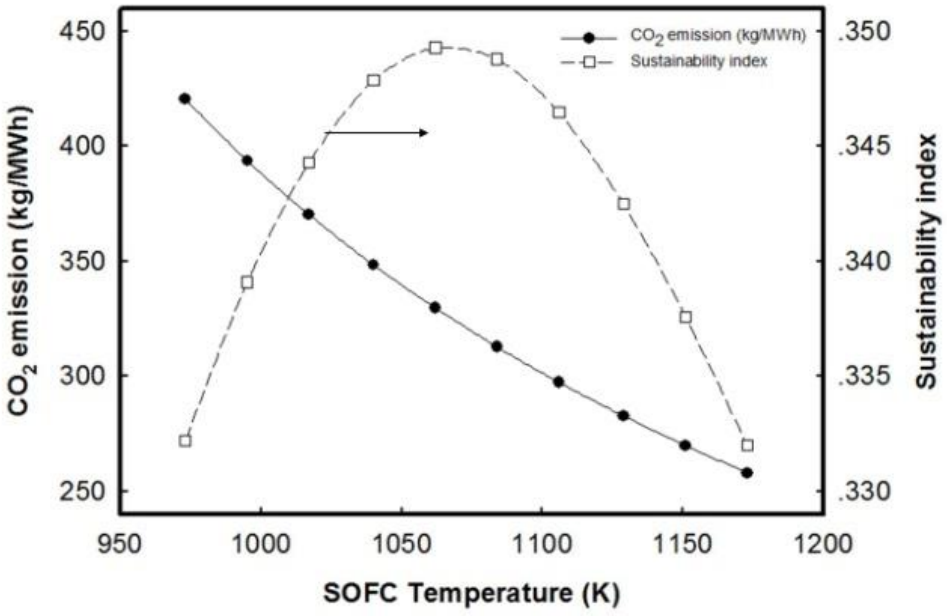

Figure 9.7 Effect of SOFC temperature on CO_2 emission and sustainability index.

The exergy destruction in system components is shown in Figure 9.8. The highest exergy destruction occurs in the afterburner mainly due to the irreversibilities associated with the combustion reaction and the large temperature difference between the gases entering the afterburner and the flame temperature. Significant exergy destruction can also be noticed in the SOFC, SG and the air pre-heater. To provide environmental insights, Figure 9.9 shows that the trigeneration system (including cooling application) has less CO_2 emission than the SOFC and the combined-heat and power cycles, providing a significant motivation for the use of heat from SOFC for cooling application as well. It is also observed that the present trigeneration system provides higher power output, compared to other types of conventional power plants.

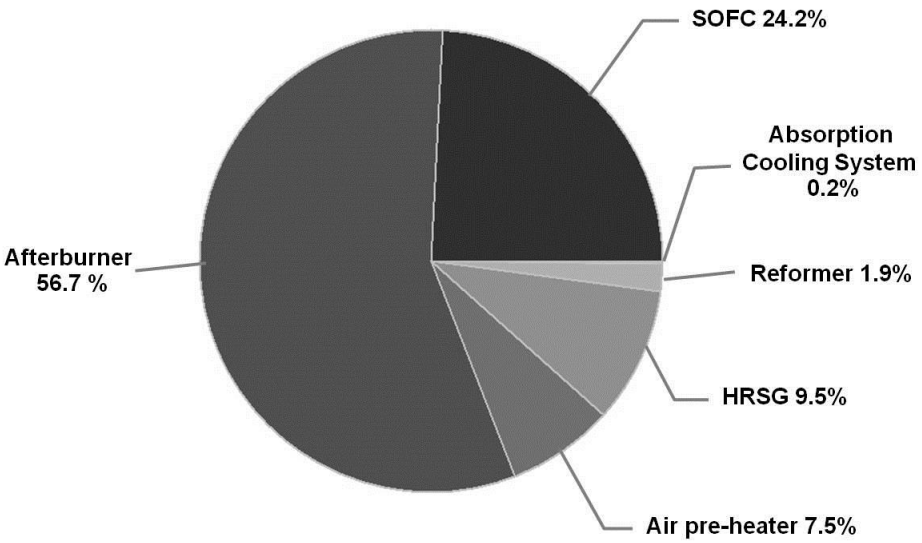

Figure 9.8 Exergy destruction in the system components.

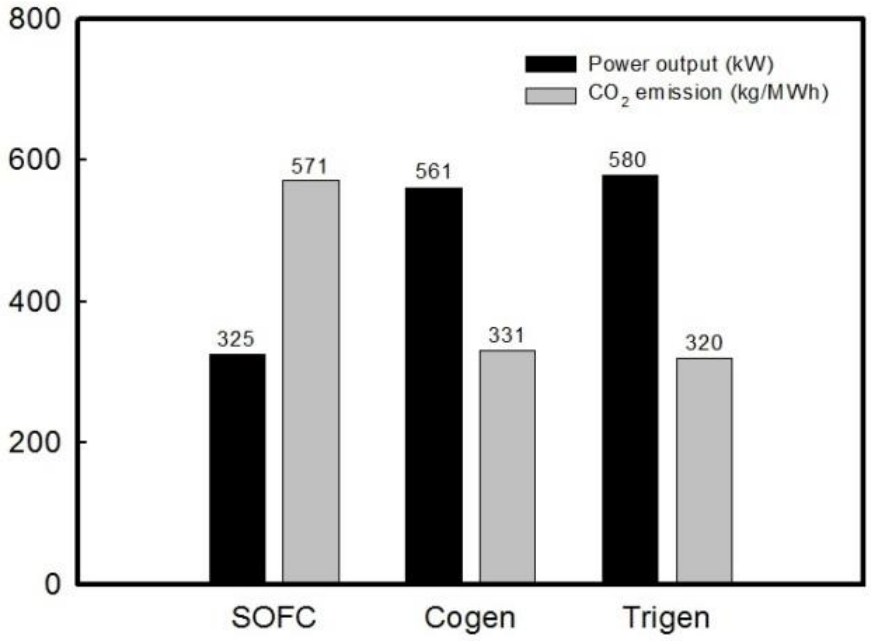

Figure 9.9 Comparison of CO_2 emission and power output of different types of plants.

Although the integration of solid oxide fuel cell and absorption chiller is feasible in term of technology and is a very promising heat recovery technique, cost is the primary constraint on the widespread adoption of absorption chiller systems. Absorption systems require greater pump energy than electric chillers. The size of condenser water pumps is generally a function of the flow rate per unit cooling capacity. Cooling technologies with lower COPs typically require a significantly higher condenser water flow rate than those technologies with higher COPs, therefore requiring larger pumps. Similarly, absorption chillers require larger cooling tower capacity than electric chillers, due to the larger volume of water. However, absorption chillers can be quite economical in the right situations, their exact economics must be worked out on a project-by-project basis.

9.4 Conclusions

Energy and exergy analyses of a trigeneration plant based on an ethanol-fueled SOFC and absorption chiller are conducted. The results highlight the benefits of considering the energy integration of the available heat within the system. In addition, energy and exergy analyses have been used successfully to estimate the energy utilization and identify the exergy losses which are leading to a better understanding, clearer problem situation and more correct use of heat in this trigeneration system. The performance of the system was studied under the variation of the SOFC current density, temperature, fuel utilization ratio and anode circulation ratio. The main findings in this study are as follows:

- The energy analysis of the trigeneration plant shows that there is at least a 32% gain in efficiency compared to the power cycle only (electrical net efficiency). The maximum energy efficiencies of the trigeneration, heating cogeneration, cooling cogeneration, and net electricity are 96%, 94%, 59% and 53%, respectively.
- The exergy analysis of the trigeneration plant shows that there is a gain of approximately 10% in efficiency compared to the power cycle only (electrical net efficiency). The maximum exergy efficiencies of the

trigeneration, heating cogeneration, cooling cogeneration, and net electricity are 64%, 63%, 55% and 53%, respectively.

- All of the examined efficiencies continuously decrease as the current density increases, except for a constant decrease in the cell voltage. Unlike the change in the SOFC temperature, the efficiencies increase as a result of the dissimilar behaviors of the voltage loss components.
- The SOFC circulation ratios have less impact on the amount of power, heating and cooling compared to other parameters. However, the change in the fuel utilization is more sensitive to the amount of trigeneration product as observed in the significant change of the electrical to heating and cooling ratios.
- The most significant sources of exergy destruction rates are the afterburner and SOFC. This is partly due to the nature of the combustion process associated with the chemical reaction and heat transfer across the large temperature. Therefore, further improvements in designing these components also need to be considered.
- The operation of the investigated double-effect absorption chiller is unchanged. Therefore, this conclusion is relatively limited to its conditions.

In an exergoenvironmental analysis, solid oxide fuel cell systems for heating, cooling and electricity generation has been performed to provide useful insights in terms of heat recovery and environmental aspects. The results show that system efficiencies, exergy destructions, the amount of CO_2 emission and sustainability index are notably affected by operating current density and SOFC temperature. The afterburner and SOFC are the two main components with the high exergy destruction while the use of absorption chillers offers effective heat recovery with the lowest exergy destruction of the whole system. In addition, chilled water generation from absorption chillers in the trigeneration system is one of the best heat recovery strategies that exhibit lesser CO_2 emissions than other types of conventional power plants.

REFERENCES

Abanades, J. C. (2002). The maximum capture efficiency of CO_2 using a carbonation/calcination cycle of $CaO/CaCO_3$. Chemical Engineering Journal 90: 303-306.

Abdullah S., Kamarudin S.K., Hasran U.A., Masdar M.S. and W.R.W., D. (2014). Review: Modeling and simulation of a direct ethanol fuel cell: An overview. Journal of Power Sources 262: 401-406.

Aguiar, P., Adjiman, C. S. and Brandon, N. P. (2004). Anode-supported intermediate temperature direct internal reforming solid oxide fuel cell. I: model-based steady-state performance. Journal of Power Sources 138: 120-136.

Ahmadi, P., Dincer, I. and Rosen, M. A. (2013). Development and assessment of an integrated biomass-based multi-generation energy system. Energy 56: 155-166.

Akiyama, M., Oki, Y. and Nagai, M. (2012). Steam reforming of ethanol over carburized alkali-doped nickel on zirconia and various supports for hydrogen production. Catalysis Today 181: 4-13.

Al-Hamamre, Z. and Hararah, M. A. (2010). Hydrogen production by thermal partial oxidation of ethanol: Thermodynamics and kinetics study. International Journal of Hydrogen Energy 35: 5367-5377.

Al-Qattan, A., ElSherbini, A. and Al-Ajmi, K. (2014). Solid oxide fuel cell application in district cooling. Journal of Power Sources 257: 21-26.

Al-Sulaiman F.A., Hamdullahpur F. and I., D. (2011). Performance comparison of three trigeneration systems using organic rankine cycles. Energy 36: 5741-5754.

Al-Sulaiman, F. A., Dincer, I. and Hamdullahpur, F. (2010a). Energy analysis of a trigeneration plant based on solid oxide fuel cell and organic Rankine cycle. International Journal of Hydrogen Energy 35: 5104-5113.

Al-Sulaiman, F. A., Dincer, I. and Hamdullahpur, F. (2010b). Exergy analysis of an integrated solid oxide fuel cell and organic Rankine cycle for cooling, heating and power production. Journal of Power Sources 195: 2346-2354.

Amiri, S., Hayes, R. E., Nandakumar, K. and Sarkar, P. (2013). Modelling heat transfer for a tubular micro-solid oxide fuel cell with experimental validation. Journal of Power Sources 233: 190-201.

Angeli, S. D., Monteleone, G., Giaconia, A. and Lemonidou, A. A. (2014). State-of-the-art catalysts for CH4 steam reforming at low temperature. International Journal of Hydrogen Energy 39: 1979-1997.

Arteaga-Perez, L. E., Casas, Y., Peralta, L. M., Kafarov, V., Dewulf, J. and Giunta, P. (2009). An auto-sustainable solid oxide fuel cell system fueled by bio-ethanol: Process simulation and heat exchanger network synthesis. Chemical Engineering Journal 150: 242-251.

Auprêtre, F., Descorme, C. and Duprez, D. (2002). Bio-ethanol catalytic steam reforming over supported metal catalysts. Catalysis Communications 3: 263-267.

Aupretre, F., Descorme, C., Duprez, D., Casanave, D. and Uzio, D. (2005). Ethanol steam reforming over MgxNi1−xAl2O3 spinel oxide-supported Rh catalysts. Journal of Catalysis 233: 464-477.

Baniasadi, E. and Dincer, I. (2011). Energy and exergy analyses of a combined ammonia-fed solid oxide fuel cell system for vehicular applications. International Journal of Hydrogen Energy 36: 11128-11136.

Basile, A., Pinacci, P., Iulianelli, A., Broglia, M., Drago, F., Liguori, S., Longo, T. and Calabrò, V. (2011). Ethanol steam reforming reaction in a porous stainless steel supported palladium membrane reactor. International Journal of Hydrogen Energy 36: 2029-2037.

Benito, M., Sanz, J. L., Isabel, R., Padilla, R., Arjona, R. and Daza, L. (2005). Bio-ethanol steam reforming: Insights on the mechanism for hydrogen production. Journal of Power Sources 151: 11-17.

Bertei, A., Thorel, A. S., Bessler, W. G. and Nicolella, C. (2012). Mathematical modeling of mass and charge transport and reaction in a solid oxide fuel cell with mixed ionic conduction. Chemical Engineering Science 68: 606-616.

Biegler, L. T., Grossman, E. I. and Westerberg, A. W. (1997). Systematic methods of chemical process design, Prentice Hall PTR.

Biswas, P. and Kunzru, D. (2007). Steam reforming of ethanol for production of hydrogen over Ni/CeO–ZrO catalyst: Effect of support and metal loading. International Journal of Hydrogen Energy 32: 969-980.

Blarke, M. B. and Lund, H. (2008). The effectiveness of storage and relocation options in renewable energy systems. Renewable Energy 33: 1499-1507.

Braun, R. J., Klein, S. A. and Reindl, D. T. (2006). Evaluation of system configurations for solid oxide fuel cell-based micro-combined heat and power generators in residential applications. Journal of Power Sources 158: 1290-1305.

Brett, D. J. L., Aguiar, P. and Brandon, N. P. (2006a). System modelling and integration of an intermediate temperature solid oxide fuel cell and ZEBRA battery for automotive applications. Journal of Power Sources 163: 514-522.

Brett, D. J. L., Aguiar, P., Brandon, N. P., Bull, R. N., Galloway, R. C., Hayes, G. W., Lillie, K., Mellors, C., Smith, C. and Tilley, A. R. (2006b). Concept and system design for a ZEBRA battery–intermediate temperature solid oxide fuel cell hybrid vehicle. Journal of Power Sources 157: 782-798.

Cai, W., Wang, F., Van Veen, A. C., Provendier, H., Mirodatos, C. and Shen, W. (2008). Autothermal reforming of ethanol for hydrogen production over an Rh/CeO2 catalyst. Catalysis Today 138: 152-156.

Calise, F., Dentice d'Accadia, M., Palombo, A. and Vanoli, L. (2006). Simulation and exergy analysis of a hybrid Solid Oxide Fuel Cell (SOFC)–Gas Turbine System. Energy 31: 3278-3299.

Cardona, C. A. and Sánchez, Ó. J. (2007). Fuel ethanol production: Process design trends and integration opportunities. Bioresource Technology 98: 2415-2457.

Casanovas, A., Roig, M., de Leitenburg, C., Trovarelli, A. and Llorca, J. (2010). Ethanol steam reforming and water gas shift over Co/ZnO catalytic honeycombs doped with Fe, Ni, Cu, Cr and Na. International Journal of Hydrogen Energy 35: 7690-7698.

Casas-Ledon, Y., Arteaga-Perez, L. E., Dewulf, J., Morales, M. C., Rosa, E., Peralta-Suáreza, L. M. and Van Langenhove, H. (2014). Health external costs associated to the integration of solid oxide fuel cell in a sugar–ethanol factory. Applied Energy 113: 1283-1292.

Casas, Y., Arteaga, L. E., Morales, M., Rosa, E., Peralta, L. M. and Dewulf, J. (2010). Energy and exergy analysis of an ethanol fueled solid oxide fuel cell power plant. Chemical Engineering Journal 162: 1057-1066.

Casas, Y., Dewulf, J., Arteaga-Pérez, L. E., Morales, M., Van Langenhove, H. and Rosa, E. (2011). Integration of Solid Oxide Fuel Cell in a sugar–ethanol factory: analysis of the efficiency and the environmental profile of the products. Journal of Cleaner Production 19: 1395-1404.

Chan, S. H., Khor, K. A. and Xia, Z. T. (2001). A complete polarization model of a solid oxide fuel cell and its sensitivity to the change of cell component thickness. Journal of Power Sources 93: 130-140.

Cheddie, D. F. (2011). Thermo-economic optimization of an indirectly coupled solid oxide fuel cell/gas turbine hybrid power plant. International Journal of Hydrogen Energy 36: 1702-1709.

Chen, D., Zeng, Q., Su, S., Bi, W. and Ren, Z. (2013a). Geometric optimization of a 10-cell modular planar solid oxide fuel cell stack manifold. Applied Energy 112: 1100-1107.

Chen, H., Yu, H., Peng, F., Yang, G., Wang, H., Yang, J. and Tang, Y. (2010). Autothermal reforming of ethanol for hydrogen production over perovskite LaNiO3. Chemical Engineering Journal 160: 333-339.

Chen, H., Yu, H., Tang, Y., Pan, M., Yang, G., Peng, F., Wang, H. and Yang, J. (2009). Hydrogen production via autothermal reforming of ethanol over noble metal catalysts supported on oxides. Journal of Natural Gas Chemistry 18: 191-198.

Chen, J. M. P. and Ni, M. (2014). Economic analysis of a solid oxide fuel cell cogeneration/trigeneration system for hotels in Hong Kong. Energy and Buildings 75: 160-169.

Chen, L., Choong, C. K. S., Zhong, Z., Huang, L., Wang, Z. and Lin, J. (2012). Support and alloy effects on activity and product selectivity for ethanol steam reforming over supported nickel cobalt catalysts. International Journal of Hydrogen Energy 37: 16321-16332.

Chen, Y., Zhao, Y., Zheng, C. and Zhang, J. (2013b). Numerical study of hydrogen production via sorption-enhanced steam methane reforming in a fluidized bed reactor at relatively low temperature. Chemical Engineering Science 92: 67-80.

Chorkendorff, I. and Niemantsverdriet, J. W. (2003). Heterogeneous catalysis in practice: hydrogen. In: Concepts of modern catalysis and kinetics. Weinheim, Germany, Wiley-VCH Verlag GmbH & Co.

Christensen, D. O., Silveston, P. L., Croiset, E. and Hudgins, R. R. (2004). Production of hydrogen from the noncatalytic partial oxidation of ethanol. Industrial & Engineering Chemistry Research 43: 2636-2642.

Cobden, P. D., Elzingaa, G. D., Booneveld, S., Dijkstra, J. W., Jansen, D. and van den Brink, R. W. (2009). Sorption-enhanced steam-methane reforming: $CaO–CaCO_3$ capture technology. Energy Procedia 1: 733-739.

Cohce, M. K., Dincer, I. and Rosen, M. A. (2011). Energy and exergy analyses of a biomass-based hydrogen production system. Bioresource Technology 102: 8466-8474.

Colpan, C. O., Dincer, I. and Hamdullahpur, F. (2007). Thermodynamic modeling of direct internal reforming solid oxide fuel cells operating with syngas. International Journal of Hydrogen Energy 32: 787-795.

Colpan, C. O., Hamdullahpur, F. and Dincer, I. (2011). Transient heat transfer modeling of a solid oxide fuel cell operating with humidified hydrogen. International Journal of Hydrogen Energy 36: 11488-11499.

Comas, J., Laborde, M. and Amadeo, N. (2004). Thermodynamic analysis of hydrogen production from ethanol using CaO as a CO_2 sorbent. Journal of Power Sources 138: 61-67.

Conte M., Mario F.D., Iacobazzi A., Mattucci A., Moreno A. and M., R. (2009). Hydrogen as Future Energy Carrier: The ENEA Point of View on Technology and Application Prospects. Energies 2: 150-179.

Cormos, A. M. and Simon, A. (2013). Dynamic modeling of CO_2 capture by calcium-looping cycle. Chemical Engineering Transactions 35: 421-426.

Costamagna, P., Selimovic, A., Del Borghi, M. and Agnew, G. (2004). Electrochemical model of the integrated planar solid oxide fuel cell (IP-SOFC). Chemical Engineering Journal 102: 61-69.

Coutelieris, F. A., Douvartzides, S. and Tsiakaras, P. (2003). The importance of the fuel choice on the efficiency of a solid oxide fuel cell system. Journal of Power Sources 123: 200-205.

Coutelieris, F. A., Douvartzides, S. L. and Tsiakaras, P. E. (2005). Heat transfer phenomena in a solid oxide fuel cell: An analytical approach. Chemical Engineering Science 60: 4423-4430.

Cunha, A. F., Wu, Y. J., Santos, J. C. and Rodrigues, A. E. (2013). Sorption enhanced steam reforming of ethanol on hydrotalcite-like compounds impregnated with active copper. Chemical Engineering Research and Design 91: 581-592.

Dawes, J. E., Hanspal, N. S., Family, O. A. and Turan, A. (2009). Three-dimensional CFD modelling of PEM fuel cells: An investigation into the effects of water flooding. Chemical Engineering Science 64: 2781-2794.

De Falco, M. (2011). Ethanol membrane reformer and PEMFC system for automotive application. Fuel 90: 739-747.

De Falco, M., Piemonte, V., Di Paola, L. and Basile, A. (2014). Methane membrane steam reforming: Heat duty assessment. International Journal of Hydrogen Energy 39: 4761-4770.

Deng, J., Cao, Z. and Zhou, B. (1995). Catalytic dehydrogenation of ethanol in a metal-modified alumina membrane reactor. Applied Catalysis A: General 132: 9-20.

Derevschikov, V. S., Lysikov, A. I. and Okunev, A. G. (2011). Sorption properties of lithium carbonate doped CaO and its performance in sorption enhanced methane reforming. Chemical Engineering Science 66: 3030-3038.

Dey, T., Singdeo, D., Bose, M., Basu, R. N. and Ghosh, P. C. (2013). Study of contact resistance at the electrode–interconnect interfaces in planar type Solid Oxide Fuel Cells. Journal of Power Sources 233: 290-298.

Diagne, C., Idriss, H. and Kiennemann, A. (2002). Hydrogen production by ethanol reforming over Rh/CeO_2–ZrO_2 catalysts. Catalysis Communications 3: 565-571.

Díaz Alvarado, F. and Gracia, F. (2010). Steam reforming of ethanol for hydrogen production: Thermodynamic analysis including different carbon deposits representation. Chemical Engineering Journal 165: 649-657.

Dincer, I. and Naterer, G. F. (2010). Assessment of exergy efficiency and Sustainability Index of an air water heat pump. International Journal of Exergy 7: 37–50.

Dincer, I. and Rosen, M. A. (2013). Exergy: energy, environment and sustainable development. San Diego, U.S.A., Elsevier.

Dou, B., Wang, C., Chen, H., Song, Y. and Xie, B. (2013). Continuous sorption-enhanced steam reforming of glycerol to high-purity hydrogen production. International Journal of Hydrogen Energy 38: 11902-11909.

Douvartzides, S., Coutelieris, F. and Tsiakaras, P. (2004a). Exergy analysis of a solid oxide fuel cell power plant fed by either ethanol or methane. Journal of Power Sources 131: 224-230.

Douvartzides, S. L., Coutelieris, F. A., Demin, A. K. and Tsiakaras, P. E. (2004b). Electricity from ethanol fed SOFCs: the expectations for sustainable development and technological benefits. International Journal of Hydrogen Energy 29: 375-379.

Ebner, J., Babbitt, C., Winer, M., Hilton, B. and Williamson, A. (2014). Life cycle greenhouse gas (GHG) impacts of a novel process for converting food waste to ethanol and co-products. Applied Energy 130: 86-93.

EG&G Technical Services, I. (2004). Fuel Cell Handbook. Virginai, U.S. Department of Energy. National Information Service.

El-Emam, R. S. and Dincer, I. (2011). Energy and exergy analyses of a combined molten carbonate fuel cell – Gas turbine system. International Journal of Hydrogen Energy 36: 8927-8935.

Elzinga, G. D., Reijers, H. T. J., Cobden, P. D., Haije, W. G. and van den Brink, R. W. (2011). CaO sorbent stabilisation for CO_2 capture applications. Energy Procedia 4: 844-851.

Fan, L., Wang, C., Chen, M., Di, J., Zheng, J. and Zhu, B. (2011). Potential low-temperature application and hybrid-ionic conducting property of ceria-carbonate composite electrolytes for solid oxide fuel cells. International Journal of Hydrogen Energy 36: 9987-9993.

Fatsikostas, A. N. and Verykios, X. E. (2004). Reaction network of steam reforming of ethanol over Ni-based catalysts. Journal of Catalysis 225: 439-452.

Feng B., Liu W., Li X. and H., A. (2007). Screening of CO2 adsorbing materials for zero emission power generation systems. Energy & Fuels 21: 426-434.

Fermoso, J., He, L. and Chen, D. (2012). Production of high purity hydrogen by sorption enhanced steam reforming of crude glycerol. International Journal of Hydrogen Energy 37: 14047-14054.

Fishtik, I., Alexander, A., Datta, R. and Geana, D. (2000). A thermodynamic analysis of hydrogen production by steam reforming of ethanol via response reactions. International Journal of Hydrogen Energy 25: 31-45.

Fong, K. F. and Lee, C. K. (2014). Investigation on zero grid-electricity design strategies of solid oxide fuel cell trigeneration system for high-rise building in hot and humid climate. Applied Energy 114: 426-433.

Freni, S., Maggio, G. and Cavallaro, S. (1996). Ethanol steam reforming in a molten carbonate fuel cell: a thermodynamic approach. Journal of Power Sources 62: 67-73.

Freni S., Mondello N., Cavallaro S., Cacciola G., Parmon V.N. and A., S. V. (2000). Hydrogen production by steam reforming of ethanol: a two step process. Reaction Kinetics and Catalysis Letters 71: 143-152.

Frusteri, F., Freni, S., Spadaro, L., Chiodo, V., Bonura, G., Donato, S. and Cavallaro, S. (2004). H2 production for MC fuel cell by steam reforming of ethanol over MgO supported Pd, Rh, Ni and Co catalysts. Catalysis Communications 5: 611-615.

Fu, P., Yi, W., Li, Z., Li, Y., Wang, J. and Bai, X. (2013). Comparative analysis on sorption enhanced steam reforming and conventional steam reforming of hydroxyacetone for hydrogen production: Thermodynamic modeling. International Journal of Hydrogen Energy 38: 11893-11901.

Fujita, K., Seyama, T., Sobue, T. and Matsuzaki, Y. (2012). Development of Segmented-in-series-type Solid Oxide Fuel Cells for Residential Applications. Energy Procedia 28: 153-161.

Gallucci, F., De Falco, M., Tosti, S., Marrelli, L. and Basile, A. (2008a). Co-current and counter-current configurations for ethanol steam reforming in a dense Pd–Ag membrane reactor. International Journal of Hydrogen Energy 33: 6165-6171.

Gallucci, F., De Falco, M., Tosti, S., Marrelli, L. and Basile, A. (2008b). Ethanol steam reforming in a dense Pd–Ag membrane reactor: A modelling work. Comparison with the traditional system. International Journal of Hydrogen Energy 33: 644-651.

Gao, P., Dai, Y., Tong, Y. and Dong, P. (2015). Energy matching and optimization analysis of waste to energy CCHP (combined cooling, heating and power) system with exergy and energy level. Energy 79: 522-535.

Gao, Z., Huang, J., Mao, Z., Wang, C. and Liu, Z. (2010). Preparation and characterization of nanocrystalline $Ce_{0.8}Sm_{0.2}O_{1.9}$ for low temperature solid oxide fuel cells based on composite electrolyte. International Journal of Hydrogen Energy 35: 731-737.

García, E. Y. and Laborde, M. A. (1991). Hydrogen production by the steam reforming of ethanol: Thermodynamic analysis. International Journal of Hydrogen Energy 16: 307-312.

Graschinsky, C., Giunta, P., Amadeo, N. and Laborde, M. (2012). Thermodynamic analysis of hydrogen production by autothermal reforming of ethanol. International Journal of Hydrogen Energy 37: 10118-10124.

Grashoff, G. J., Pilkington, C. E. and Corti, C. W. (1983). The Purification of Hydrogen: A review of the technology emphasizing the current status of Palladium membrane diffusion. Platinum Metals Review 27: 157-169.

Gutierrez, A., Karinen, R., Airaksinen, S., Kaila, R. and Krause, A. O. I. (2011). Autothermal reforming of ethanol on noble metal catalysts. International Journal of Hydrogen Energy 36: 8967-8977.

Halabi, M. H., de Croon, M. H. J. M., van der Schaaf, J., Cobden, P. D. and Schouten, J. C. (2012). Kinetic and structural requirements for a CO2 adsorbent in sorption enhanced catalytic reforming of methane – Part I: Reaction kinetics and sorbent capacity. Fuel 99: 154-164.

Harriman, L. G. (1990). The Dehumidification Handbook. Amesbury, Massachusetts, U.S.A., Munters Cargocaire.

Harrison, D. P. (2008). Sorption-enhanced hydrogen production-a review. Industrial & Engineering Chemistry Research 47: 6486–6501.

Haryanto A., Fernando S., Murali N. and S., A. (2005). Current Status of Hydrogen Production Techniques by Steam Reforming of Ethanol: A Review. Energy & Fuels 19: 2098-2106.

Haseli, Y., Dincer, I. and Naterer, G. F. (2008). Thermodynamic analysis of a combined gas turbine power system with a solid oxide fuel cell through exergy. Thermochimica Acta 480: 1-9.

He, Z., Li, H. and Birgersson, E. (2013). Reduced model for the planar solid oxide fuel cell. Computers & Chemical Engineering 52: 155-167.

Hernández, L. and Kafarov, V. (2009). Thermodynamic evaluation of hydrogen production for fuel cells by using bio-ethanol steam reforming: Effect of carrier gas addition. Journal of Power Sources 192: 195-199.

Herold, K. E., Radermacher, R. and Klein, S. A. (1996). Absorption chillers and heat pumps, CRC press.

Hofmann, P. and Panopoulos, K. D. (2010). Detailed dynamic Solid Oxide Fuel Cell modeling for electrochemical impedance spectra simulation. Journal of Power Sources 195: 5320-5339.

Holladay, J. D., Hu, J., King, D. L. and Wang, Y. (2009). An overview of hydrogen production technologies. Catalysis Today 139: 244-260.

Hong, T., Kim, D., Koo, C. and Kim, J. (2014). Framework for establishing the optimal implementation strategy of a fuel-cell-based combined heat and power system: Focused on multi-family housing complex. Applied Energy 127: 11-24.

Hong, W.-T., Yen, T.-H., Chung, T.-D., Huang, C.-N. and Chen, B.-D. (2011). Efficiency analyses of ethanol-fueled solid oxide fuel cell power system. Applied Energy 88: 3990-3998.

Huang, J., Xie, F., Wang, C. and Mao, Z. (2012). Development of solid oxide fuel cell materials for intermediate-to-low temperature operation. International Journal of Hydrogen Energy 37: 877-883.

Huang, S., Feng, S., Wang, H., Li, Y. and Wang, C. (2011). $LaNi_{0.6}Fe_{0.4}O_3$–$Ce_{0.8}Sm_{0.2}O_{1.9}$–Ag composite cathode for intermediate temperature solid oxide fuel cells. International Journal of Hydrogen Energy 36: 10968-10974.

Iordanidis, A. A., Kechagiopoulos, P. N., Voutetakis, S. S., Lemonidou, A. A. and Vasalos, I. A. (2006). Autothermal sorption-enhanced steam reforming of bio-oil/biogas mixture and energy generation by fuel cells: Concept analysis and process simulation. International Journal of Hydrogen Energy 31: 1058-1065.

Ishak, F., Dincer, I. and Zamfirescu, C. (2012). Energy and exergy analyses of direct ammonia solid oxide fuel cell integrated with gas turbine power cycle. Journal of Power Sources 212: 73-85.

Iwasa, N. and Takezawa, N. (1991). Reforming of ethanol-Dehydrogenation to Ethyl Acetate and Steam Reforming to Acetic over Copper-Based Catalysts. Bulletin of the Chemical Society of Japan 64.

Jamsak, W., Assabumrungrat, S., Douglas, P. L., Laosiripojana, N., Suwanwarangkul, R., Charojrochkul, S. and Croiset, E. (2007). Performance of ethanol-fuelled solid oxide fuel cells: Proton and oxygen ion conductors. Chemical Engineering Journal 133: 187-194.

Jia, J., Abudula, A., Wei, L., Jiang, R. and Shen, S. (2007). A mathematical model of a tubular solid oxide fuel cell with specified combustion zone. Journal of Power Sources 171: 696-705.

Johnsen, K., Ryu, H. J., Grace, J. R. and Lim, C. J. (2006). Sorption-enhanced steam reforming of methane in a fluidized bed reactor with dolomite as -acceptor. Chemical Engineering Science 61: 1195-1202.

Kaddouri, A. and Mazzocchia, C. (2004). A study of the influence of the synthesis conditions upon the catalytic properties of Co/SiO2 or Co/Al2O3 catalysts used for ethanol steam reforming. Catalysis Communications 5: 339-345.

Klein, S. A. (2014). Engineering equation solver, F-Chart Software.

Kromp, A., Geisler, H., Weber, A. and Ivers-Tiffée, E. (2013). Electrochemical impedance modeling of gas transport and reforming kinetics in reformate fueled solid oxide fuel cell anodes. Electrochimica Acta 106: 418-424.

Liguras, D. K., Goundani, K. and Verykios, X. E. (2004). Production of hydrogen for fuel cells by catalytic partial oxidation of ethanol over structured Ru catalysts. International Journal of Hydrogen Energy 29: 419-427.

Lima da Silva, A., Malfatti, C. d. F. and Müller, I. L. (2009). Thermodynamic analysis of ethanol steam reforming using Gibbs energy minimization method: A detailed study of the conditions of carbon deposition. International Journal of Hydrogen Energy 34: 4321-4330.

Lima da Silva, A. and Müller, I. L. (2011). Hydrogen production by sorption enhanced steam reforming of oxygenated hydrocarbons (ethanol, glycerol, n-butanol and methanol): Thermodynamic modelling. International Journal of Hydrogen Energy 36: 2057-2075.

Lin, J., Babbitt, C. W. and Trabold, T. A. (2013). Life cycle assessment integrated with thermodynamic analysis of bio-fuel options for solid oxide fuel cells. Bioresource Technology 128: 495-504.

Lin, W.-H. and Chang, H.-F. (2004). A study of ethanol dehydrogenation reaction in a palladium membrane reactor. Catalysis Today 97: 181-188.

Lin, Y.-T., Lin, C.-T., Chen, Y.-C., Yin, K.-M. and Yang, C.-T. (2007). An analytical study of the PEM fuel cell with axial convection in the gas channel. International Journal of Hydrogen Energy 32: 4477-4488.

Llorca, J., Homs, N. s., Sales, J. and de la Piscina, P. R. r. (2002). Efficient Production of Hydrogen over Supported Cobalt Catalysts from Ethanol Steam Reforming. Journal of Catalysis 209: 306-317.

Lo Faro, M., Stassi, A., Antonucci, V., Modafferi, V., Frontera, P., Antonucci, P. and Aricò, A. S. (2011). Direct utilization of methanol in solid oxide fuel cells: An electrochemical and catalytic study. International Journal of Hydrogen Energy 36: 9977-9986.

Lopes, D. G., da Silva, E. P., Pinto, C. S., Neves Jr, N. P., Camargo, J. C., Ferreira, P. F. P., Furlan, A. L. and Lopes, D. G. (2012). Technical and economic analysis of a power supply system based on ethanol reforming and PEMFC. Renewable Energy 45: 205-212.

Ma, S., Wang, J., Yan, Z., Dai, Y. and Lu, B. (2011). Thermodynamic analysis of a new combined cooling, heat and power system driven by solid oxide fuel cell based on ammonia–water mixture. Journal of Power Sources 196: 8463-8471.

Mahishi, M. R., Sadrameli, M. S., Vijayaraghavan, S. and Goswami, D. Y. (2008). A Novel Approach to Enhance the Hydrogen Yield of Biomass Gasification Using CO_2 Sorbent. Journal of Engineering for Gas Turbines and Power 130: 011501.

Maidment, G. G., Zhao, X., Riffat, S. B. and Prosser, G. (1999). Application of combined heat-and-power and absorption cooling in a supermarket. Applied Energy 63: 169-190.

Manzolini, G. and Tosti, S. (2008). Hydrogen production from ethanol steam reforming: energy efficiency analysis of traditional and membrane processes. International Journal of Hydrogen Energy 33: 5571-5582.

Markova, D., Bazbauers, G., Valters, K., Alhucema Arias, R., Weuffen, C. and Rochlitz, L. (2009). Optimization of bio-ethanol autothermal reforming and carbon monoxide removal processes. Journal of Power Sources 193: 9-16.

Martavaltzi, C. S. and Lemonidou, A. A. (2010). Hydrogen production via sorption enhanced reforming of methane: Development of a novel hybrid material—reforming catalyst and CO_2 sorbent. Chemical Engineering Science 65: 4134-4140.

Mat, M. D., Liu, X., Zhu, Z. and Zhu, B. (2007). Development of cathodes for methanol and ethanol fuelled low temperature (300–600°C) solid oxide fuel cells. International Journal of Hydrogen Energy 32: 796-801.

Mattos, L. V. and Noronha, F. B. (2005a). Hydrogen production for fuel cell applications by ethanol partial oxidation on Pt/CeO_2 catalysts: the effect of the reaction conditions and reaction mechanism. Journal of Catalysis 233: 453-463.

Mattos, L. V. and Noronha, F. B. (2005b). Partial oxidation of ethanol on supported Pt catalysts. Journal of Power Sources 145: 10-15.

Moné, C. D., Chau, D. S. and Phelan, P. E. (2001). Economic feasibility of combined heat and power and absorption refrigeration with commercially available gas turbines. Energy Conversion and Management 42: 1559-1573.

Morgenstern, D. A. and Fornango, J. P. (2005). Low-Temperature Reforming of Ethanol over Copper-Plated Raney Nickel: A New Route to Sustainable Hydrogen for Transportation. Energy & Fuels 19: 1708-1716.

Nedyalkova, R., Torras, C., Salvadó, J. and Montané, D. (2010). Electrophoretic deposition of ethanol steam-reforming catalysts on metal plates for the development of catalytic-wall reactors. Fuel Processing Technology 91: 1040-1048.

Ni, M., Leung, D. Y. C. and Leung, M. K. H. (2007a). A review on reforming bio-ethanol for hydrogen production. International Journal of Hydrogen Energy 32: 3238-3247.

Ni, M., Leung, M. K. H. and Leung, D. Y. C. (2007b). Parametric study of solid oxide fuel cell performance. Energy Conversion and Management 48: 1525-1535.

Nishiguchi, T., Matsumoto, T., Kanai, H., Utani, K., Matsumura, Y., Shen, W.-J. and Imamura, S. (2005). Catalytic steam reforming of ethanol to produce hydrogen and acetone. Applied Catalysis A: General 279: 273-277.

Noren, D. A. and Hoffman, M. A. (2005). Clarifying the Butler–Volmer equation and related approximations for calculating activation losses in solid oxide fuel cell models. Journal of Power Sources 152: 175-181.

Novaresio, V., García-Camprubí, M., Izquierdo, S., Asinari, P. and Fueyo, N. (2012). An open-source library for the numerical modeling of mass-transfer in solid oxide fuel cells. Computer Physics Communications 183: 125-146.

Paglieri, S. N. and Way, J. D. (2002). Innovations in palladium membrane research. Separation & Purification Review 31: 1-169.

Park, J. and Bae, J. (2012). Characterization of electrochemical reaction and thermo-fluid flow in metal-supported solid oxide fuel cell stacks with various manifold designs. International Journal of Hydrogen Energy 37: 1717-1730.

Park, J., Bae, J. and Kim, J.-Y. (2012). A numerical study on anode thickness and channel diameter of anode-supported flat-tube solid oxide fuel cells. Renewable Energy 42: 180-185.

Park, S. K., Ahn, J.-H. and Kim, T. S. (2011). Performance evaluation of integrated gasification solid oxide fuel cell/gas turbine systems including carbon dioxide capture. Applied Energy 88: 2976-2987.

Parthasarathy, P. and Narayanan, K. S. (2014). Hydrogen production from steam gasification of biomass: Influence of process parameters on hydrogen yield – A review. Renewable Energy 66: 570-579.

Patcharavorachot, Y., Arpornwichanop, A. and Chuachuensuk, A. (2008). Electrochemical study of a planar solid oxide fuel cell: Role of support structures. Journal of Power Sources 177: 254-261.

Petruzzi, L., Cocchi, S. and Fineschi, F. (2003). A global thermo-electrochemical model for SOFC systems design and engineering. Journal of Power Sources 118: 96-107.

Pirkandi, J., Ghassemi, M., Hamedi, M. H. and Mohammadi, R. (2012). Electrochemical and thermodynamic modeling of a CHP system using tubular solid oxide fuel cell (SOFC-CHP). Journal of Cleaner Production 29–30: 151-162.

Piroonlerkgul, P., Assabumrungrat, S., Laosiripojana, N. and Adesina, A. A. (2008). Selection of appropriate fuel processor for biogas-fuelled SOFC system. Chemical Engineering Journal 140: 341-351.

Piroonlerkgul, P., Kiatkittipong, W., Arpornwichanop, A., Soottitantawat, A., Wiyaratn, W., Laosiripojana, N., Adesina, A. A. and Assabumrungrat, S. (2010). Technical and economic study of integrated system of solid oxide fuel cell, palladium membrane reactor, and CO_2 sorption enhancement unit. Chemical Engineering and Processing: Process Intensification 49: 1006-1016.

Qin, H., Zhu, B., Raza, R., Singh, M., Fan, L. and Lund, P. (2012). Integration design of membrane electrode assemblies in low temperature solid oxide fuel cell. International Journal of Hydrogen Energy 37: 19365-19370.

Rabenstein, G. and Hacker, V. (2008). Hydrogen for fuel cells from ethanol by steam-reforming, partial-oxidation and combined auto-thermal reforming: A thermodynamic analysis. Journal of Power Sources 185: 1293-1304.

Rosen, M. A., Dincer, I. and Kanoglu, M. (2008). Role of exergy in increasing efficiency and sustainability and reducing environmental impact. Energy Policy 36: 128-137.

Rossi, C. C. R. S., Alonso, C. G., Antunes, O. A. C., Guirardello, R. and Cardozo-Filho, L. (2009). Thermodynamic analysis of steam reforming of ethanol and glycerine for hydrogen production. International Journal of Hydrogen Energy 34: 323-332.

Rostrup-Nielsen, J. R. (1984). Catalytic Steam Reforming. In Catalysis Science and Technology. Berlin, Springer.

Saebea, D., Arpornwichanop, A., Patcharavorachot, Y. and Assabumrungrat, S. (2011). Adsorption-membrane hybrid system for ethanol steam reforming: Thermodynamic analysis. International Journal of Hydrogen Energy 36: 14428-14434.

Saebea, D., Authayanun, S., Patcharavorachot, Y., Paengjuntuek, W. and Arpornwichanop, A. (2013). Use of different renewable fuels in a steam reformer integrated into a solid oxide fuel cell: Theoretical analysis and performance comparison. Energy 51: 305-313.

Sakadjian B.B., Iyer M.V., Gupta H. and L., F. (2007). Kinetics and structural characterization of calcium-based sorbents calcined under subatmospheric conditions for the high-temperature CO_2 capture process. Industrial & Engineering Chemistry Research 46: 35–42.

Sanaye, S. and Katebi, A. (2014). 4E analysis and multi objective optimization of a micro gas turbine and solid oxide fuel cell hybrid combined heat and power system. Journal of Power Sources 247: 294-306.

Sánchez, D., Chacartegui, R., Muñoz, A. and Sánchez, T. (2006). Thermal and electrochemical model of internal reforming solid oxide fuel cells with tubular geometry. Journal of Power Sources 160: 1074-1087.

Seelam, P. K., Liguori, S., Iulianelli, A., Pinacci, P., Calabrò, V., Huuhtanen, M., Keiski, R., Piemonte, V., Tosti, S., De Falco, M. and Basile, A. (2012). Hydrogen production from bio-ethanol steam reforming reaction in a Pd/PSS membrane reactor. Catalysis Today 193: 42-48.

Silva, A. M., Farias, A. M. D. d., Costa, L. O. O., Barandas, A. P. M. G., Mattos, L. V., Fraga, M. A. and Noronha, F. B. (2008). Partial oxidation and water–gas shift reaction in an integrated system for hydrogen production from ethanol. Applied Catalysis A: General 334: 179-186.

Sohn, S., Nam, J. H., Jeon, D. H. and Kim, C.-J. (2010). A micro/macroscale model for intermediate temperature solid oxide fuel cells with prescribed fully-developed axial velocity profiles in gas channels. International Journal of Hydrogen Energy 35: 11890-11907.

Solieman, A. A. A., Dijkstra, J. W., Haije, W. G., Cobden, P. D. and van den Brink, R. W. (2009). Calcium oxide for CO_2 capture: Operational window and efficiency penalty in sorption-enhanced steam methane reforming. International Journal of Greenhouse Gas Control 3: 393-400.

Somers, C., Mortazavi, A., Hwang, Y., Radermacher, R., Rodgers, P. and Al-Hashimi, S. (2011). Modeling water/lithium bromide absorption chillers in ASPEN Plus. Applied Energy 88: 4197-4205.

Song, S., Douvartzides, S. and Tsiakaras, P. (2005). Exergy analysis of an ethanol fuelled proton exchange membrane (PEM) fuel cell system for automobile applications. Journal of Power Sources 145: 502-514.

Srinivas, D., Satyanarayana, C. V. V., Potdar, H. S. and Ratnasamy, P. (2003). Structural studies on NiO-CeO_2-ZrO_2 catalysts for steam reforming of ethanol. Applied Catalysis A: General 246: 323-334.

Stamatis A., Vinni C., Bakalis D., Tzorbatzoglou F. and P., T. (2012). Exergy Analysis of an Intermediate Temperature Solid Oxide Fuel Cell-Gas Turbine Hybrid System Fed with Ethanol. Energies 5: 4268-4287.

Sun, S., Yan, W., Sun, P. and Chen, J. (2012). Thermodynamic analysis of ethanol reforming for hydrogen production. Energy 44: 911-924.

Suwanwarangkul, R., Croiset, E., Fowler, M. W., Douglas, P. L., Entchev, E. and Douglas, M. A. (2003). Performance comparison of Fick's, dusty-gas and Stefan–Maxwell models to predict the concentration overpotential of a SOFC anode. Journal of Power Sources 122: 9-18.

Suzuki, T., Takahashi, Y., Hamamoto, K., Yamaguchi, T. and Fujishiro, Y. (2011). Low temperature processed composite cathodes for Solid-oxide fuel Cells. International Journal of Hydrogen Energy 36: 10998-11003.

Szargut, J., Morris, D. R. and Steward, F. R. (1988). Exergy Analysis of Thermal, Chemical, and Metallurgical Processes, Springer.

Tanim, T., Bayless, D. J. and Trembly, J. P. (2014). Modeling a 5 kWe planar solid oxide fuel cell based system operating on JP-8 fuel and a comparison with tubular cell based system for auxiliary and mobile power applications. Journal of Power Sources 245: 986-997.

Tippawan, P. and Arpornwichanop, A. (2014). Energy and exergy analysis of an ethanol reforming process for solid oxide fuel cell applications. Bioresource Technology 157: 231-239.

Tosti, S., Basile, A., Borgognoni, F., Capaldo, V., Cordiner, S., Di Cave, S., Gallucci, F., Rizzello, C., Santucci, A. and Traversa, E. (2008a). Low-temperature ethanol steam reforming in a Pd–Ag membrane reactor: Part 2. Pt-based and Ni-based catalysts and general comparison. Journal of Membrane Science 308: 258-263.

Tosti, S., Basile, A., Borgognoni, F., Capaldo, V., Cordiner, S., Di Cave, S., Gallucci, F., Rizzello, C., Santucci, A. and Traversa, E. (2008b). Low temperature ethanol steam reforming in a Pd-Ag membrane reactor: Part 1: Ru-based catalyst. Journal of Membrane Science 308: 250-257.

Tosti, S., Fabbricino, M., Moriani, A., Agatiello, G., Scudieri, C., Borgognoni, F. and Santucci, A. (2011). Pressure effect in ethanol steam reforming via dense Pd-based membranes. Journal of Membrane Science 377: 65-74.

Tse, L. K. C., Wilkins, S., McGlashan, N., Urban, B. and Martinez-Botas, R. (2011). Solid oxide fuel cell/gas turbine trigeneration system for marine applications. Journal of Power Sources 196: 3149-3162.

Tseronis, K., Bonis, I., Kookos, I. K. and Theodoropoulos, C. (2012). Parametric and transient analysis of non-isothermal, planar solid oxide fuel cells. International Journal of Hydrogen Energy 37: 530-547.

Tseronis, K., Kookos, I. K. and Theodoropoulos, C. (2008). Modelling mass transport in solid oxide fuel cell anodes: a case for a multidimensional dusty gas-based model. Chemical Engineering Science 63: 5626-5638.

Tzanetis, K. F., Martavaltzi, C. S. and Lemonidou, A. A. (2012). Comparative exergy analysis of sorption enhanced and conventional methane steam reforming. International Journal of Hydrogen Energy 37: 16308-16320.

Vasudeva, K., Mitra, N., Umasankar, P. and Dhingra, S. C. (1996). Steam reforming of ethanol for hydrogen production: Thermodynamic analysis. International Journal of Hydrogen Energy 21: 13-18.

Verda, V. and Calí Quaglia, M. (2008). Solid oxide fuel cell systems for distributed power generation and cogeneration. International Journal of Hydrogen Energy 33: 2087-2096.

Virkar, A. V., Chen, J., Tanner, C. W. and Kim, J.-W. (2000). The role of electrode microstructure on activation and concentration polarizations in solid oxide fuel cells. Solid State Ionics 131: 189-198.

Wanat, E. C., Venkataraman, K. and Schmidt, L. D. (2004). Steam reforming and water–gas shift of ethanol on Rh and Rh–Ce catalysts in a catalytic wall reactor. Applied Catalysis A: General 276: 155-162.

Wang, K., Ran, R., Hao, Y., Shao, Z., Jin, W. and Xu, N. (2008). A high-performance no-chamber fuel cell operated on ethanol flame. Journal of Power Sources 177: 33-39.

Wang, S., Worek, W. M. and Minkowycz, W. J. (2012). Performance comparison of the mass transfer models with internal reforming for solid oxide fuel cell anodes. International Journal of Heat and Mass Transfer 55: 3933-3945.

Wang, W. and Wang, Y. (2008). Thermodynamic analysis of hydrogen production via partial oxidation of ethanol. International Journal of Hydrogen Energy 33: 5035-5044.

Wang, Z., Lü, Z., Wei, B., Huang, X., Chen, K., Pan, W. and Su, W. (2011). A right-angular configuration for the single-chamber solid oxide fuel cell. International Journal of Hydrogen Energy 36: 3147-3152.

Wu, Y. J., Li, P., Yu, J. G., Cunha, A. F. and Rodrigues, A. E. (2013). Sorption-enhanced steam reforming of ethanol on NiMgAl multifunctional materials: Experimental and numerical investigation. Chemical Engineering Journal 231: 36-48.

Yan, D., Bin, Z., Fang, D., Luo, J., Wang, X., Pu, J., Chi, B., Jian, L. and Zhang, Y. (2013). Feasibility study of an external manifold for planar intermediate-temperature solid oxide fuel cells stack. International Journal of Hydrogen Energy 38: 660-666.

Yu, C.-Y., Lee, D.-W., Park, S.-J., Lee, K.-Y. and Lee, K.-H. (2009). Study on a catalytic membrane reactor for hydrogen production from ethanol steam reforming. International Journal of Hydrogen Energy 34: 2947-2954.

Yu, Z., Han, J. and Cao, X. (2011). Investigation on performance of an integrated solid oxide fuel cell and absorption chiller tri-generation system. International Journal of Hydrogen Energy 36: 12561-12573.

Yu, Z., Han, J., Cao, X., Chen, W. and Zhang, B. (2010). Analysis of total energy system based on solid oxide fuel cell for combined cooling and power applications. International Journal of Hydrogen Energy 35: 2703-2707.

Yun, S. and Ted Oyama, S. (2011). Correlations in palladium membranes for hydrogen separation: A review. Journal of Membrane Science 375: 28-45.

Zhang, X., Su, S., Chen, J., Zhao, Y. and Brandon, N. (2011). A new analytical approach to evaluate and optimize the performance of an irreversible solid oxide fuel cell-gas turbine hybrid system. International Journal of Hydrogen Energy 36: 15304-15312.

Zhao, F. and Virkar, A. V. (2005). Dependence of polarization in anode-supported solid oxide fuel cells on various cell parameters. Journal of Power Sources 141: 79-95.

Zhao, L., He, B., Gu, J., Liu, F., Chu, X. and Xia, C. (2012). Reaction model for cathodes cooperated with oxygen-ion conductors for solid oxide fuel cells using proton-conducting electrolytes. International Journal of Hydrogen Energy 37: 548-554.

Zhao, Y., Xia, C., Jia, L., Wang, Z., Li, H., Yu, J. and Li, Y. (2013). Recent progress on solid oxide fuel cell: Lowering temperature and utilizing non-hydrogen fuels. International Journal of Hydrogen Energy 38: 16498-16517.

Zhu, B. (2001). Advantages of intermediate temperature solid oxide fuel cells for tractionary applications. Journal of Power Sources 93: 82-86.

Zhu, H. and Kee, R. J. (2003). A general mathematical model for analyzing the performance of fuel-cell membrane-electrode assemblies. Journal of Power Sources 117: 61-74.

APPENDIX

Appendix A List of international publications

1. **Tippawan, P.**, Arpornwichanop, A. (2014). Energy and exergy analysis of an ethanol reforming process for solid oxide fuel cell applications. Bioresource Technology, 157, 231–239.
2. **Tippawan, P.**, Assabumrungrat, S., Arpornwichanop, A. (2014). Theoretical Study on the Ethanol-Fueled SOFC System Integrated with Dehumidifier. Chemical Engineering Transactions, 39, 1465-1470.
3. **Tippawan, P.**, Arpornwichanop, A., Dincer, I. (2015). Exergoenvironmental Analysis of Heat Recovery from Solid Oxide Fuel Cell System for Cooling Applications. Chemical Engineering Transactions, 43, 2203-2208.
4. **Tippawan, P.**, Arpornwichanop, A., Dincer, I. (2015). Energy and exergy analyses of an ethanol-fueled solid oxide fuel cell for a trigeneration system. Energy, 87, 228-239.

Appendix B List of International conferences

1. **Tippawan, P.**, Patcharavorachot, Y., Assabumrungrat, S., Arpornwichanop, A. (2011). Thermodynamic Evaluation of Ethanol Steam Reforming via Acetaldehyde as an Intermediate. Thailand Chemical Engineering and Applied Chemistry International Conference 2011 (TIChE 2011), 10-11 November 2011, Hatyai, Thailand.
2. **Tippawan, P.**, Arpornwichanop, A. (2012). Energy and exergy analysis of hydrogen production from different ethanol reforming processes. XX International Conference on Chemical Reactors (Chemreactor-20), 3-7 December 2012, Luxemburg city, Luxemburg.
3. **Tippawan, P.**, Arpornwichanop, A. (2013). Performance improvement of a solid oxide fuel cell system with a two-step ethanol reforming process using CO_2 sorbent. The 9^{th} European congress of Chemical Engineering and 2^{nd} European congress of Appiled Biotechnology (ECCE9-ECAB2), 21-24 April 2013, The Hague, The Netherlands.
4. **Tippawan, P.**, Assabumrungrat, S., Arpornwichanop, A. (2014). Theoretical Study on the Ethanol-Fueled SOFC System Integrated with Dehumidifier. The

17th Conference Process Integration Modelling and Optimisation for Energy Saving and Pollution Reduction (PRES 2014) 23-27 August 2014, Prague, Czech Republic.

5. **Tippawan, P.**, Arpornwichanop, A., Dincer, I. (2015). Exergoenvironmental Analysis of Heat Recovery from Solid Oxide Fuel Cell System for Cooling Applications. The 12th International Conference on Chemical & Process Engineering (ICheaP12) 19-22 May 2015, Milan, Italy.

VITA

Miss Phanicha Tippawan was born in Bangkok, on January 1, 1988. She received the Bachelor Degree in Chemical Engineering from King Mongkut Institute of Technology Ladkrabang in 2009. She began her doctoral study in June 2009 and received Ph.D. scholarship "Dutsadiphiphat Scholarship, Ratchadaphiseksomphot Endowment Fund" from Chulalongkorn University. During her study, she spent her eight months in Clean Energy Research Laboratory (CERL), Faculty of Engineering and Applied Science, University of Ontario Institute of Technology (UOIT), Ontario, Canada, to undertake parts of the Ph.D. research.